AD-A049 278 GULF AND WESTERN APPLIED SCIENCE LABS WALTHAM MA F/G 6/16
SENSORY MECHANISM MODELING.(U)
OCT 77 J BORAH, L R YOUNG, R E CURRY F33615-76-C-0039
AFHRL-TR-77-70 NL

UNCLASSIFIED

1 OF 2
AD
A049278

AFHRL-TR-77-70

(2)

AIR FORCE

HUMAN RESOURCES

LABORATORY

AD A049278

AD NO. ____
DDC FILE COPY

SENSORY MECHANISM MODELING

By

Joshua Borah
Laurence R. Young
Renwick E. Curry
Gulf + Western
Applied Science Laboratories
335 Bear Hill Road
Waltham, Massachusetts 02154

ADVANCED SYSTEMS DIVISION
Wright-Patterson Air Force Base, Ohio 45433

October 1977
Interim Report for Period 26 January 1976 – 20 July 1977

AIR FORCE SYSTEMS COMMAND
BROOKS AIR FORCE BASE, TEXAS 78235

NOTICE

When U.S. Government drawings, specifications, or other data are used for any purpose other than a definitely related Government procurement operation, the Government thereby incurs no responsibility nor any obligation whatsoever, and the fact that the Government may have formulated, furnished, or in any way supplied the said drawings, specifications, or other data is not to be regarded by implication or otherwise, as in any manner licensing the holder or any other person or corporation, or conveying any rights or permission to manufacture, use, or sell any patented invention that may in any way be related thereto.

This interim report was submitted by Gulf + Western, Applied Science Laboratories, 335 Bear Hill Road, Waltham, Massachusetts 02154, under contract F33615-76-C-0039, project 6114, with Advanced Systems Division, Air Force Human Resources Laboratory (AFSC), Wright-Patterson Air Force Base, Ohio 45433. Mr. William B. Albery, Simulation Techniques Branch, was the contract monitor.

This report has been reviewed and cleared for open publication and/or public release by the appropriate Office of Information (OI) in accordance with AFR 190-17 and DoDD 5230.9. There is no objection to unlimited distribution of this report to the public at large, or by DDC to the National Technical Information Service (NTIS).

This technical report has been reviewed and is approved for publication.

GORDON A. ECKSTRAND, Director
Advanced Systems Division

DAN D. FULGHAM, Colonel, USAF
Commander

Unclassified

SECURITY CLASSIFICATION OF THIS PAGE (When Data Entered)

REPORT DOCUMENTATION PAGE

READ INSTRUCTIONS BEFORE COMPLETING FORM

1. REPORT NUMBER: AFHRL-TR-77-78
2. GOVT ACCESSION NO.
3. RECIPIENT'S CATALOG NUMBER

4. TITLE (and Subtitle): SENSORY MECHANISM MODELING
5. TYPE OF REPORT & PERIOD COVERED: Interim rept. 26 January 1976 – 29 July 1977
6. PERFORMING ORG. REPORT NUMBER

7. AUTHOR(s): Joshua Borah, Laurence R. Young, Renwick E. Curry
8. CONTRACT OR GRANT NUMBER(s): F33615-76-C-0039

9. PERFORMING ORGANIZATION NAME AND ADDRESS: Gulf + Western Applied Science Laboratories, 335 Bear Hill Road, Waltham, Massachusetts 02154
10. PROGRAM ELEMENT, PROJECT, TASK AREA & WORK UNIT NUMBERS: 62205F, 61141901

11. CONTROLLING OFFICE NAME AND ADDRESS: HQ Air Force Human Resources Laboratory (AFSC), Brooks Air Force Base, Texas 78235
12. REPORT DATE: October 1977
13. NUMBER OF PAGES: 138

14. MONITORING AGENCY NAME & ADDRESS (if different from Controlling Office): Advanced Systems Division, Air Force Human Resources Laboratory, Wright-Patterson Air Force Base, Ohio 45433
15. SECURITY CLASS. (of this report): Unclassified
15a. DECLASSIFICATION/DOWNGRADING SCHEDULE

16. DISTRIBUTION STATEMENT (of this Report)

Approved for public release; distribution unlimited.

DDC RECEIVED FEB 1 1978 B

17. DISTRIBUTION STATEMENT (of the abstract entered in Block 20, if different from Report)

18. SUPPLEMENTARY NOTES

19. KEY WORDS (Continue on reverse side if necessary and identify by block number)

aircraft simulation	motion effects	proprioceptive system
circular vection	motion perception	sensory system modeling
haptic system	neural sensory receptors	tactile system
linear vection	optimal control theory	vestibular system
manned simulation	orientation perception	visual effects

20. ABSTRACT (Continue on reverse side if necessary and identify by block number)

The purpose of this study was to model human motion and orientation sensing mechanisms so that simulator motion cueing systems can be designed to take full advantage of the characteristics of these sensory mechanisms. Individual models for vestibular, visual, tactile, and proprioceptive sensors have been either adapted from previous modeling work or formulated from available psychophysical and neurophysiological data. A computer-aided literature search was conducted to help identify material in the area of mechanoreceptor systems, and the resulting bibliography is included in the report.

A composite model structure has been proposed, using a Kalman filter blending technique to integrate information from the different sensory modalities into a single estimate of state. The Kalman filter represents the

DD FORM 1 JAN 73 1473 EDITION OF 1 NOV 65 IS OBSOLETE

Unclassified

SECURITY CLASSIFICATION OF THIS PAGE (When Data Entered)

410 539

Item 20 Continued:

presumed function of neural central processing. The model has been implemented in the form of a digital computer program, and promising preliminary results, in qualitative agreement with known human responses, have been obtained using only vestibular model components.

Ongoing work is directed at exercising the nonvestibular modalities, performing thorough validation and exercise of the entire model, and extending the model where possible. Modifications are expected as this work is pursued.

1473B

FORWARD

This report documents a study conducted by Gulf + Western Applied Science Laboratories under Contract No. F33605-76-C-0039, and covers the period from January 1976 through July 1977. The project was managed by Dr. David Sheena, with Joshua Borah as project engineer and Drs. Laurence Young and Renwick Curry as consultants.

The sponsoring agency was the Air Force Human Resources Lab at Wright-Patterson Air Force Base, where William Albery served as contract monitor and the program was overseen by Don Gum. Several other people at WPAFB assisted in reviewing the work, among them Max Fiore, Andrew Junker, Patricia Knoop, and Dr. David Quam.

TABLE OF CONTENTS

TABLE OF CONTENTS (Cont'd.)

LIST OF FIGURES

LIST OF FIGURES (Cont'd.)

LIST OF FIGURES (Cont'd.)

LIST OF FIGURES (Cont'd.)

LIST OF TABLES

SENSORY MECHANISM MODELING

1.0 INTRODUCTION

Reliance on aircraft simulation, both for pilot training and experimentation, is expanding rapidly. There exists a need to learn more about human sensory systems in order to discover what motion cues are important for training, face validity, and manual control research in a simulation, and how best to provide them. Current motion cueing systems, for instance, often emphasize matching simulator motion with aircraft motion and use "washout" logic to keep motion within hardware limitations. Although physiological thresholds and sensitive frequencies are sometimes considered, the special characteristics of the pilot's sensory system are not used to full advantage. Utilization of these characteristics may result in more effective simulations, but will require some understanding of how the various sensors interact to produce a certain overall sensation of orientation and motion. The purpose of this sensory mechanism modeling project is to further the understanding of multi-sensory integration in spatial orientation, and to aid in its application to simulator requirements.

Currently the "fidelity," or realism, of a simulated maneuver is evaluated either by subjective pilot opinion, or by comparing aircraft specific forces, accelerations, visual field motions, and tactile forces, with those produced by the simulator. In our view, the appropriate comparison should be between the pilot's perception of motion in the simulator and aircraft, rather than between the simulator and aircraft motions themselves. Figure 1.1 shows a scheme that uses sensory system models to compare perception in the simulator to that which would be produced in the aircraft. Several elements shown in this block diagram are under the control of the simulator designer and user, including, for example, the limits on a motion drive and the logic used to control it in conjunction with visual and tactile cues. In order to specify these for sufficient simulator fidelity, however, the block labelled "Motion Sensing Model of Pilot" must be developed. That development is the subject of this research.

In addition to the model development, a number of important ancillary issues are raised. For example, how much realism, or fidelity, is necessary for a given purpose, such as pilot training or aircraft handling quality evaluation? What is the least amount of simulator motion

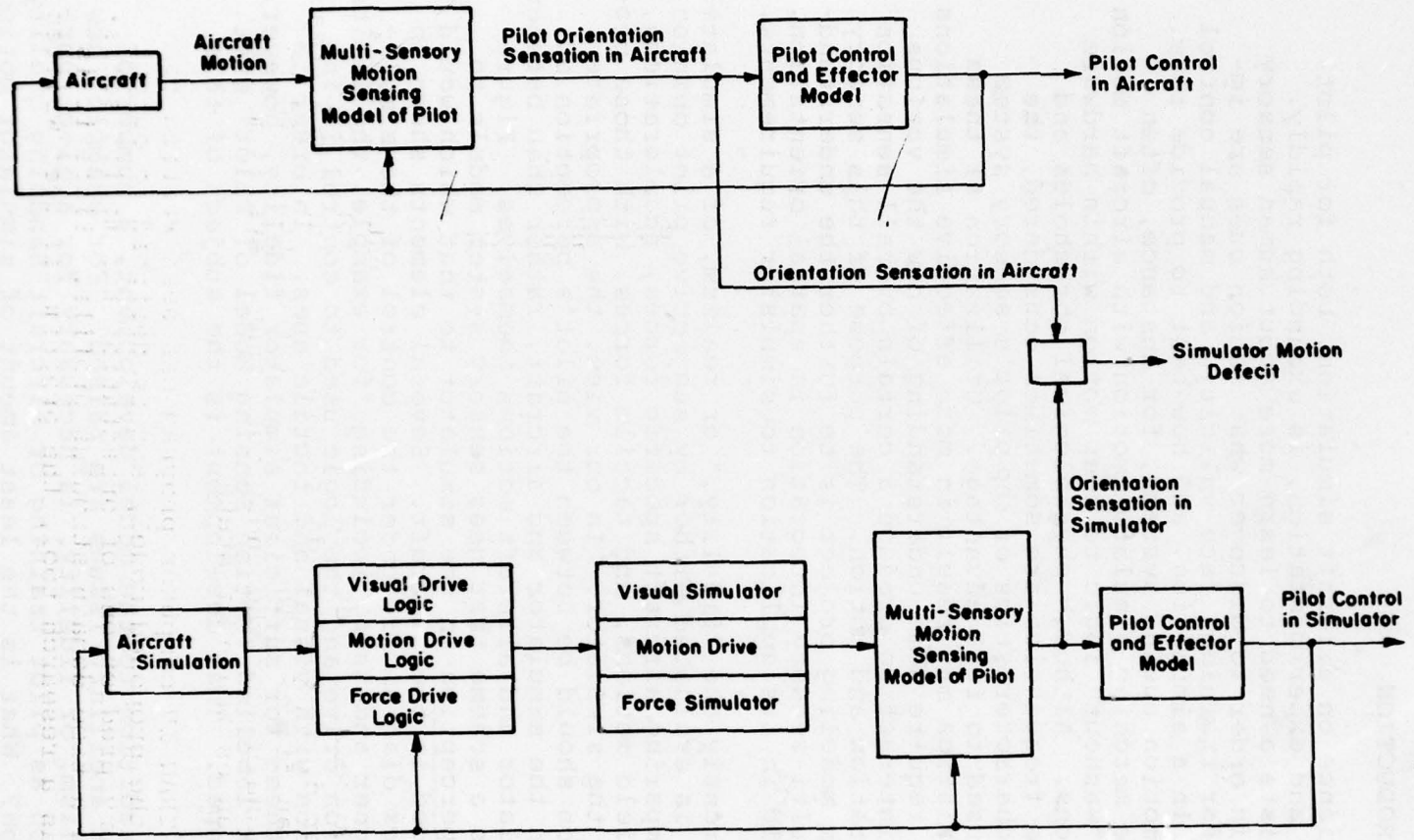

Figure 1.1 Comparison of sensation in real aircraft and simulator based on pilot Sensory Mechanism Models.

necessary to achieve a given degree of fidelity? How much simulator motion can be "traded" for more compelling visual scene displays, more elaborate tactile force devices, etc? All of these questions demand a greater understanding of the underlying sensory mechanisms, and the overall affect of multisensory stimulation.

1.1 Summary

The specific objective of the work described by this report has been to create a unified, or composite, model for motion and orientation perception able to integrate four sensory modalities: vestibular, visual, proprioceptive, and tactile. Theoretical models for nearly all the individual sensor systems exist in the literature, based on varying amounts of data, and in the case of the vestibular and visual systems interaction between modalities has been studied as well. Data relating mechanoreceptor function to perceived motion and orientation is relatively sparse, and a computer literature search has been conducted to identify available information in this area. Although there are many gaps in our knowledge of all sensory modes, it is felt that there is now enough information to warrant a first attempt at a unified perception model with the goal of making reasonable predictions of subjective orientation.

The biological central processor, charged with integrating information from various sensors, may have evolved to perform something akin to an optimal estimation process. Under certain linearity and noise spectrum assumptions, the least mean squared error estimator is the well known Kalman filter. Although nonlinear processes may also play a part, it was decided to model integration of the various information channels with a Kalman filter blending approach.

An internal model, representing the central processor's view of the relation between biological sensors and the outside world, is used to derive optimal gains for a steady-state Kalman filter. The Kalman filter is then used to process signals from the individual sensor system models, producing an estimate of state.

A FORTRAN IV computer program has been written to implement the proposed model, and is designed to output time history predictions of orientation and motion sensation given a time domain stimulus profile. Since it is intended as a research tool, the program has been written

in as flexible a form as possible allowing the model structure to be changed or adjusted easily.

Employing only vestibular sensor components (semicircular canals and otoliths), the model has been exercised with yaw step acceleration, linear step acceleration, and with rapid pitch to a constant pitch angle. All stimuli were above threshold levels and threshold effects have not yet been considered. Initial results appear quite promising and are qualitatively consistent with psychophysical data. In the case of yaw step acceleration, which stimulates only the semicircular canals, the model predicts an initially accurate perception of yaw velocity, which then levels off and decays. The time course is consistent with experimental data. The step in forward linear acceleration is "felt" by the model as an initial acceleration which rapidly decays and is replaced by a pitched-back sensation. This phenomena is well known during aircraft catapult launches. When the stimulus is a true pitch-back, the same steady-state perception results, but the time course of perceived pitch orientation closely follows true pitch orientation. The change in specific force direction is no longer felt as a large initial acceleration. This is also consistent with known human responses.

Model exercise up to this point, although encouraging, has been very preliminary. Additional work is needed to test threshold phenomena and to match quantitative model responses with psychophysical data. Model parameters probably will need to be adjusted or "tuned" so that response time constants and magnitudes fit experimental data as closely as possible. As of this writing, interaction of visual, tactile and proprioceptive sensors with the semicircular canals and otoliths has not been tested. Work is ongoing to implement these additional modalities and to make any model modifications indicated by the results.

1.2 Report Organization

This report is divided into six sections. Section 2.0 describes a computer literature search for mechanoreceptor data. The references generated by the search are listed, by categories, in Appendix A.

Section 3.0 details pertinent knowledge about each of the four sensory modalities under consideration, and presents our modeling approach to each individual sensor system. The modalities being considered are: visual, vestibular, tactile and proprioceptive.

Section 4.0 is devoted to the unified model. First, three previous models that integrate two or more sensory modalities are described very briefly (Section 4.1). Next, our approach to the current effort is discussed (Section 4.2), followed by a detailed description of the proposed "unified model" (Section 4.3).

Section 5.0 presents and discusses results so far obtained from a computer implementation of the model. System matrices and parameters used to generate these results are listed in Appendix B. Conclusions appear in Section 6.0.

2.0 LITERATURE SEARCH

A computer literature search was conducted to identify available material in the area of neural mechanoreceptor systems. The NASIC service was used to search three files: MEDLINE (Index Medicus), NTIS (Government reports), and PSYCHABS (Psychological Abstracts). In addition to these sources the Defense Documentation Center (DDC) service was employed.

Some of the key words used in the searches were:

Perceptual Orientation
Space perception
Space orientation
Kinesthetic perception
Cutaneous Sense
Proprioception
Tactile
Haptic
Vibrotactile
Mechanoreceptor
Pacini corpuscles
Golgi and Mazzoni corpuscles
Neuromuscular spindles

The descriptive paragraph sent to the DDC was:

"We are searching for literature describing human mechanoreceptor systems and the perceptions (sensations) caused by stimulation of mechanoreceptors. We are especially interested in models relating mechanical stimulation to resulting perception, or to afferent nerve responses from tactile and proprioceptive receptors. Of even more specific interest is work relating sensation of motion and orientation to mechanoreceptor stimulation. The heading 'Mechanoreceptor' may include such subheadings as cutaneous sensors, tactile receptor, proprioceptor, haptic sensor, deep pressure sensor; or more specifically Pacini corpuscle, Mazzoni corpuscle, Iggo corpuscles, muscle spindle, Golgi tendon organ, neuromuscular spindles, etc."

Table 2.1 specifies the total number of references generated by each search and the number of references considered pertinent after inspection (in the latter category duplicate references are counted only for the first index in which they were found). Copies of pertinent references were obtained and organized by category (see Table 2.2). Table 2.2 includes secondary references cited by other articles. All references generated by this search are listed by categories in Appendix A.

COMPUTER LITERATURE SEARCHES

INDEX	TOTAL REFERENCES GENERATED	PERTINENT REFERENCES GENERATED
MEDLINE	133	16
PSYCHABS	258	10
NTIS	264	7
DDC	14	2
TOTAL	669	35

TABLE 2.1

CLASSIFICATION OF MECHANORECEPTOR LITERATURE

	NO. OF ARTICLES
TACTILE SENSOR SYSTEMS	
- NEUROPHYSIOLOGY	21
- PSYCHOPHYSICS	12
- NEUROPHYSIOLOGY & PSYCHOPHYSICS	1
PROPRIOCEPTIVE SENSOR SYSTEMS	
- NEUROPHYSIOLOGY	11
- PSYCHOPHYSICS	1
GENERAL MECHANORECEPTOR MODELS & PHYSIOLOGY	2
TOTAL	48

TABLE 2.2

3.0 SENSOR SUBSYSTEMS

3.1 Visual System

3.1.1 Scope of the Visual Cues Considered

Of the wide variety of visual cues available to the pilot in simulation this section considers only one aspect, namely the sensation of continuous motion, or of steady pitch or roll angle, induced by the movement of a large field visual scene. It specifically excludes two large and important classes of visual cues. One is information available to the pilot on his display instruments, such as the artificial horizon or rate of turn indicator. The other is information from specific external visual field structure, such as an horizon.

Sufficient attention has been devoted to the instrument flight rules (IFR) case in the manual control literature that one can safely assume that those models are valid for perception of movement. Specifically, the pilot is assumed able to perceive, with a processing time of the order of 100 to 300 msecs, each state variable explicitly displayed on a dial or other indicator, and its first derivative. The approximate observation noises associated with these indications is 20 db below the signal level (Curry, Hoffman & Young, 1976; Kleinman, Baron, & Levison, 1970).

The visual cues considered in this section are limited to out the window visual scenes as provided in an aircraft or in a wide field visual scene flight simulator. They do not, however, include any elements in the structure of the scene such as recognizable landmarks, orientation cues, or even the horizon line. The descriptions are limited to the peripheral motion cues which are equivalent to the passage of stars or clouds in a wide field simulation.

3.1.2 Characteristics of Vection

The visually induced effects on orientation and motion perception are referred to in general as "vection," with circularvection referring to visually induced motion in yaw and linearvection referring to visually induced translatory motion. The common experience of linearvection is the illusion of moving backwards while actually stationary when the adjacent train in a station begins to slowly move forward, or when the neighboring car at a stop light begins to

creep forward. Circularvection, or a sustained sensation of yaw rate when the entire visual field rotates about a vertical axis, is somewhat less common but is experienced by many in 360° motion picture theaters, and especially in good wide field visual simulators. Least well known of all are the phenomena of visually induced pitch or roll resulting from a steady pitch or roll rate of the entire visual surround. The interest in these phenonena has increased markedly over the past five years resulting in a great deal of quantitative data on all forms of vection, and attempts to understand the interaction between visually induced motion and vestibular responses. Some general facts can be summarized as they apply to all forms of visually induced motion:

1. The peripheral, rather than the central visual fields, must be stimulated.

2. Background stimulation is more important than foreground stimulation.

3. Up to a certain spatial frequency, the increase in the number of clearly defined moving borders enhances the onset and magnitude of the vection.

4. The visually induced effect is proportional to the stimulus velocity up to a saturation velocity.

5. The time delay to onset of visually induced motion is highly variable, both among individuals and for any one individual.

6. Brief vestibular cues in the appropriate direction hasten the onset of visually induced motion and those in the conflicting direction delay its onset.

7. Continuous constant velocity stimulation results in a slight long term adaptation in the effect and in occasional losses of the visual effect, possibly correlated with eye movements.

8. The visually induced motion effect is, in most respects, identical to that produced by the vestibular stimulation with the exception that no sensation of acceleration or deceleration is felt to accompany the observed changes in velocity.

9. The frequency response of visually induced motion effects depends upon the predictability of the signal; it is wider band for predictable than for random motions.

10. The approximate frequency response for each of the modes tested is modeled by a first-order low-pass filter with break frequency at 0.1 Hz.

3.1.3 Dynamic Model for Vection

For the purposes of the Kalman filter model, it would be desirable to have a model of the visually induced motion effects obtained in the absence of any vestibular stimulation. This would be apparently analogous to the vestibular models obtained for rotation in the dark. Unfortunately, experiments on visually induced motion in the absence of any vestibular information cannot be performed on normal subjects possessing a functioning vestibular system. Simply stated, either the vestibular system will yield signals confirming the direction of visually induced motion, as when a cab is rotated relative to a stationary surround, or, in the absence of any vestibular stimulation, the semicircular canal and otolith cues will indicate that the subject is not accelerating or changing orientation with respect to gravity, which is a signal in direct conflict with the visually induced motion sets. Therefore, we are left in somewhat of a quandary since the Kalman filter itself should lead to the development of the appropriate strategy for visual-vestibular interaction and yet each of the psychophysical experiments upon which the model is developed involves vestibular cues which either confirm or conflict with visual field motion. Finally, to complicate matters even further, the development of visually induced motion effects is a very strong function of the mental set of the subject. Having frequently experienced true motion or visually induced motion, and being placed in the situation in which such motion seems possible (as for example in a movable trainer), the onset and strength of the visually induced motion is enhanced.

The rationale for picking a low-pass filter with break frequency at 0.1 Hz stems from both linearvection and circularvection experiments with sinusoidal random input stimuli, and from time domain recordings of the development of circularvection or linearvection following a step change in field velocity. In the latter case as shown in Figure 3.1 for circularvection and Figure 3.2 for linearvection,

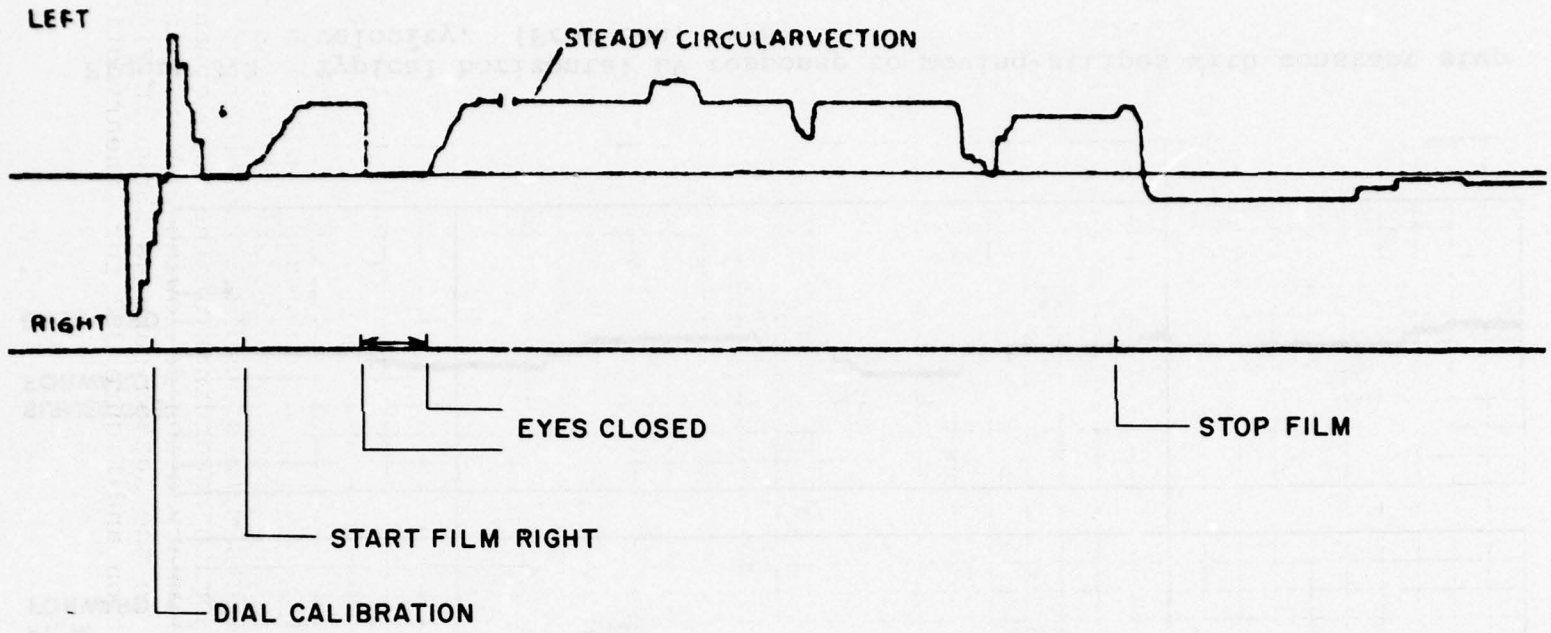

Figure 3.1 Typical recording of magnitude estimation showing dial calibration, onset of circularvection, waxing and waning of circularvection with trainer stationary, outlasting circularvection following stopping of film, and long lasting aftereffect in opposite direction (after Young, et. al., 1973).

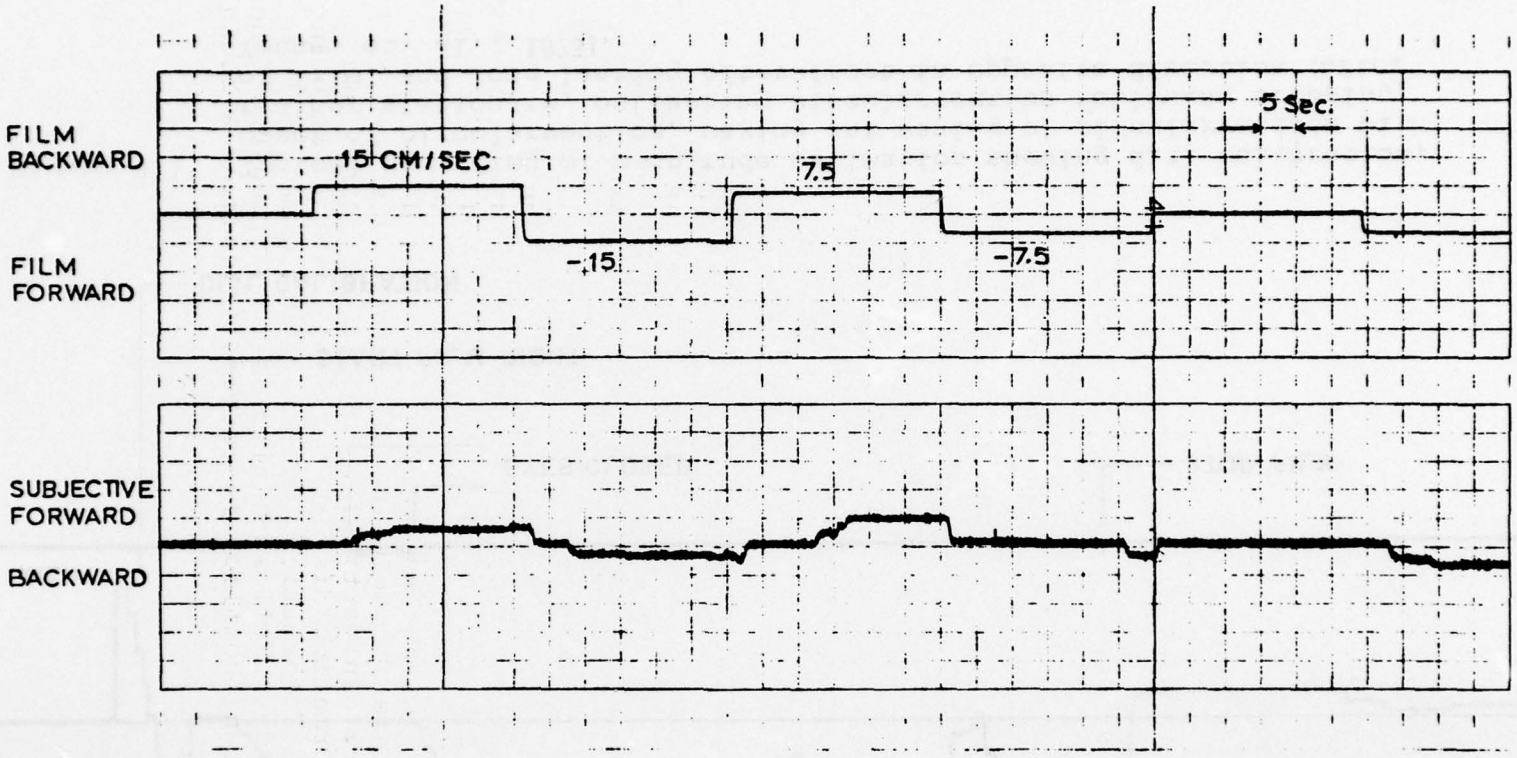

Figure 3.2 Typical horizontal LV response to moving stripes with constant step velocity. (From Chu, 1976)

after the delay in onset, the sensation rises rapidly in an almost exponential fashion to its final value in a period of usually 3 to 5 seconds, consistent with a first-order system having a time constant of approximately 1.5 seconds. In the case of vertical linearvection with a stationary cab, we have shown that the amplitude ratio and phase lag of self-induced velocity as a function of field velocity breaks at approximately 0.1 Hz but that this break is more noticeable and the amplitude ratio decreases more markedly when the input is a random signal as would typically be the case in most flight simulation conditions. Figures 3.3 and 3.4 from Chu, (1976) show these frequency responses for the linearvection case. In the case of circularvection, or rotation about a yaw axis, similar measurements were taken under conditions in which the cab was actually moved but subject to a vestibular simulation which was independent of the visual field motion. Measurements of the describing function between visual input velocity, vestibular stimulus velocity, and the presumed perception of velocity, as reflected in the subject's control stick motions to zero the cab velocity, yielded the manual control frequency responses shown in Figure 3.5 from Zacharias and Young (1977). Some adaptation to prolonged stimulation is also evident in the linearvection experiments of Bertoz et al (1975), in which it was seen that during prolonged stimulation the subject requires ever increasing field velocities to maintain a perception of constant linear velocity. It was felt that the long term adaptation associated with time constants on the order of a minute or more is not required for the initial modeling effort.

Although the basic model used in this contract is a linear Kalman filter model, it should be pointed out that certain success has been achieved in modeling visual interactions with a nonlinear "cue conflict model" in which certain sensory channels are in effect turned off when their outputs are strongly in disagreement with those of other channels. In particular, when short term visual transient information disagrees strongly with vestibular induced motion information, the visual information is largely discarded until such time as the strength of the vestibular-visual conflict is reduced (Zacharias & Young, 1977).

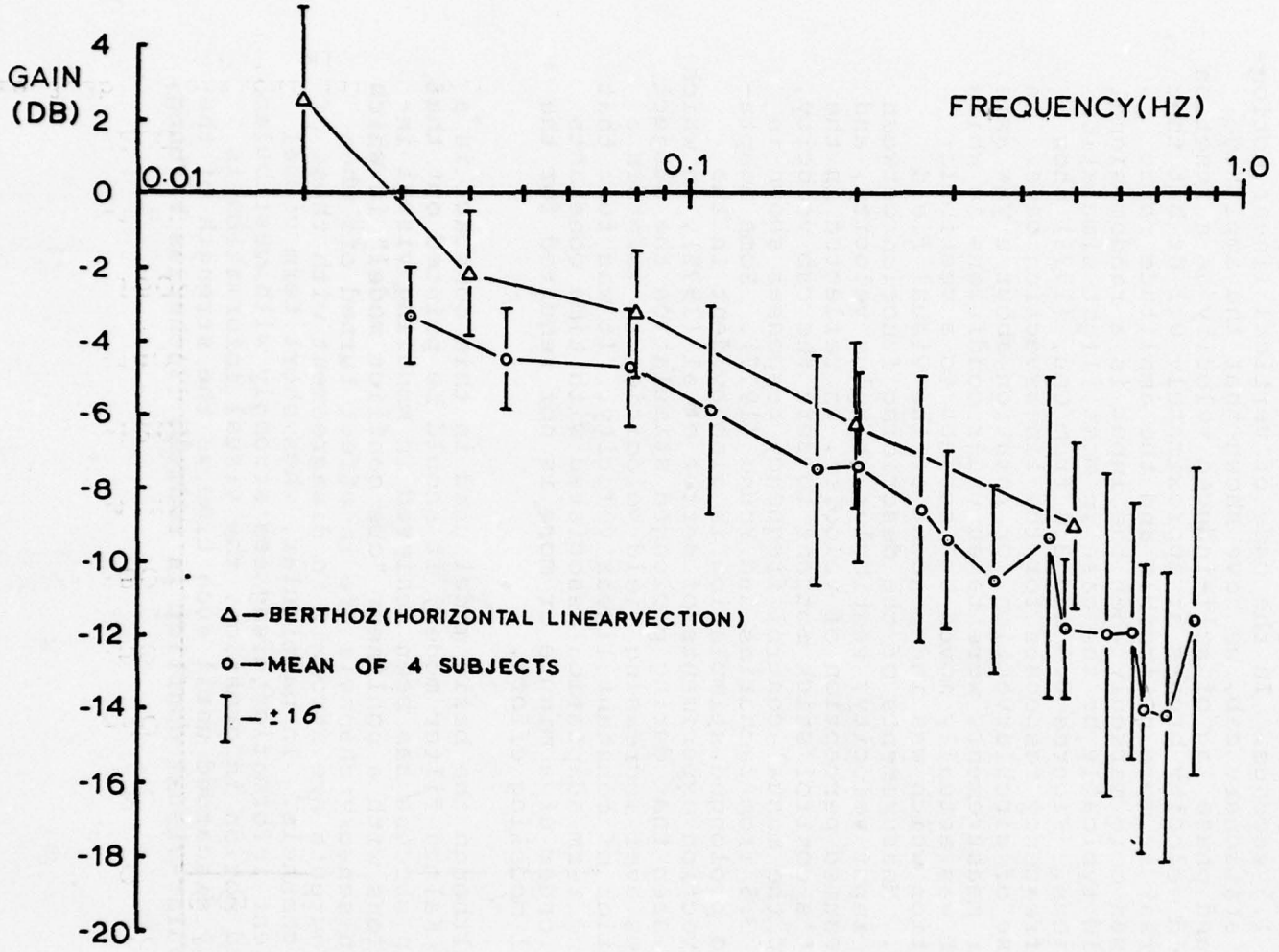

77339

Figure 3.3a Vertical linearvection: frequency response to moving stripes with sinusoidal velocity; gain vs. frequency. (From Chu, 1976)

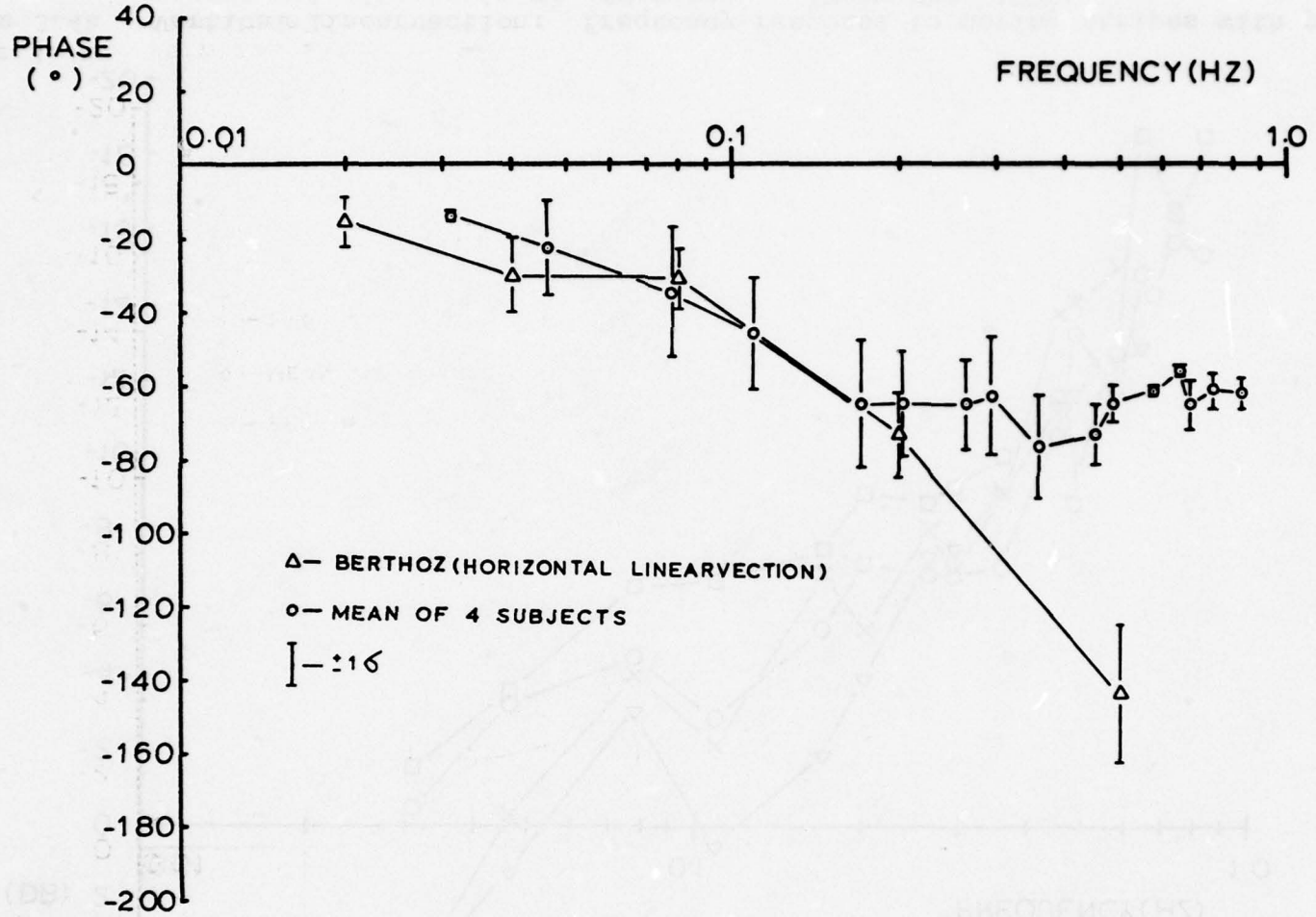

Figure 3.3b Vertical linearvection: frequency response to moving stripes with sinusoidal velocity; phase vs. frequency. (From Chu, 1976)

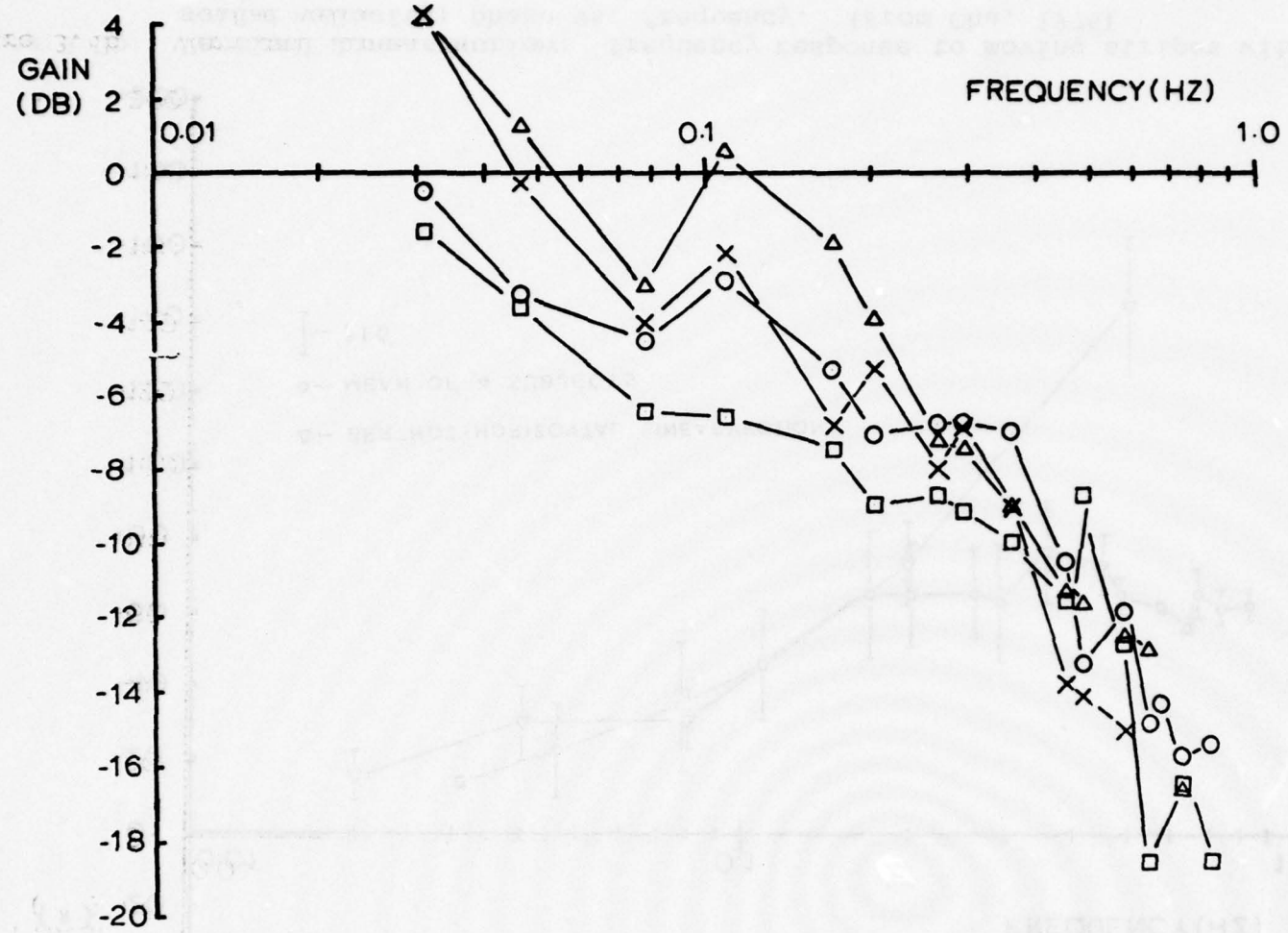

Figure 3.4a Vertical linearvection: frequency response to moving stripes with pseudo-random velocity; gain vs. frequency. (From Chu, 1976)

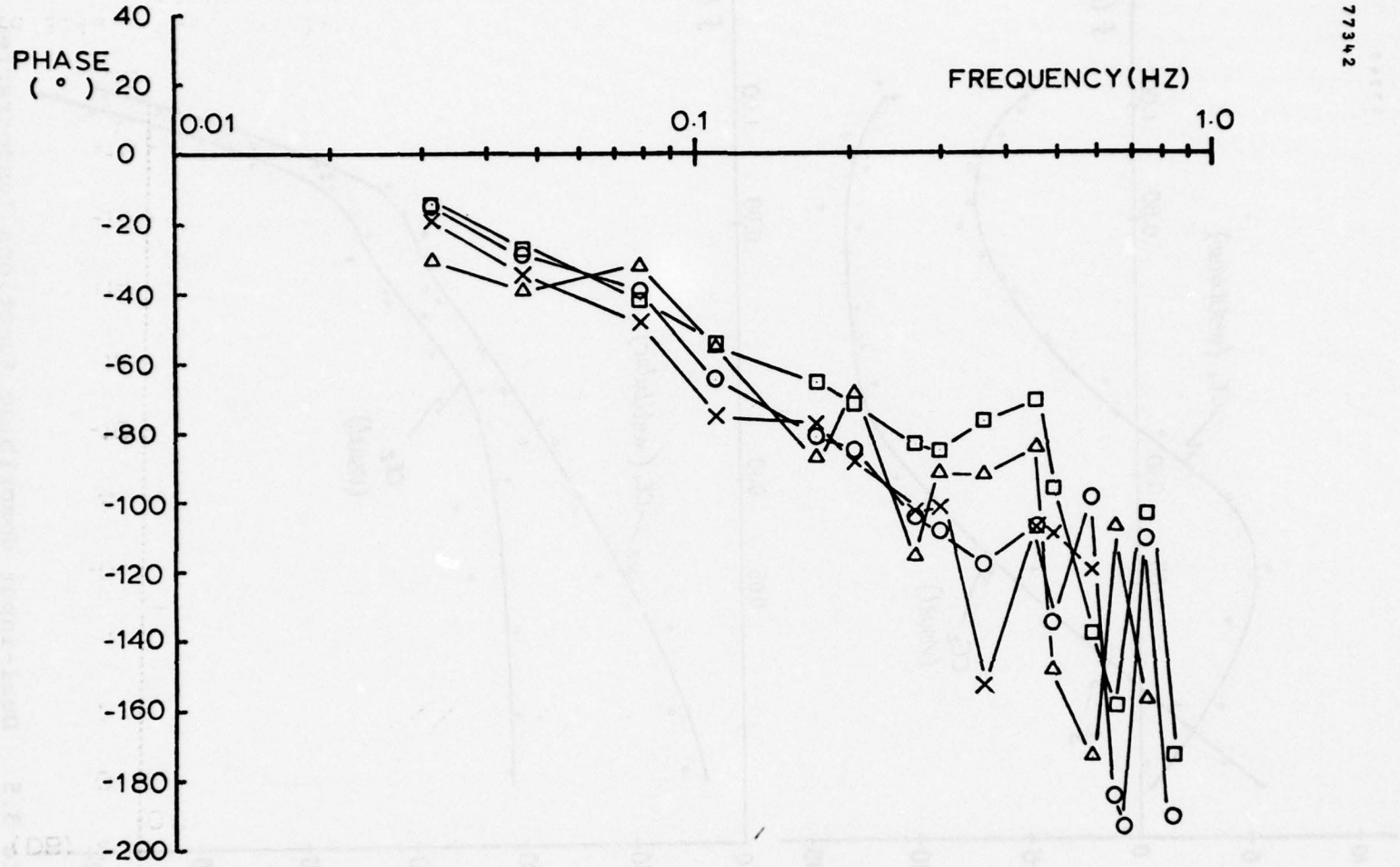

Figure 3.4b Vertical linearvection: frequency response to moving stripes with pseudo-random velocity; phase vs. frequency (from Chu, 1976)

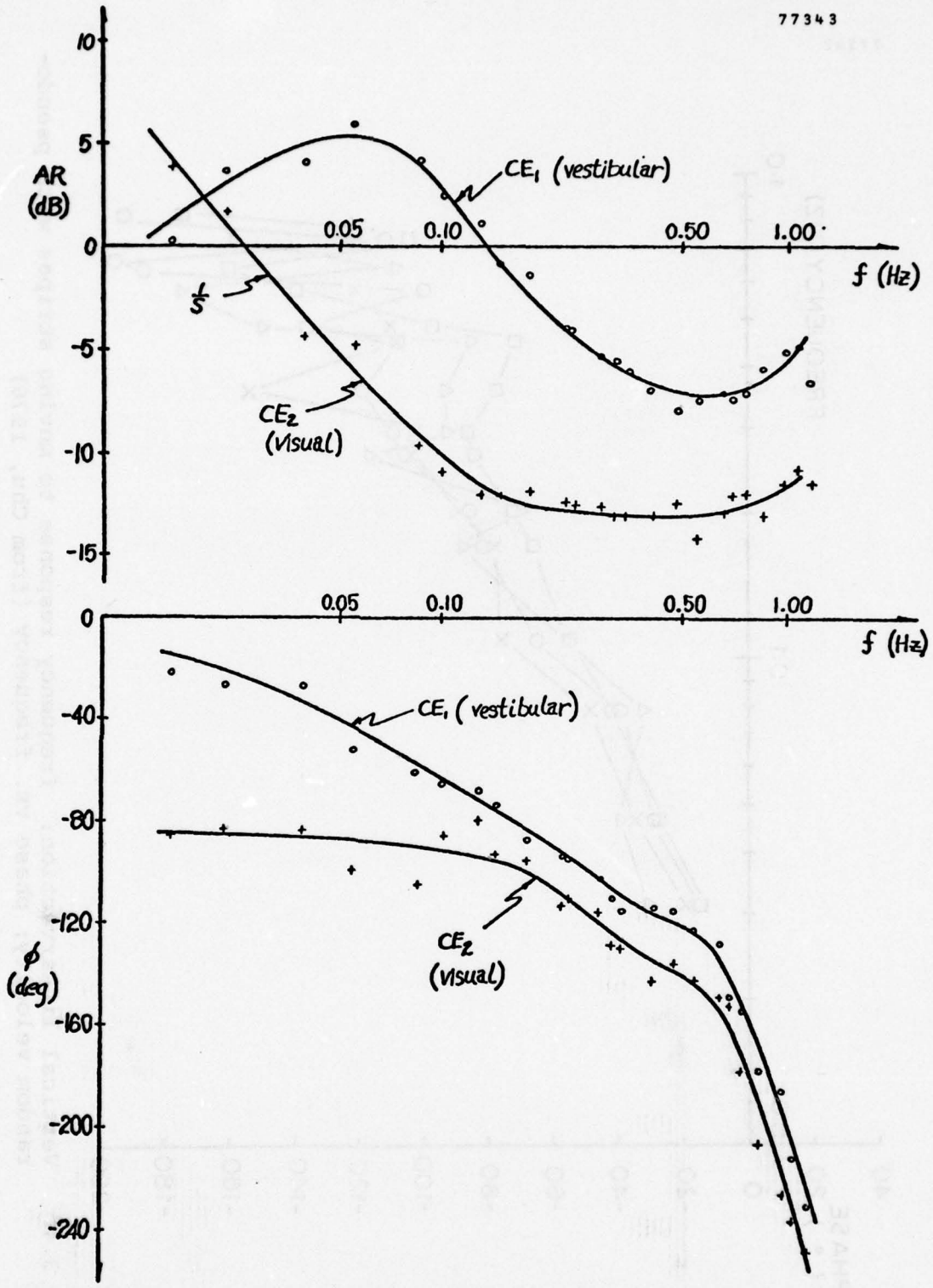

Figure 3.5 Dual-input describing functions (uncorrected for operator dynamics) (from Zacharias, 1977).

3.1.4 Electrophysiological Measures

The psychophysical measures reviewed above are more reliable, for the purposes of modeling at the present time, than are any physiological measures associated with vection. Although eye movement records, and especially nystagmus velocity, provides a convenient measure, highly correlated with circularvection, the functional relationship between the two is far from clear. At the electrophysiological level, single unit recordings at various sites in the brain stem and cerebellum have been shown to be influenced by visual field velocity. In particular, evidence is rapidly accumulating to implicate the vestibular nucleus as a site at which body rotation signals from various sensory modalities are represented, and perhaps integrated (see Henn et. al., 1974; Dichgans et. al., 1973; Thomsen, 1976). However, the case is not yet made that these signals represent the visual input to vection and, therefore, the modeling effort will remain primarily based on the magnitude estimate data.

3.2 Vestibular System

The vestibular system resides in a labyrinthine structure behind the auditory portion of the ear. It is composed of a set of rotation sensing organs known as the semicircular canals and a set of specific force sensors called the otoliths. These organs have been studied extensively over many years and are the most well-defined of the four sensory systems under consideration.

3.2.1 Semicircular Canals

The semicircular canal model used for this work closely follows the model for canal afferent firing rate used by Ormsby (1974) and relies heavily on work by Young and Oman (1969) and Goldberg and Fernandez (1971). The two sets of canals are replaced by a single Cyclopean set of three canals with sensitive axes oriented as shown in Figure 3.6.

The response of each canal along its sensitive axis is modeled as a highly overdamped torsion pendulum with added afferent processing. The resulting transfer function is shown below.

77344

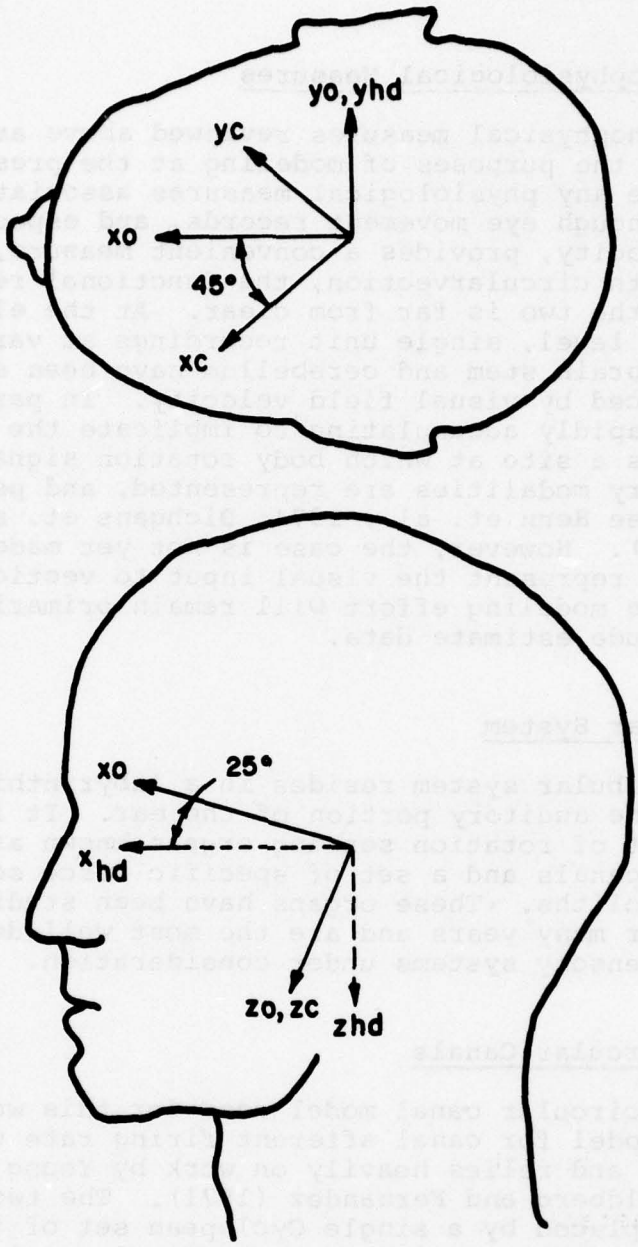

HEAD COORDINATES ≡ (xhd , yhd , zhd)

CANAL COORDINATES ≡ (xc , yc , zc)

OTOLITH COORDINATES ≡ (xo , yo , zo)

Figure 3.6 Cyclopian Sensor Coordinates

$$\frac{AFR}{\alpha} = (.574)\ \underbrace{\frac{1}{(s+1)(s+200)}}_{\text{torsion pend.}}\ \underbrace{\frac{s}{(s+.0333)}}_{\text{adaptation}}\ \underbrace{(s+100)}_{\substack{\text{rate}\\ \text{sensitivity}}} \qquad (3.1)$$

where AFR = afferent firing rate

α = angular acceleration

This differs from Ormsby's model only in that Ormsby's 18-second torsion pendulum time constant has been changed to 10 seconds in order to match more recent information, and a .005-second time constant from the torsion pendulum model has been omitted. It is not anticipated that there will be a need to use the model at iteration intervals of much less than .1 seconds and the .005-second time constant would, therefore, be invisible.

The absolute canal threshold is usually taken as the acceleration step which a subject has a 75% probability of detecting. Above absolute threshold, detection latency is a function of angular acceleration magnitude. Figure 3.7 shows response latency as a function of angular acceleration. This curve can be fit with the equation

$$\alpha(T - T_r) = k_\omega \qquad (3.2)$$

where α = angular acceleration

T = response latency

T_r = reaction time

k_ω = constant

k_ω has units of angular velocity and is approximately 2° per second. Thus, an angular acceleration below absolute threshold will never be felt while an acceleration above absolute threshold will be felt only after angular velocity reaches k_ω.

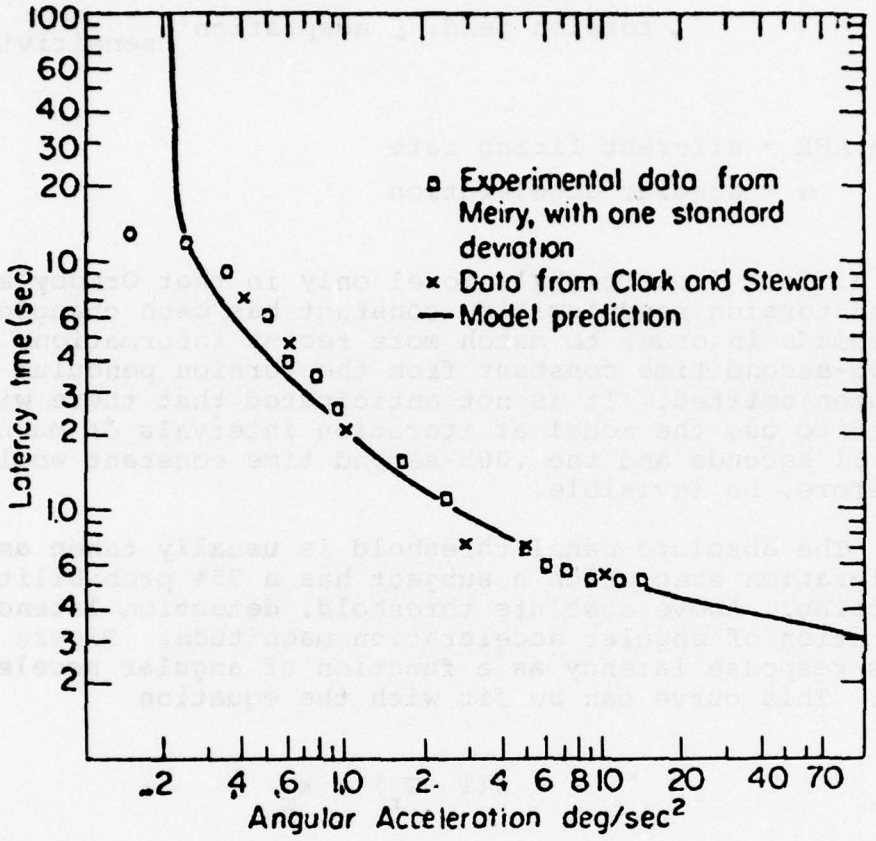

Figure 3.7 Adaptation model for subjective response latency to constant angular acceleration. (From Young & Oman, 1969) (Used with permission of Aerospace Medical Association.)

The velocity threshold is usually the most important one, and the overdamped quality of Equation 3.1 allows ω to be associated with an afferent firing rate. Threshold has, therefore, been modeled as shown in Figure 3.8. TH_C in Figure 3.8 is the afferent firing rate reached during a 10°/sec angular acceleration step after .2 seconds (i.e., when angular velocity reaches 2°/sec).

3.2.2 Otoliths

The otoliths are modeled using Ormsby's Cyclopean system of coordinates shown in Figure 3.6. The xo and yo axes represent the utricular otolith, while the zo axis represents the saccular otolith. Response dynamics along each sensitive axis are modeled as an accelerometer with added rate senstivity presumably due to neural processing.

The transfer function used by Ormsby (1974) is

$$\frac{AFR}{sf} = \frac{18000(s + .1)}{(s + .2)(s + 200)} \qquad (3.3)$$

AFR = afferent firing rate

sf = specific force

This differs from a model proposed by Young and Meiry in 1968, in that the pole at 200 rad/sec in Equation 3.3 appears at 1.5 rad/sec in the Young and Meiry model.

Fernandez and Goldberg (1976) recorded from squirrel monkey otolith afferents and found that they could divide units into two populations based on the regularity (i.e., coefficient of variation) of discharge rate. Regular units (coefficient of variation < .075) represented approximately 70% of the sample, irregular units (coefficient of variation > .15) represented approximately 25% of the sample and the remaining units were not clearly defined.

Figure 3.9 shows amplitude ratio Bode plots of the regular and irregular units found by Fernandez and Goldberg, and also plots the Ormsby, and Young and Meiry models. Comparison with the Goldberg and Fernandez data suggests that the 1.5 rad/sec (.24 Hz) pole in the Young and Meiry model

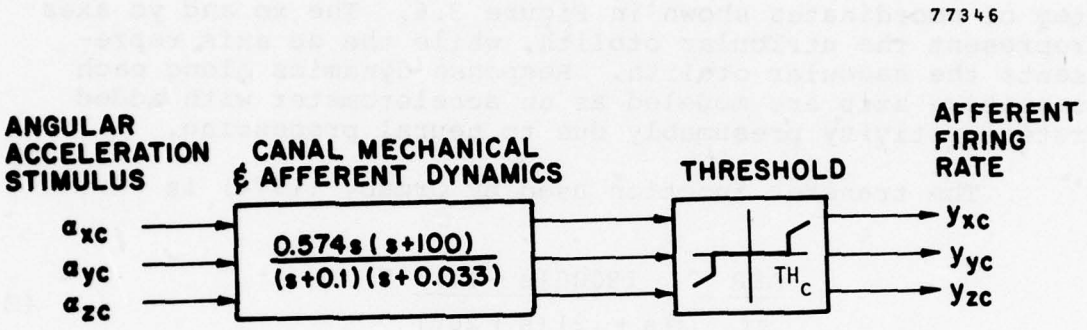

Figure 3.8 Semicircular Canal Model.

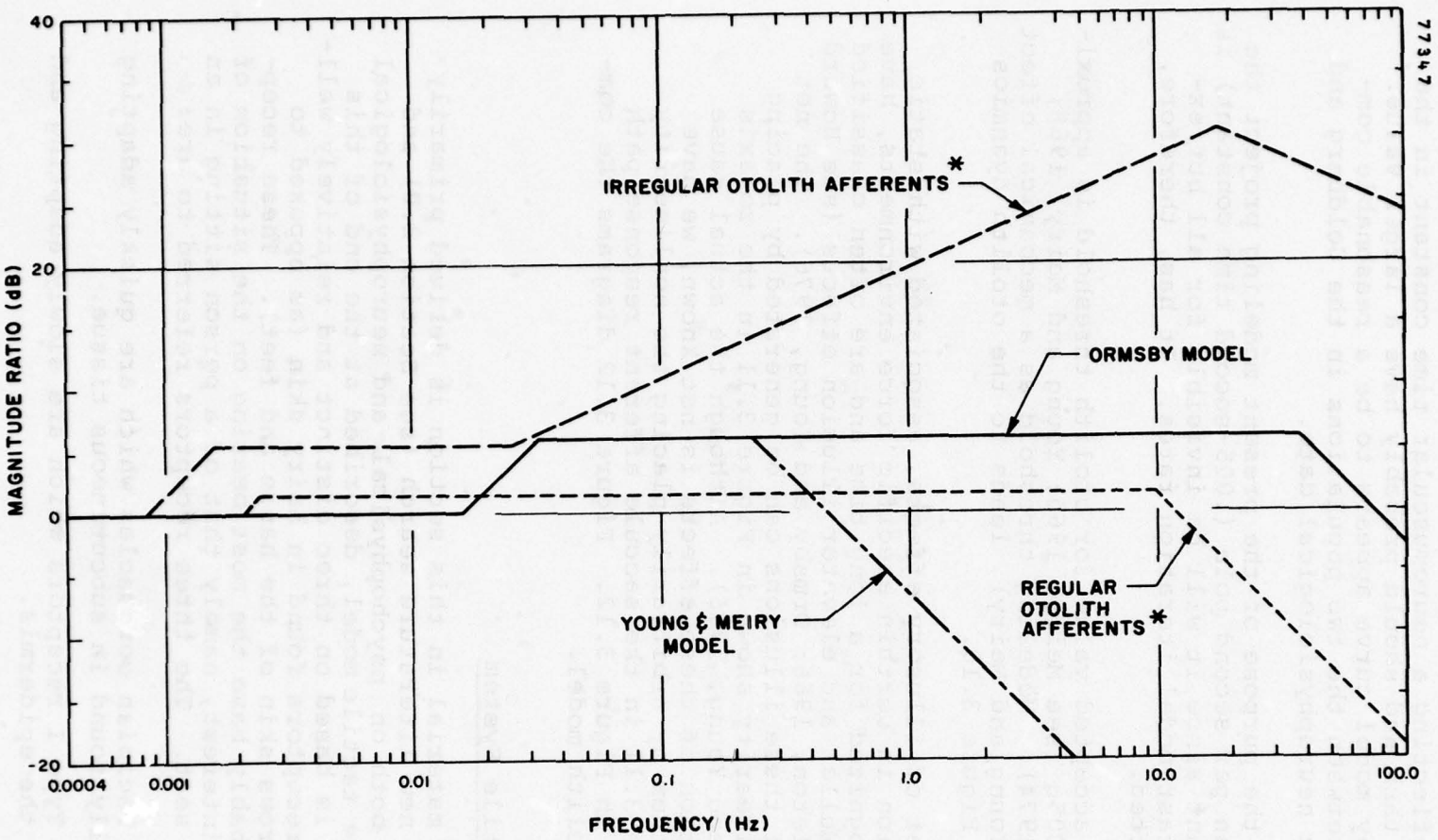

Figure 3.9 Bode Asymptote Plots, Frequency vs. Magnitude Ratio. (Steady state gain has been arbitrarily chosen as unity in all three cases.)

* Plotted using median values from Fernandez and Goldberg's (1976) data.

may be reflecting a neuromuscular time constant in the response task and should probably have a larger value. The Ormsby model curve appears to be a reasonable compromise between the two populations in the Goldberg and Fernandez neurophysiological data.

For the purpose of the present modeling project the 200 radian per second pole (.005-second time constant) is unimportant since it will be invisible for all but extremely fast model iteration rates. It has, therefore, been omitted.

The accepted value for otolith threshold is approximately .005g (see Meiry, 1965; Young and Meiry, 1968; Ormsby, 1974). Modeling threshold as a mechanical effect (as did Young and Meiry), leads to the otolith dyanmics shown in Figure 3.10.

A set of illusory effects, associated with static orientation in certain specific force environments, have been recognized for a long time and are often classified Aubert, Müller and elevator illusion effects (see Howard and Templeton, 1966; Ormsby and Young, 1976). The net effect of these illusions can be generated by placing the nonlinearity shown in Figure 3.11 in the zo axis (Ormsby and Young, 1976). Although the actual cause and location of these effects is not known, we have modeled them by arbitrarily placing the nonlinearity of Figure 3.11 in the saccule afferent response path as shown in Figure 3.12. Figure 3.12 diagrams the complete otolith model.

3.3 Tactile System

The material in this section is derived primarily from the new literature search (see Section 2.0) and is based both on psychophysical and neurophysiological data. The tactile model, described at the end of this section, is based on three distinct and relatively well-defined receptors found in hairy skin (as opposed to the glabrous skin of the hands and feet). These receptors probably have the most bearing on the situation of primary interest, namely that of a person sitting in an aircraft seat. The three receptors referred to are:

1. Pacinian corpuscles which are quickly adapting and usually found in subcutaneous tissue.

2. Type I receptors which are slowly adapting and found in the epidermis.

77348

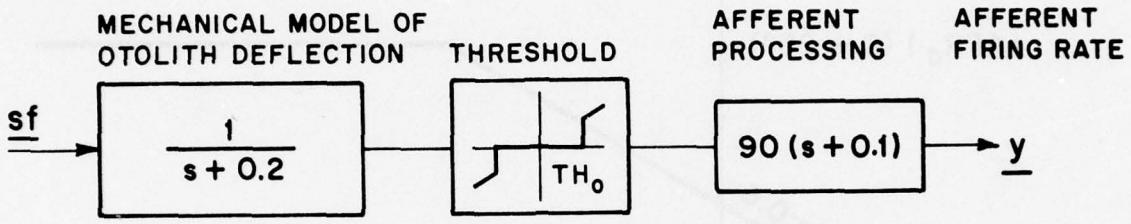

Figure 3.10 Otolith Dynamics.

77349

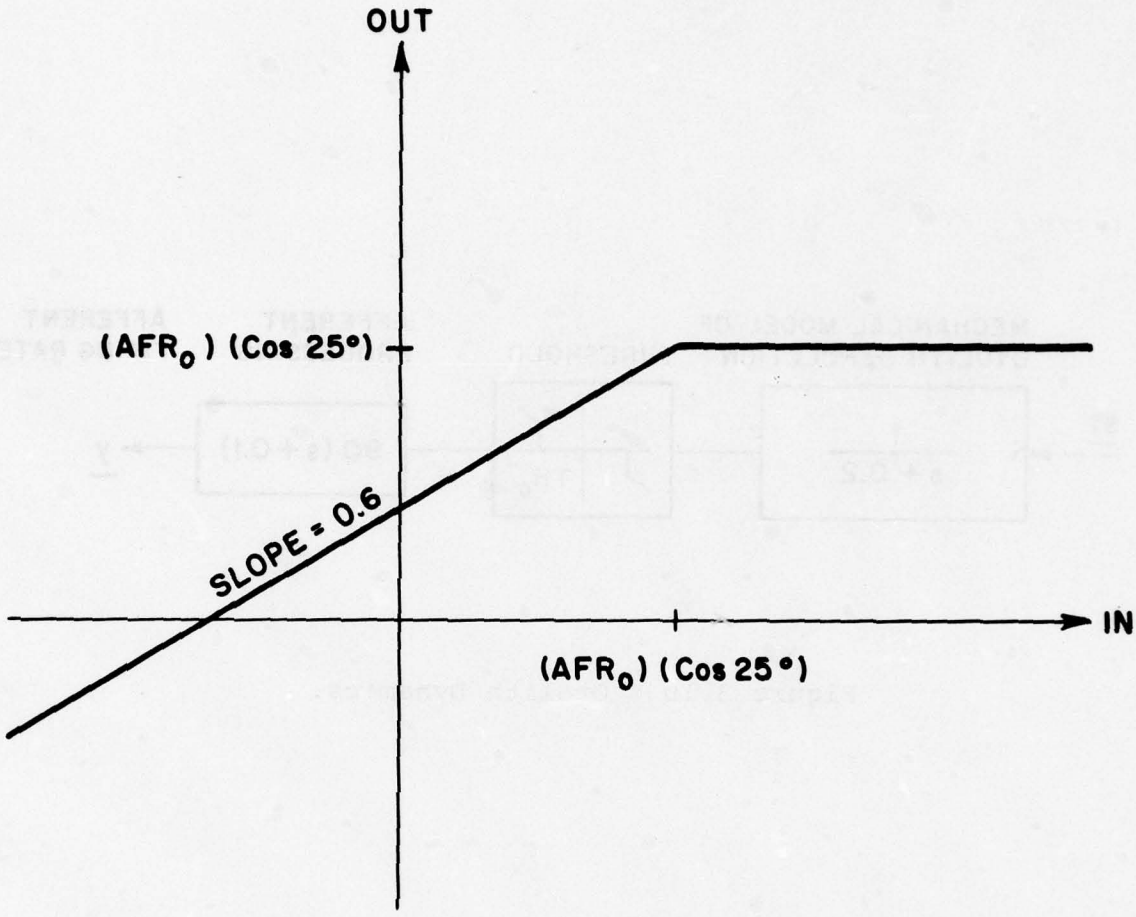

$$AFR_0 \equiv \frac{\text{AFFERENT FIRING RATE}}{g}$$

Figure 3.11 Saccule Non-linearity (redrawn from Ormsby & Young, 1976).

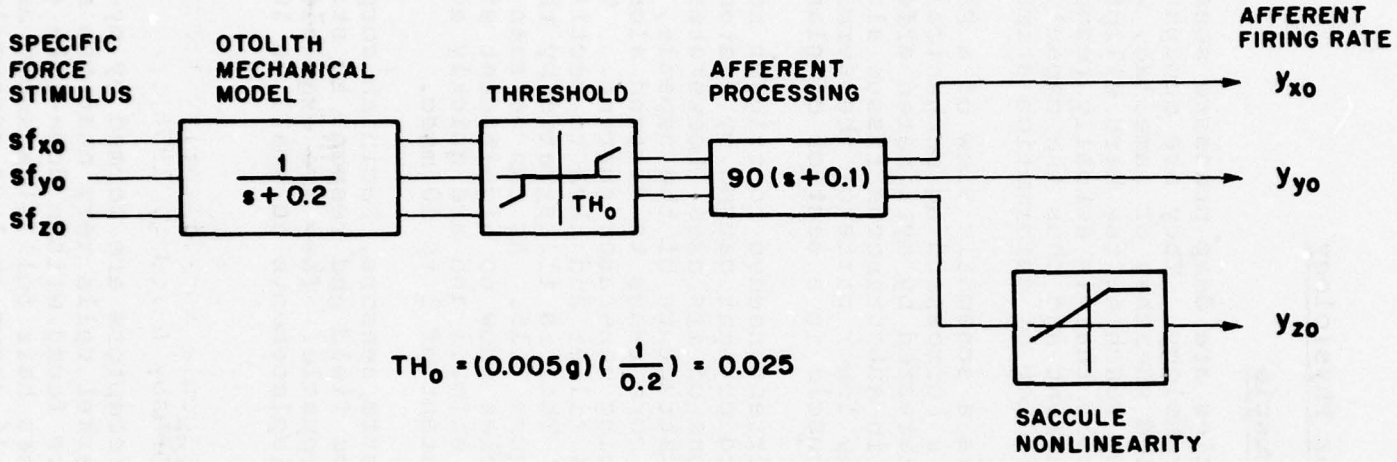

Figure 3.12 Otolith Model.

3. Type II receptors which are also slowly adapting and found in the dermis.

3.3.1 Tactile Receptor Physiology

3.3.1.1 Pacinian Corpuscle

Pacinian corpuscles are deep pressure sensors with a rather distinctive morphology. They are encapsulated by cylindrical fluid-filled sheaths, or lamellae, which prevent static deformation from reaching the hard elliptical core. It is this dendritic core that is actually responsible for producing generator current and thus the capsule acts as a mechanical high-pass filter of deformation stimuli.

Figure 3.13 shows a schematic view of a Pacinian corpuscle, as well as a corresponding mechanical model. The corpuscles are innervated by myelinated afferent fibers and are usually found in subcutaneous tissue although they sometimes appear in the lower parts of the dermis. Figure 3.14 shows such a corpuscle in a section of glabrous skin.

The generator current needed to trigger nerve firing is apparently an inward current caused by distention of the dendritic core along one of its axes (Loewenstein, 1971). Due to the mechanical structure of the capsule, when a pressure is released, the core tends to distend along the orthogonal axis also producing generator current. The net effect is to high-pass filter and then to rectify the actual compression stimulus. This is illustrated by the cellular recording shown in Figure 3.15. As can be seen in Figure 3.15, Pacinian corpuscles show no significant static response to compression stimuli and are quickly adapting, displaying a time constant of 1 to 10 msec.

Being deep pressure sensors, Pacinian corpuscles have a fairly wide receptive field and respond to stimuli not directly above the corpuscle. They are exquisitely sensitive and respond to displacements as small as 10 μm (Loewenstein, 1971).

3.3.1.2 Type I Receptor

Type I tactile receptors are formed by myelinated fibers which end in Merkel cells very near the skin's surface. Merkel cells are found within dome-like elevations of the epidermis between hair follicles known as Iggo corpuscles. Figure 3.16 shows an Iggo corpuscle and a detail of one Merkel cell ending.

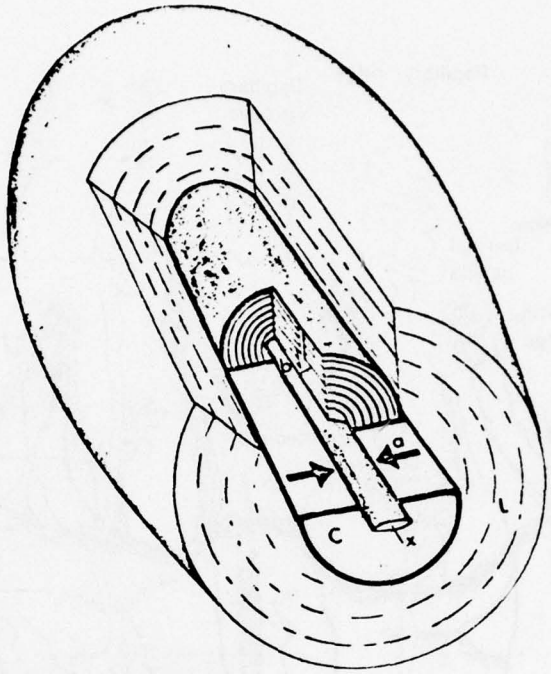

Figure 3.13a Schematic view of a Pacinian corpuscle.

L, outer lamellae; C, core lamellae; the unmyelinated dendrite is at the center. The arrows, b and a, illustrate situations of compression in the plane of the minor and major elliptical axes of the dendrite respectively. (Lowenstein, 1971) (Used with permission of Springer-Verlag.)

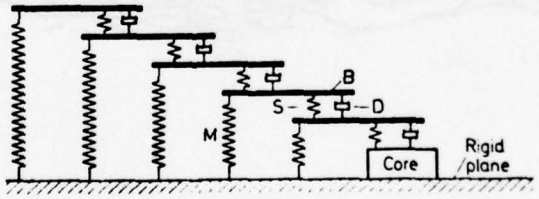

Figure 3.13b. Mechanical model of the corpuscle.

The model incorporates the main structural elements of the capsule: rigid bars B represent the positions of the lamellae; springs M, their compliance; springs S, the compliance of the weak lamellar interconnections; and dashpots D, the resistance of the interlamellar fluid (viscosity of water). (Lowenstein, 1971) (Used with permission of Springer-Verlag.)

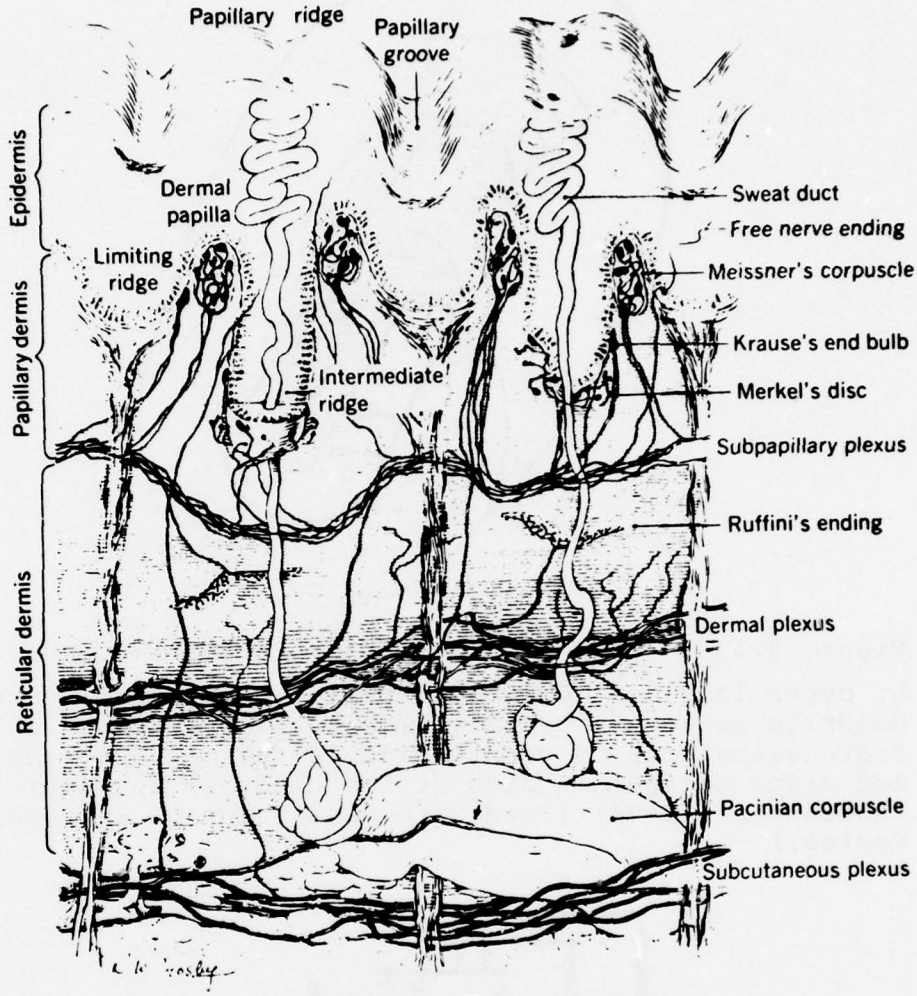

Figure 3.14 Section of glabrous skin. (From Mountcastle, Vernon B.: Sensory receptors and neural encoding: introduction to sensory processes. In Mountcastle, Vernon B., editor: Medical physiology, ed. 13, St. Louis, 1974, The C.V. Mosby Co.; courtesy Dr. M.E. Jabaley.)

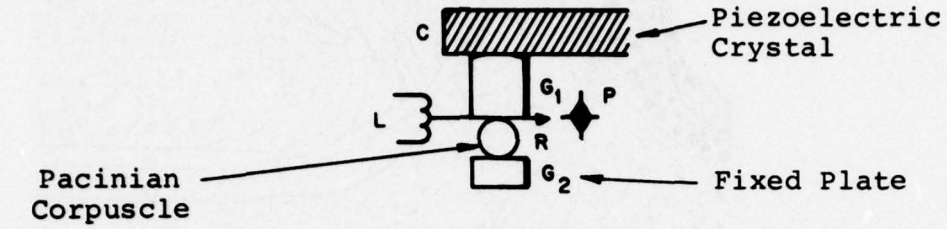

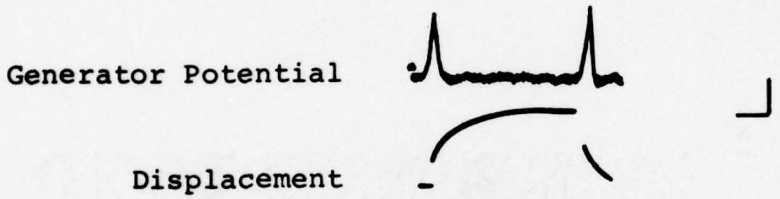

Figure 3.15. Generator potential in response to compressions of intact Pacinian corpuscle. Calibration is 10 msec and 50μv. (From Lowenstein, 1971). (Used with permission of Springer-Verlag.)

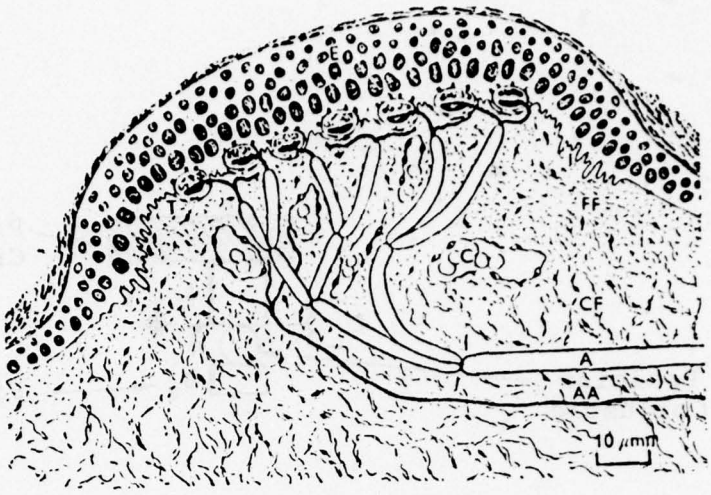

Figure 3.16a. Iggo Corpuscle

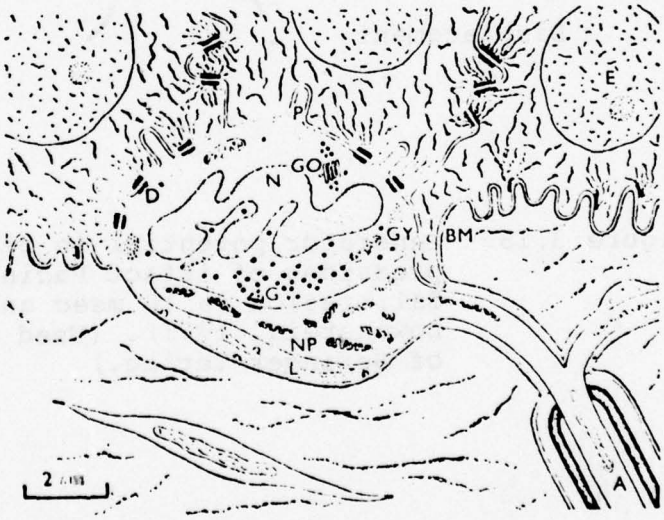

Figure 3.16b. Detail showing merkel cell ending. (From Iggo and Muir, 1969)(Used with permission of The Physiological Society.)

Type I receptors exhibit highly focused receptive fields and respond only to direct stimulation of the touch corpuscle. They respond dynamically to stimuli as small as from 1 to 5 mm of skin displacement. Figures 3.17 and 3.18 show typical time responses to step displacements for Type I afferents. The step response adapts with time constants of about 1 second and 30 seconds. Type I receptors do show a static response but it is characterized by a highly irregular afferent rate. These fibers usually do not exhibit any resting discharge (see Iggo and Muir, 1969).

3.3.1.3 Type II Receptor

Type II receptors are formed by myelinated fibers ending in lightly encapsulated Ruffini endings. The end organ is situated in the dermis but is not as close to the skin surface as the Type I receptors. Figure 3.19 shows a typical Ruffini ending in hairy skin of the cat.

Figures 3.20 and 3.21, recorded from Type II receptors in hairy skin of the cat, show typical time responses of the receptors to vertical skin displacement. The semi-log plots of Figure 3.21 can be fit with three adaptation time constants of approximately 1, 5 and 20 seconds. Type II receptors do exhibit a regular static response as well as a regular resting discharge, and have a relatively wide receptive field responsive to stretch (see Chambers et al, 1972).

3.3.1.4 Comparative Physiology

The receptors described in the preceding sections appear to be common to mammalian hairy skin. Receptors with very similar properties have been identified in cats, monkeys, humans and even reptiles (Iggo & Muir, 1969; Knibestol and Vallbo, 1970; Kenton et. al., 1971; Chambers et. al., 1972; Burgess, 1973). For example, Figure 3.22 from Knibestol and Vallbo (1970) shows a recording from a receptor in human hairy skin that was found to closely resemble the cat Type II cutaneous receptors described in detail by Chambers et. al. (1972).

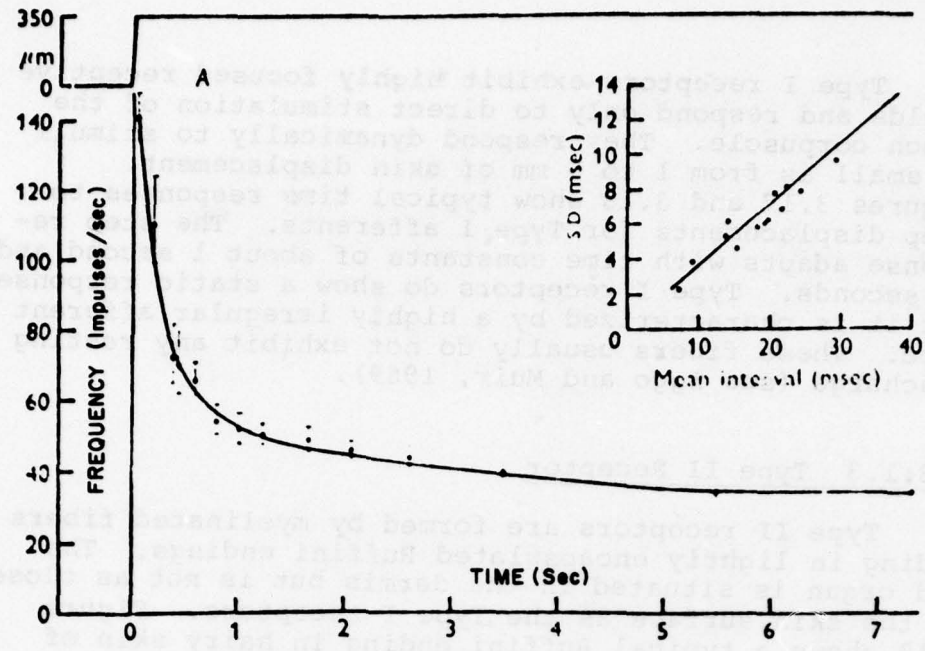

Figure 3.17a. Mean step response of Type I unit.

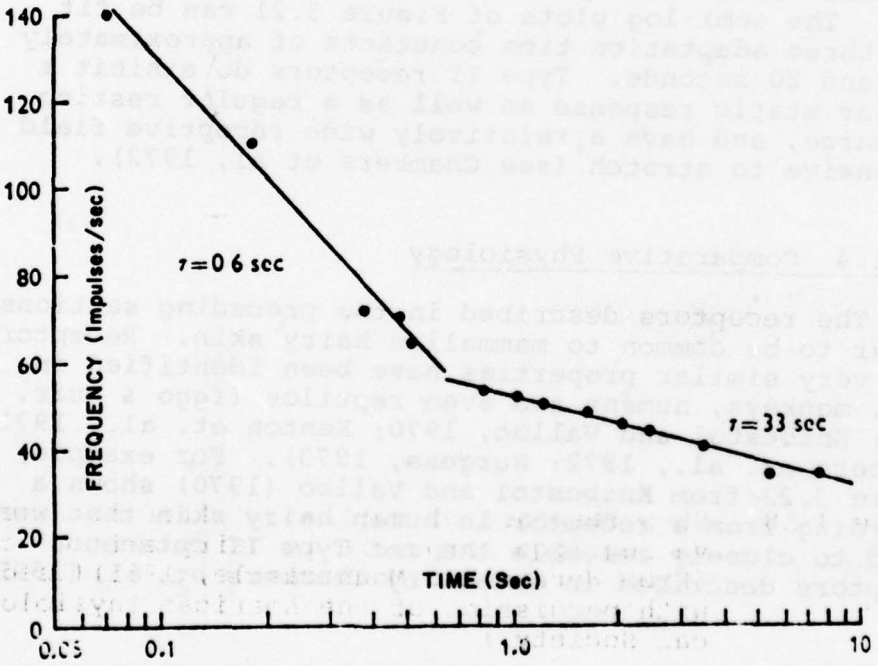

Figure 3.17b Step response of Type I plotted on semi-log scale. (From Iggo & Muir, 1969)(Used with permission of the Physiological Society.)

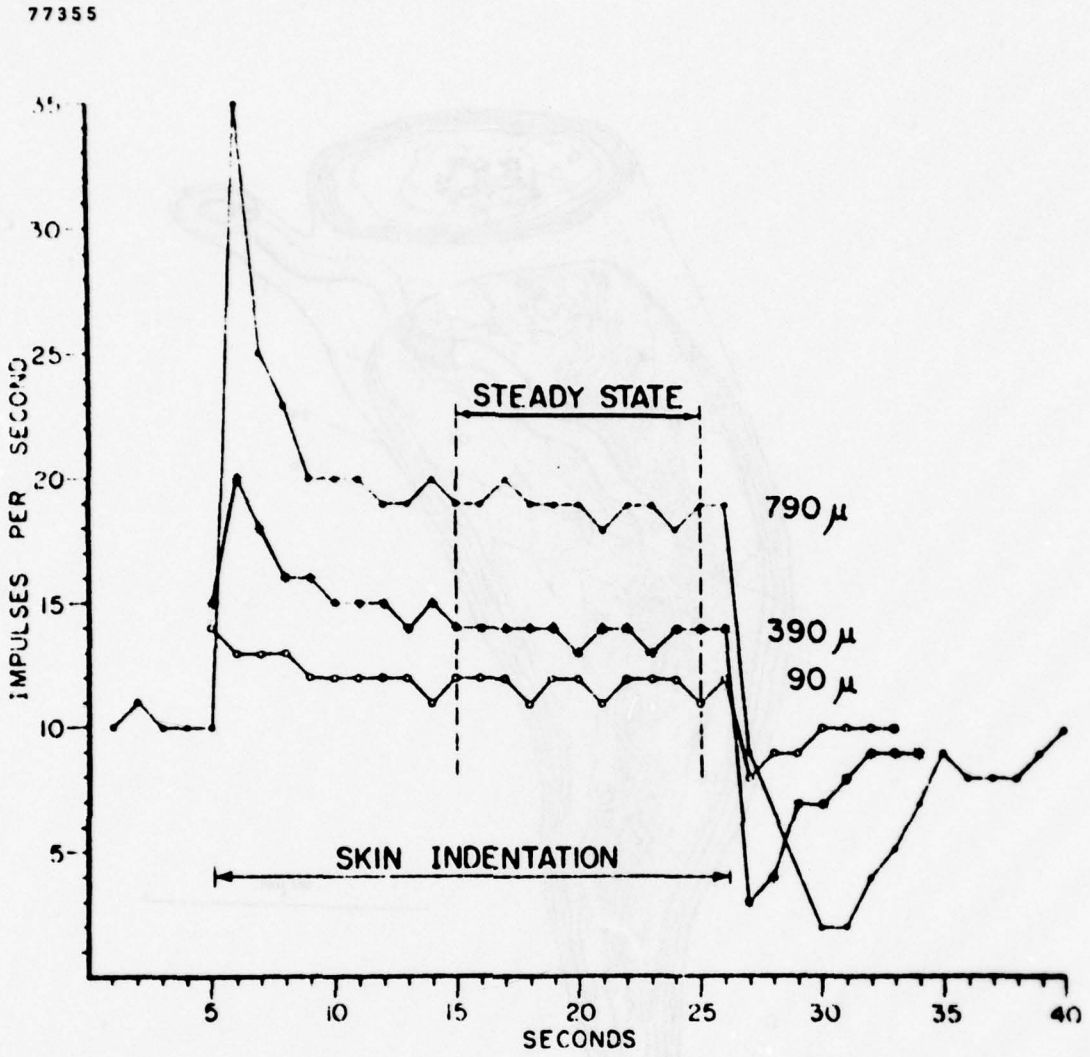

Figure 3.18 Step response of cutaneous afferent innervating Iggo corpuscle in hairy skin of cat. (From Werner and Mountcastle, 1965)(Used with permission of the American Physiological Society.)

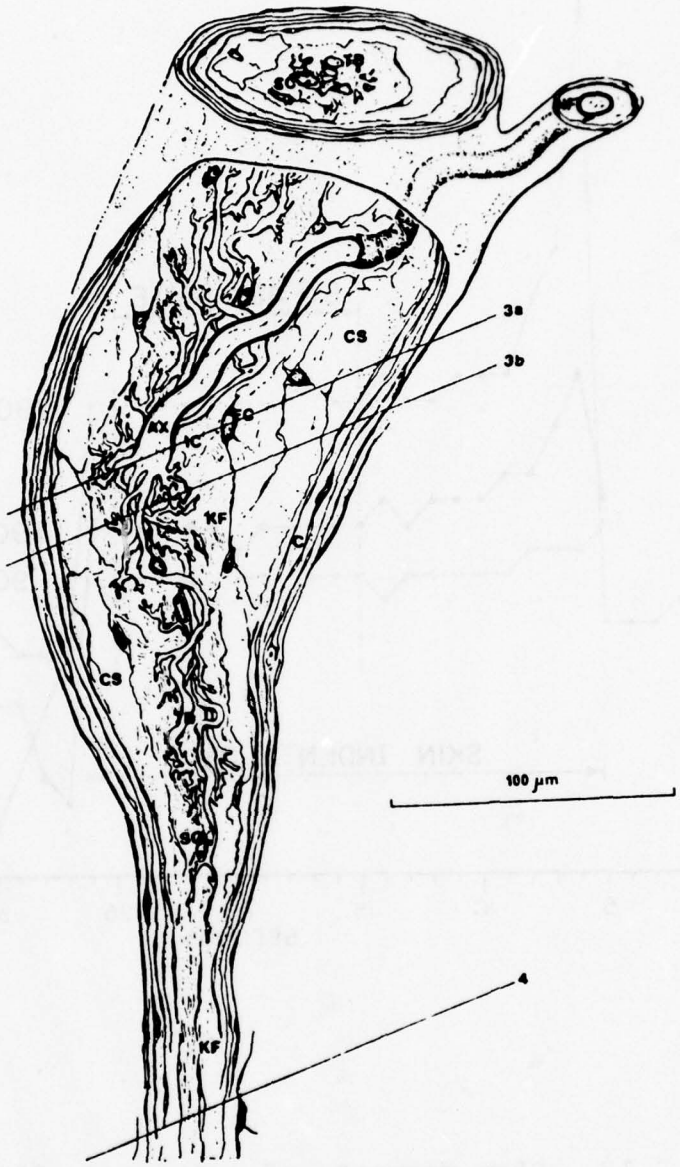

Figure 3.19 Lightly encapsulated Ruffini ending situated in the dermis, in hairy skin of the cat. (From Chambers, Andres, Duering, & Iggo, 1972) (Used with permission of Longman Group Ltd.)

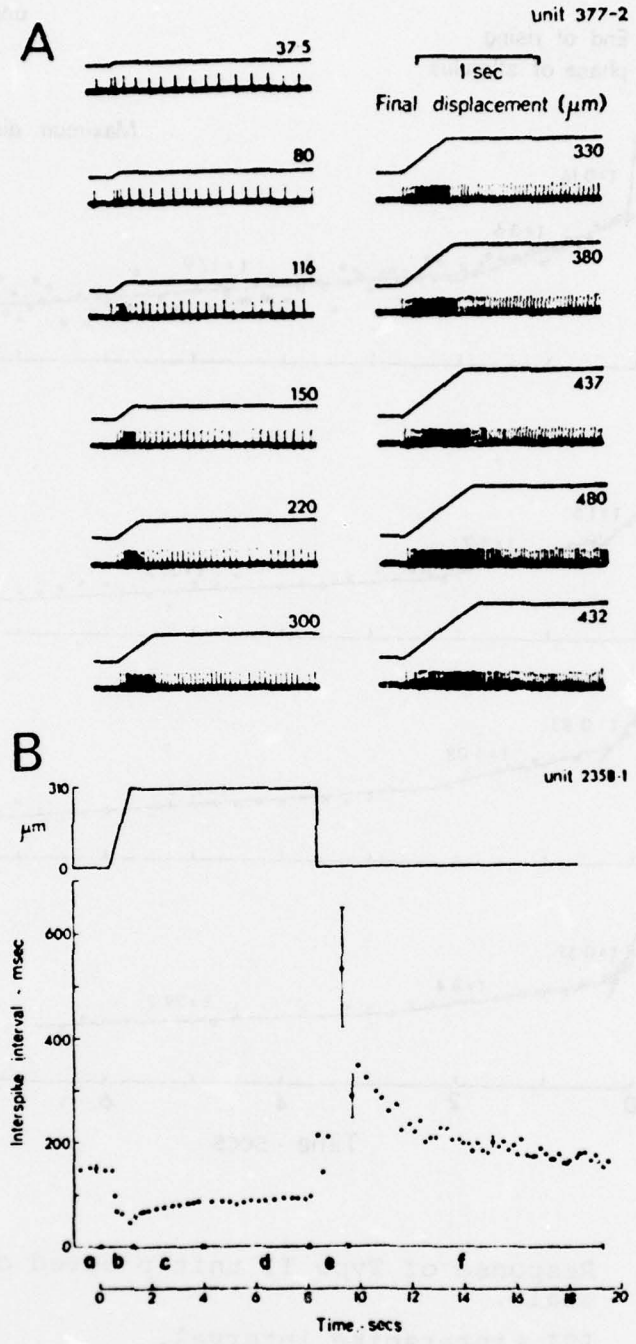

Figure 3.20 Time response of time unit to vertical displacement of the skin. A, single records. B, each print is the mean of 6 recordings; (a) resting discharge; (b) dynamic discharge; (c) adapting discharge; (d) adapted discharge; (e) silent period; (f) recovery of resting discharge. (From Chambers, Andres, Duering, and Iggo, 1972)(Used with permission of Longman Group, Ltd.)

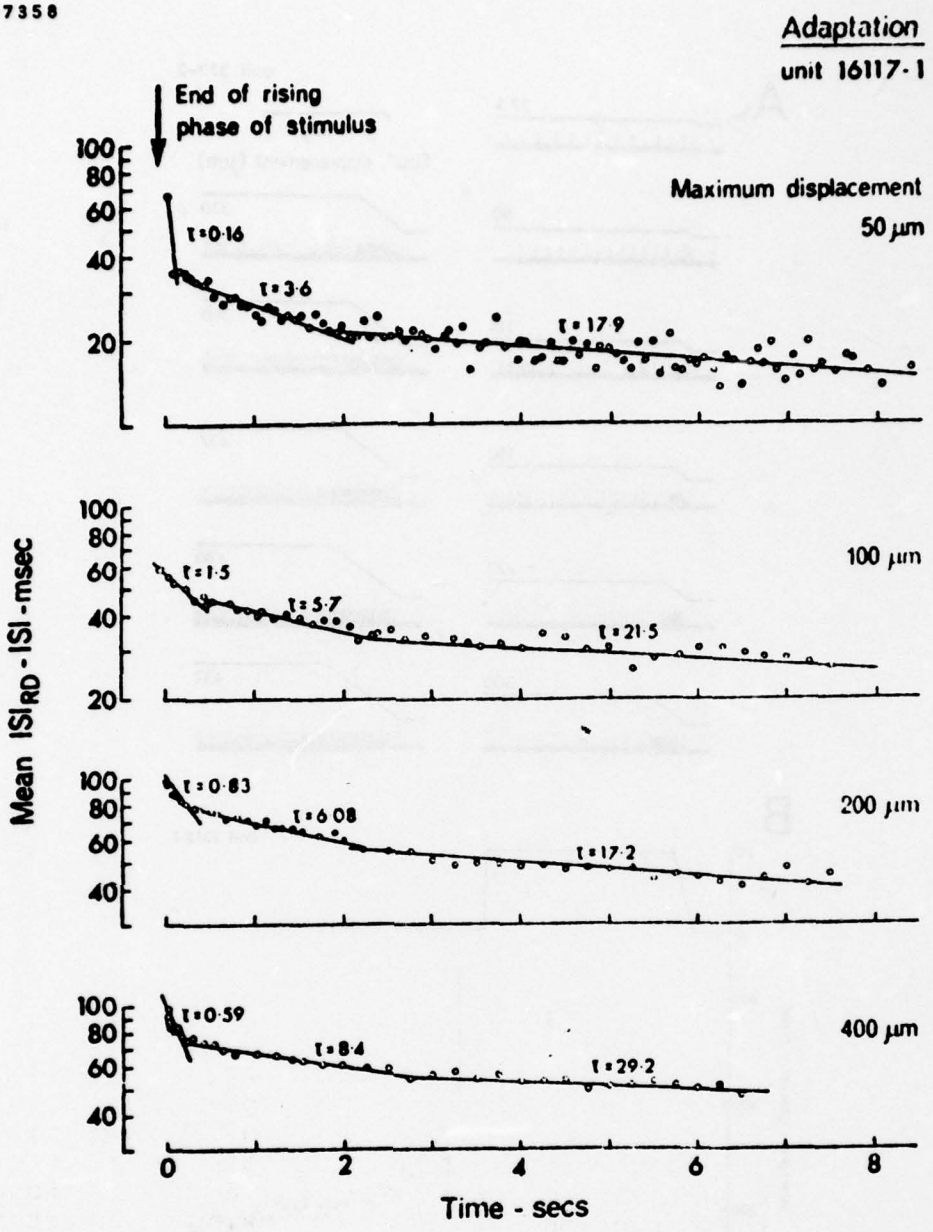

Figure 3.21 Response of Type II unit plotted on semi-log scale.

ISI ≡ interspike interval.

ISI_{RD} ≡ interspike interval during resting discharge.

(From Chambers, Andres, Duering, & Iggo, 1972)
(Used with permission of Longman Group, Ltd.)

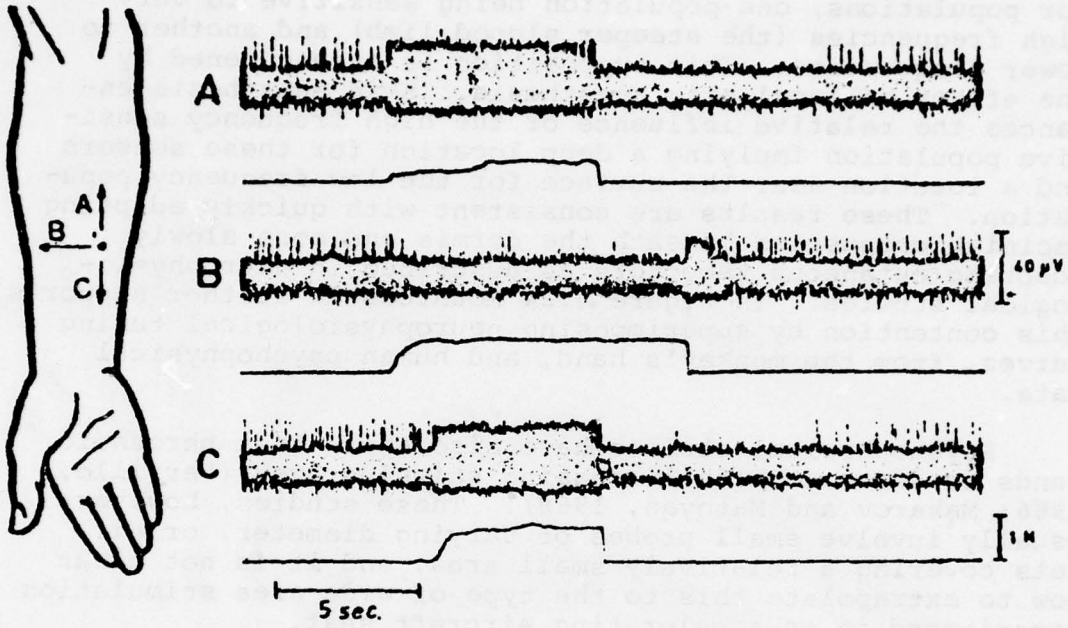

Figure 3.22 Responses to skin stretch of a slowly adapting unit with indistinct receptive field borders in the hairy skin. In the drawing, the black dot indicates the point of maximal sensitivity of the unit. The arrows indicate the directions in which the skin was stretched when the records in A, B and C respectively were obtained. (From Knibestol & Vallbo, 1970) (Used with permission of the Scandinavian Physiological Society.)

3.3.2 Psychophysical Data

Figure 3.23 shows human threshold to flutter vibration over a range of frequencies under normal conditions and after skin surface has been anesthetized. Both curves have a double limb characteristic that suggests two receptor populations, one population being sensitive to very high frequencies (the steeper sloped limb) and another to lower frequencies. This supposition is strengthened by the effect of local skin anesthesia. Skin anesthesia enhances the relative influence of the high frequency sensitive population implying a deep location for these sensors and a location near the surface for the low frequency population. These results are consistent with quickly adapting Pacinian corpuscles beneath the dermis and more slowly adapting cutaneous receptors as described in neurophysiological studies. In Figure 3.24 Mountcastle further supports this contention by superimposing neurophysiological tuning curves, from the monkey's hand, and human psychophysical data.

Psychophysical studies have also shown that threshold tends to decrease with increasing stimulus area (Verrillo, 1966; Makarov and Matoyan, 1968). These studies, however, usually involve small probes of varying diameter, or air jets covering a relatively small area, and it is not clear how to extrapolate this to the type of wide area stimulation experienced in an accelerating aircraft seat.

The shape of the steady-state input/output function for tactile sensation is still not clear. Mountcastle (Mountcastle, 1971) has found that linear functions provide good fits to his data for glabrous skin but that power functions seem more appropriate in the case of hairy skin. Kruger and Kenton (1973) have disputed this contention, however. For preliminary modeling purposes we will assume a linear relation.

3.3.3 Weber Fractions for the Tactile System

Werner and Mountcastle (1965) have calculated Weber fractions for mechanoreceptors innervating hairy skin of the cat, both empirically and theoretically. The curves of Figure 3.25 were determined theoretically by using previously calculated input/output functions. The dashed line assumes the least discriminable response to be always

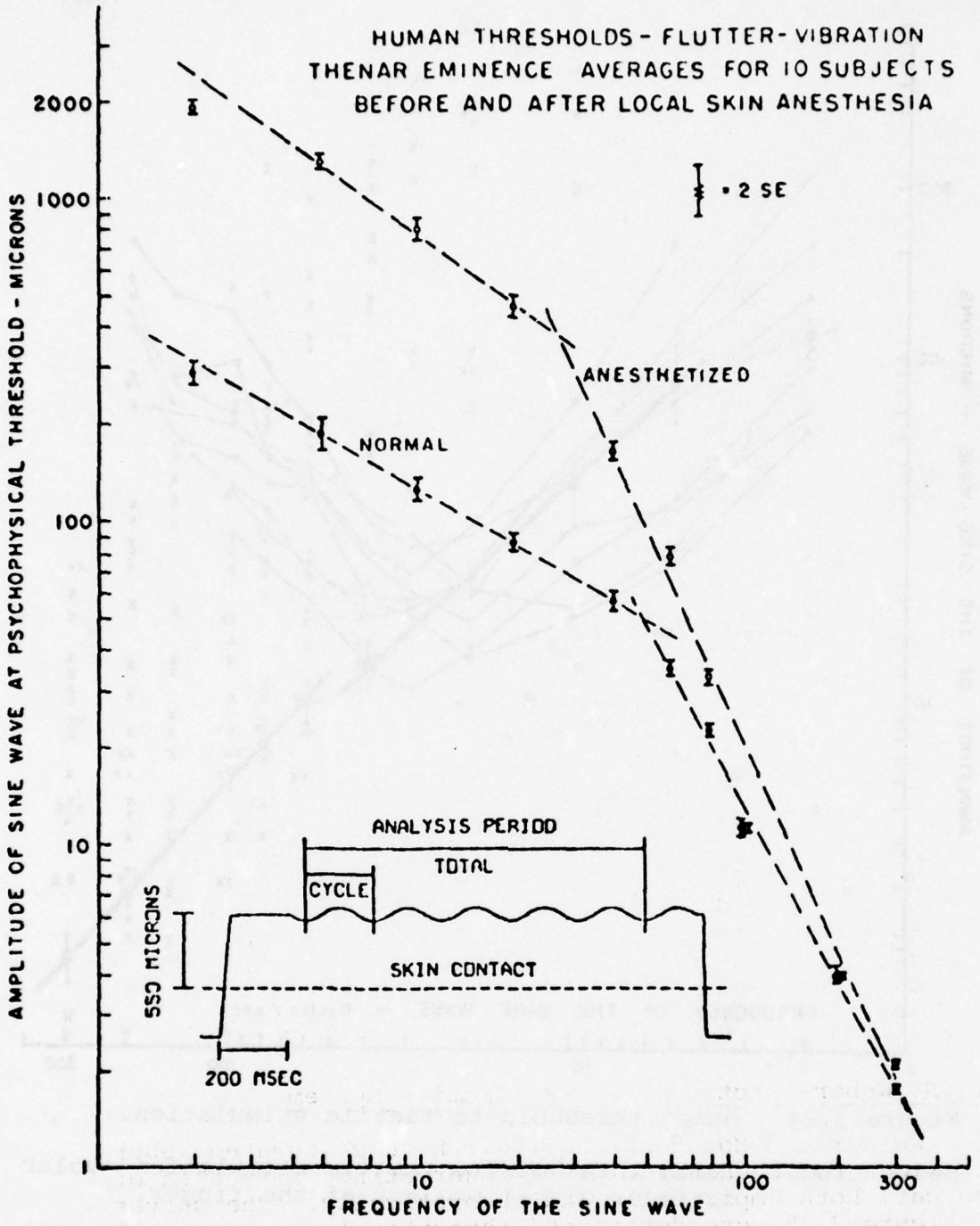

Figure 3.23 Psychophysical tuning curve for human threshold to tactile stimulus--glabrous skin, thenar eminence. (From Mountcastle, 1967) (Used with permission of Rockefeller University Press.)

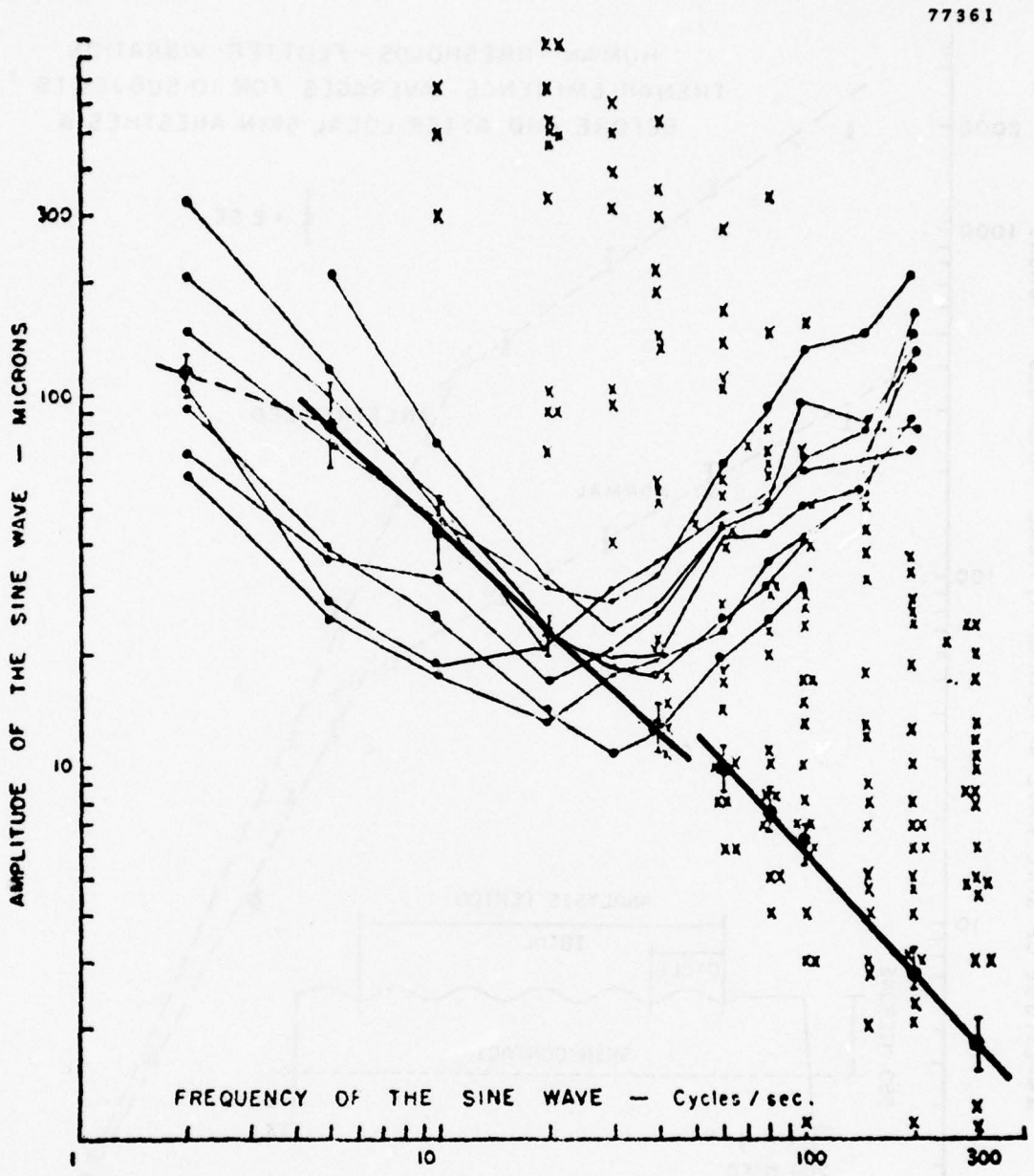

Figure 3.24 Human threshold to tactile stimulation.

Heavy Lines: Human threshold to tactile stimulation--volar surface, distal phalanx of the finger.

Light Lines: Tuning points--myelinated cutaneous afferents ending in glabrous skin of monkey hand.

Crosses: Tuning points--myelinated afferents ending in Pacinian corpuscles of monkey hand.

(From Mountcastle, 1967) (Used with permission of Rockefeller University Press.)

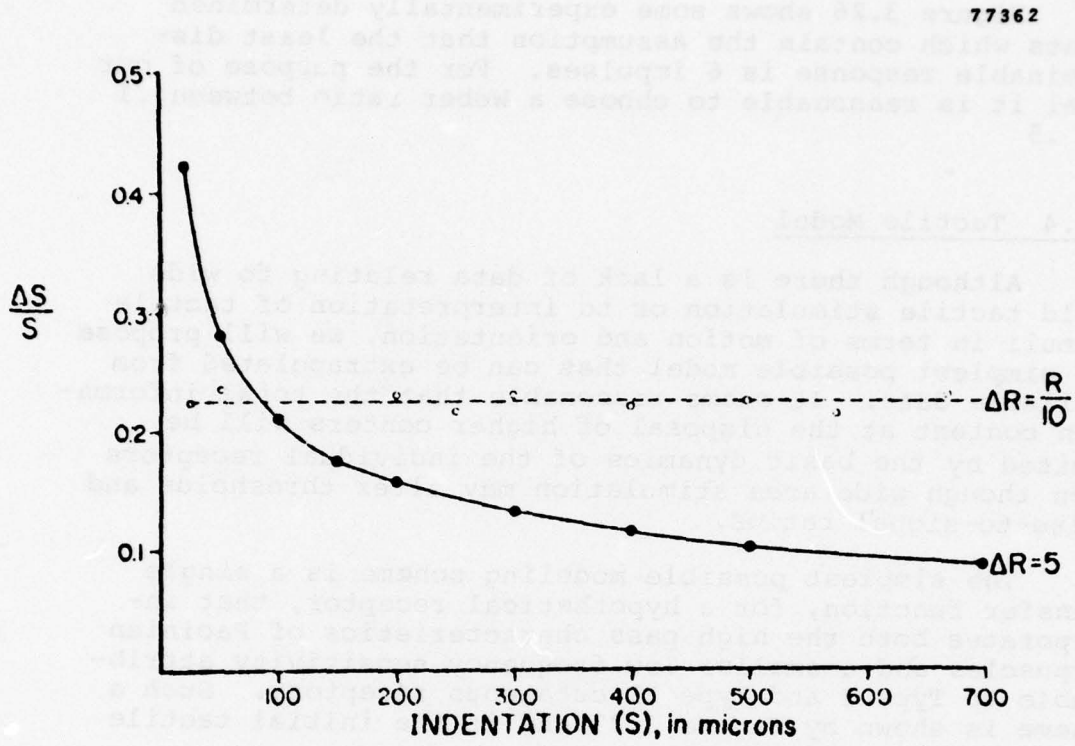

Figure 3.25 Weber fraction $(\frac{\Delta S}{S})$ based on input/output function calculated for mechanoreceptor afferent innervating hairy skin of cat.

Dashed Line: Assume least discriminable response increment (ΔR) is always one-tenth of the total response (R).

Solid Line: Assume least discriminable response increment is always 5 impulses.

$\Delta S \equiv$ Least discriminable stimulus; $S \equiv$ total stimulus.

(From Werner and Mountcastle, 1965) (Used with permission of the American Physiological Society.)

1/10 of the total response, while the solid line assumes that the least discriminable response is always 5 impulses.

Figure 3.26 shows some experimentally determined points which contain the assumption that the least discriminable response is 6 impulses. For the purpose of our model it is reasonable to choose a Weber ratio between .1 and .5

3.3.4 Tactile Model

Although there is a lack of data relating to wide field tactile stimulation or to interpretation of tactile stimuli in terms of motion and orientation, we will propose the simplest possible model that can be extrapolated from available data. It seems reasonable that the total information content at the disposal of higher centers will be limited by the basic dynamics of the individual receptors even though wide area stimulation may alter thresholds and noise-to-signal ratios.

The simplest possible modeling scheme is a single transfer function, for a hypothetical receptor, that incorporates both the high pass characteristics of Pacinian corpuscles and a smaller low frequency sensitivity attributable to Type I and Type II cutaneous receptors. Such a scheme is shown by Figure 3.27 and is the initial tactile model used in our program.

The Pacinian corpuscles are rectifiers as well as high-pass filters and no directional information is available from them. Some of the slowly adapting receptors, on the other hand, do provide directional information. The nonlinear two channel output allows the central processor (in the case of our model a Kalman filter) to gain directional information by noticing which channel the information comes from, but results in greater measurement noise than would be the case for a single linear channel.

Body seat compression dynamics can be modeled as a spring dashpot system as shown in Figure 3.28 (see Gum, 1973). For initial trial of the model the seat is assumed to be very hard since this condition will maximize the contribution of the tactile system. Later a more realistic seat compliance can be used, thus decreasing the effective bandwidth of the tactile system.

77363

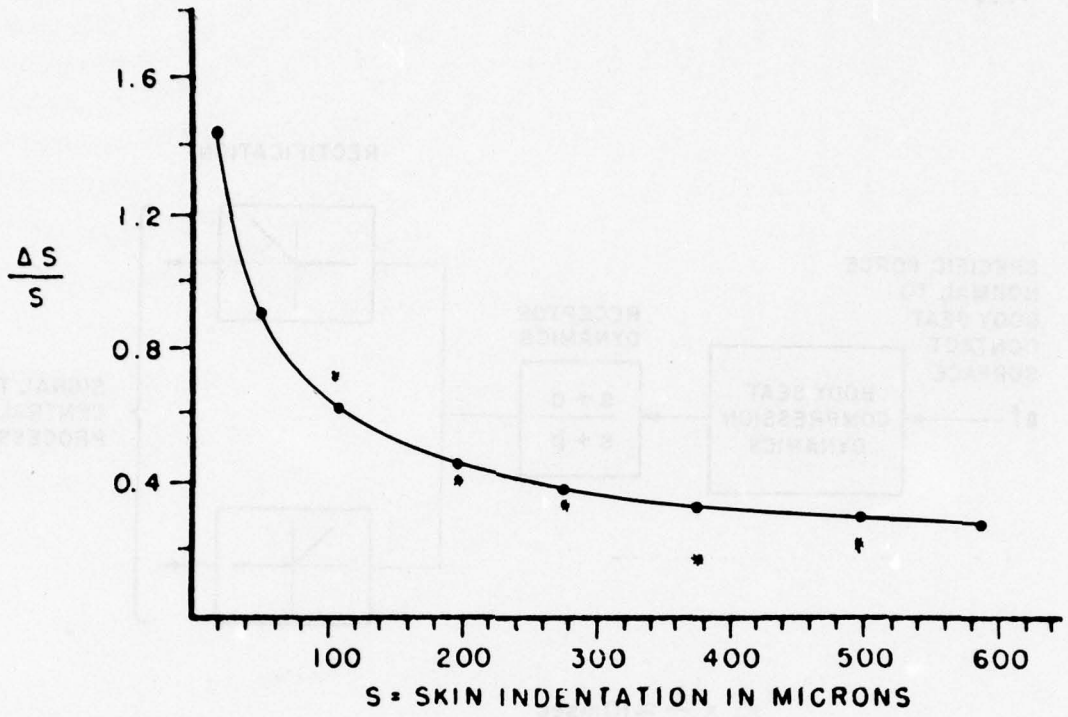

Figure 3.26 Weber fraction ($\frac{\Delta S}{S}$)

Dots: Based on Input/Output power function calculated for mechanoreceptor afferent innervating hairy skin of cat.

Asterisks: Points determined experimentally for same unit.

All points assume least discriminable response is 6 impulses.

(From Werner and Mountcastle, 1965)(Used with permission of the American Physiological Society.)

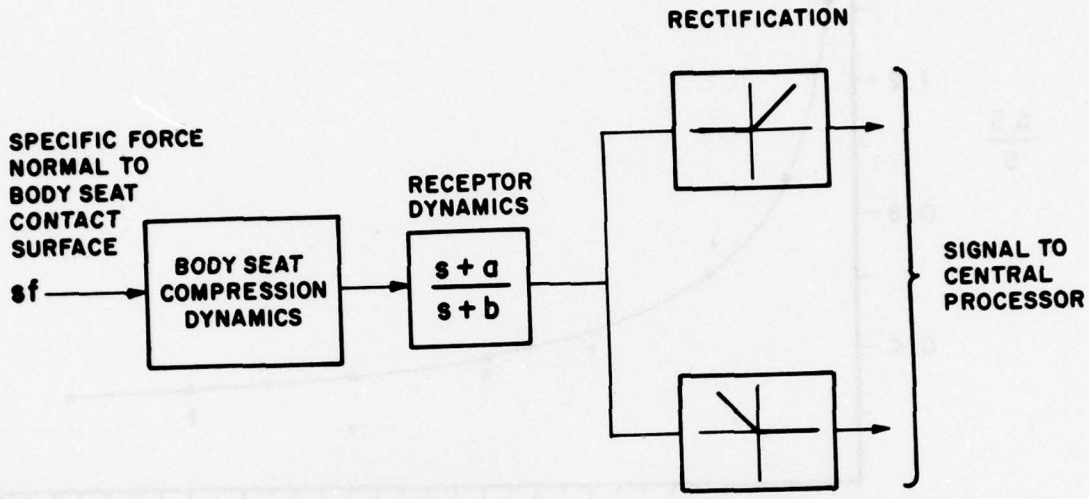

$$\tau_b = \frac{1}{b} \approx 10\,\text{msec}$$

$$\frac{a}{b} = \frac{1}{10}$$

Figure 3.27 Tactile Model.

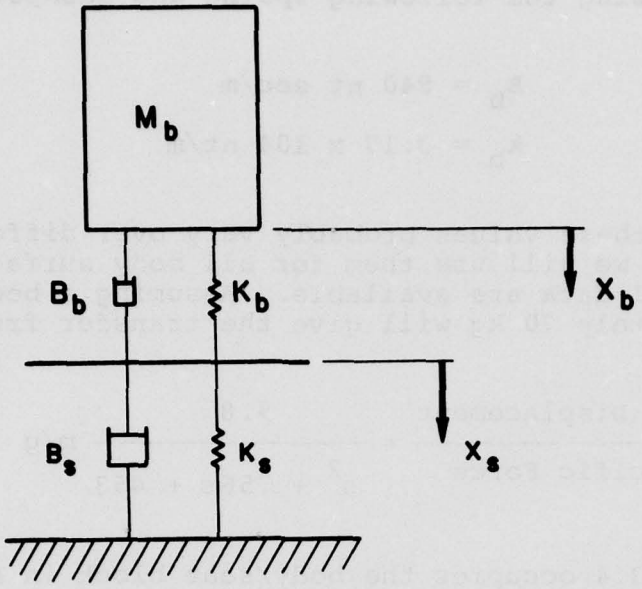

One-half Body/Buttocks/Seat Model

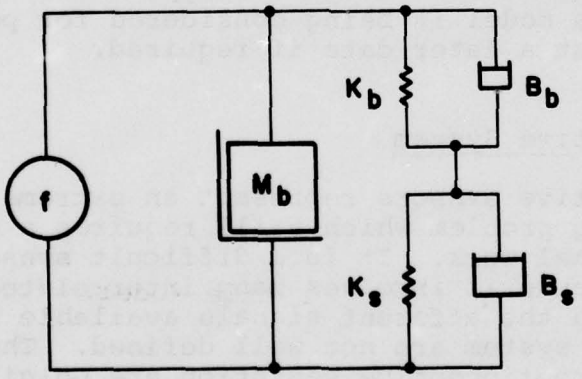

Mechanical Circuit Diagram

Figure 3.28 Buttocks/Seat Model
(From Gum, 1973)

Gum (1973) has modeled the buttocks seat contact surface using the following spring and dashpot constants:

$$B_b = 840 \text{ nt sec/m}$$

$$k_b = 3.17 \times 104 \text{ nt/m}$$

Although these values probably vary over different body surfaces, we will use them for all body surfaces until additional data are available. Assuming a body mass of approximately 70 kg will give the transfer frunction

$$\frac{\text{Skin Displacement}}{\text{Specific Force}} = \frac{9.8}{s^2 + .56s + 453} \text{ m/g} \qquad (3.4)$$

Equation 3.4 occupies the body/seat block in Figure 3.27. Since there is no good threshold information concerning the broad area tactile stimulus, we will take threshold as zero for the time being.

Figure 3.29 shows an alternate, more complex tactile model using two completely separate channels, one employing high-pass dynamics characteristic of Pacinian corpuscle, and another employing more slowly adapting dynamics characteristic of Type I and Type II receptors. This model is being considered for possible implementation at a later date if required.

3.4 Proprioceptive System

Proprioceptive sensors represent an extremely challenging modeling problem which still requires a great deal of additional work. It is a difficult sensory mode to approach because it involves many interrelated joints and muscles, and the afferent signals available to the central nervous system are not well defined. The basic components of proprioceptive sensation are Golgi tendon organs, muscle spindles and joint receptors. Golgi tendon organs transduce muscle tension and Figure 3.30 shows one model proposed for tendon organ response. Muscle spindles appear to be primarily muscle length sensors. Figure 3.31 is a diagram of a typical muscle spindle and Figure 3.32 shows a lumped parameter model for spindle function.

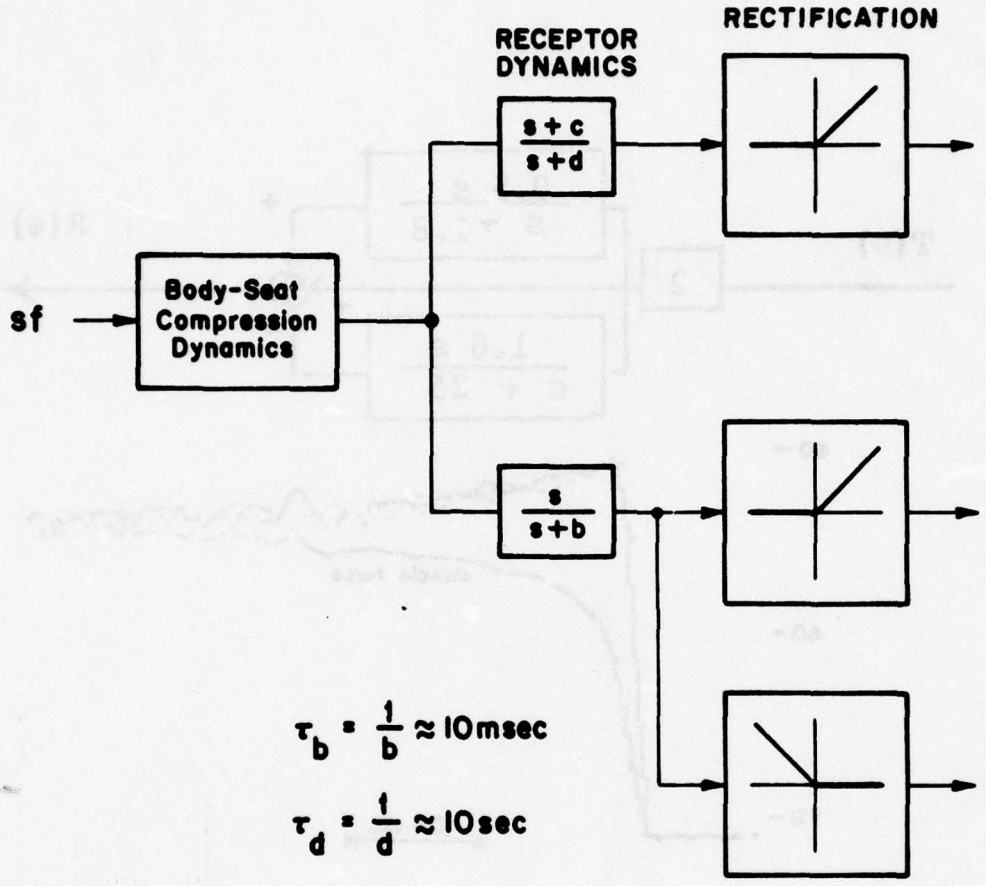

Figure 3.29 Alternate Tactile Model.

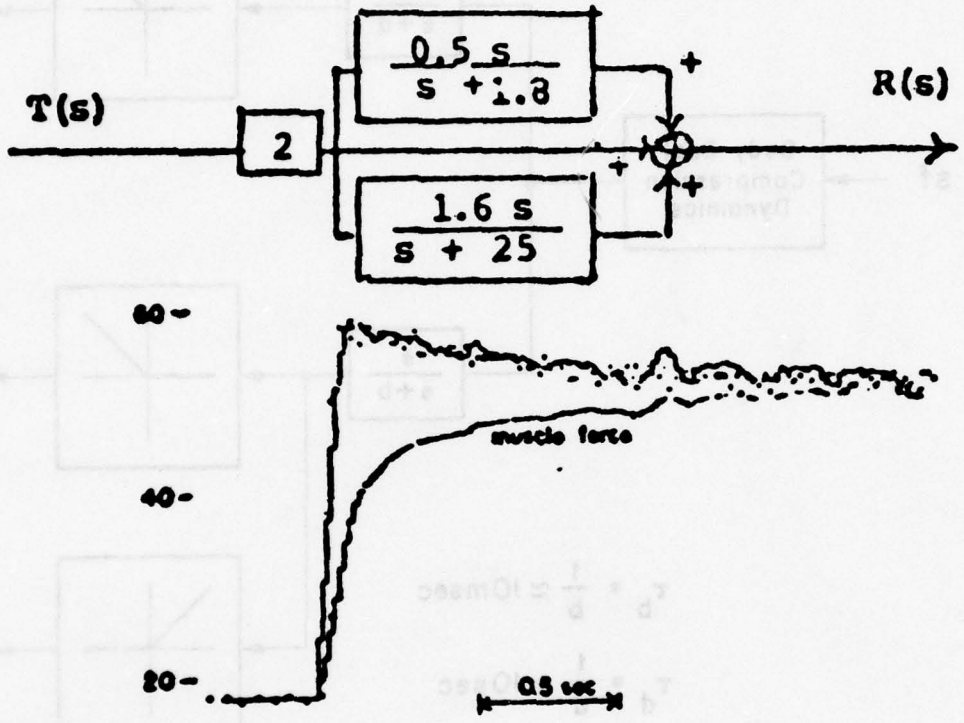

Figure 3.30 Model for Golgi tendon organ function and experimental result of increasing muscle tension. (From Houk and Henneman, 1967, as modified by Oman, class notes, MIT, 1975.)

77368

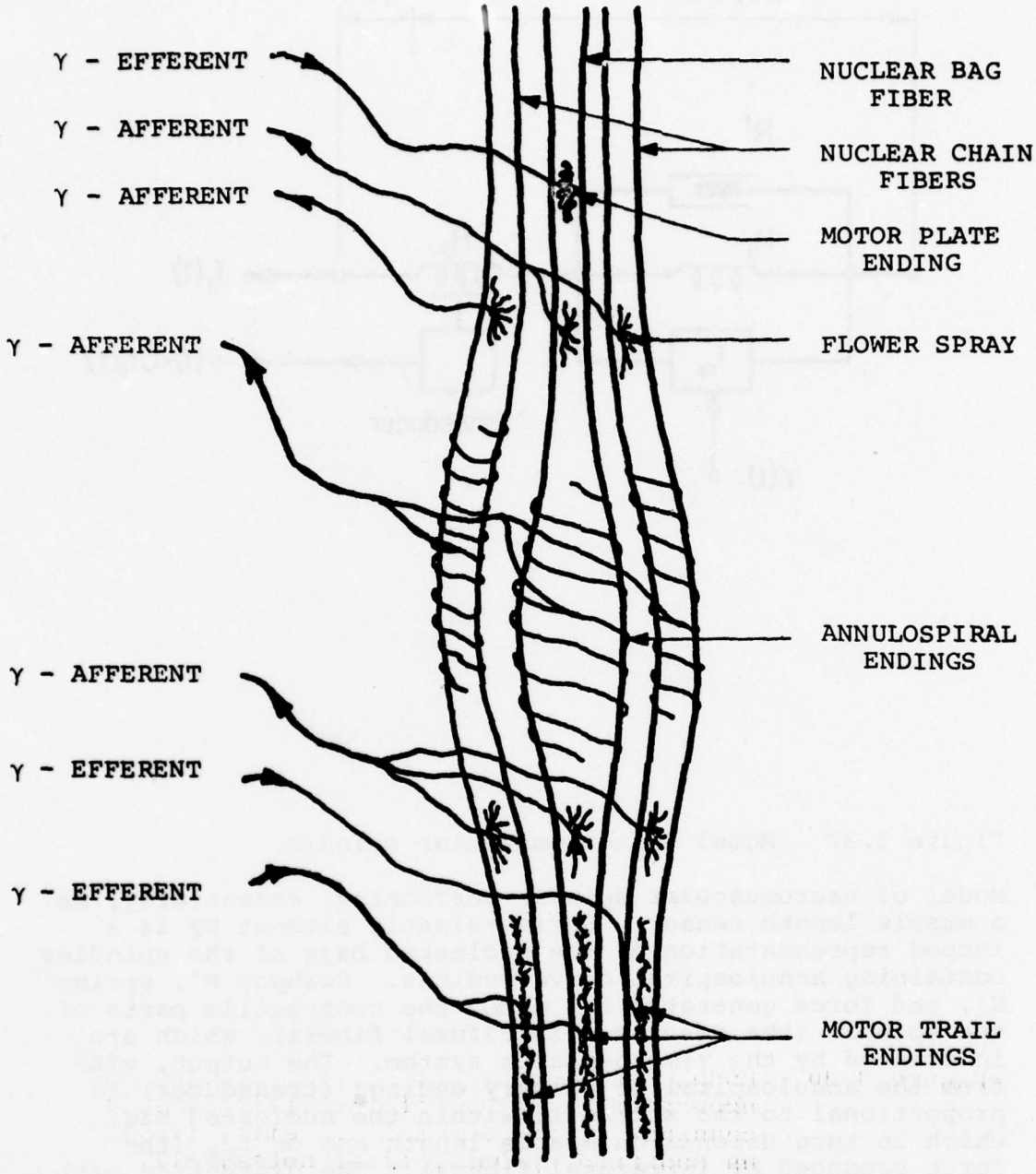

Figure 3.31. Muscle Spindle Diagram (from Gum, after Nashner, 1970).

77367

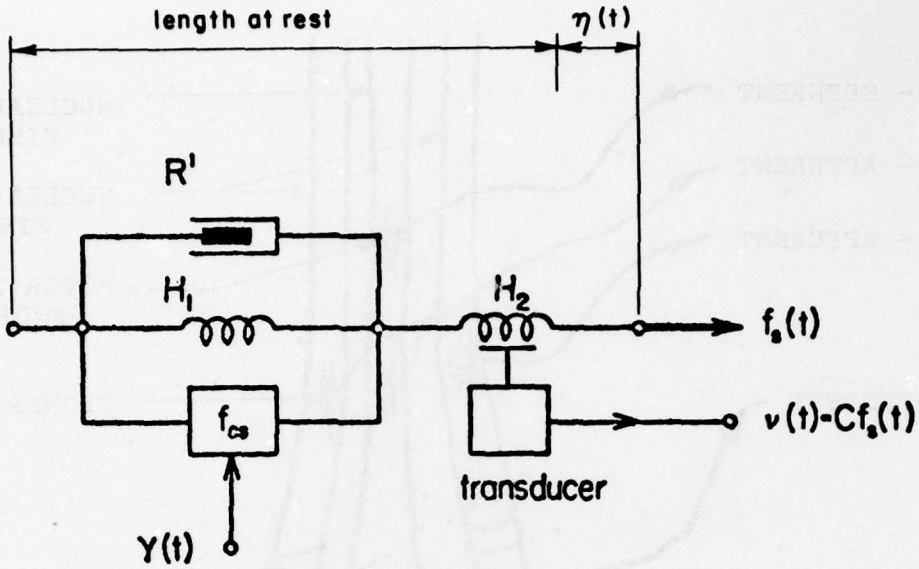

Figure 3.32 Model of neuromuscular spindle.

Model of neuromuscular spindle performing, essentially, as a muscle length sensor. Series-elastic element H_2 is a lumped representation of the nucleated bags of the spindles containing annulospiral nerve endings. Dashpot R', spring H_1, and force generator f_{cs} model the contractile parts of the spindle (the so-called intrafusal fibers), which are innervated by the γ-moto-neuron system. The output, v(t) from the annulospiral or primary endings (transducer) is proportional to the stress f_s within the nucleated bag, which in turn depends on muscle length and on f_{cs} (the force produced by intrafusal fibers). The distension η(t) is beyond resting length of the spindle. (After Talbot & Gessner, 1973)

As an initial attempt to include proprioceptive input in the unified model, we have chosen to consider one very specific proprioceptive input. This input is muscle spindle response to lateral head motion with respect to the body trunk. Gum (1973) has proposed a model for the head/neck control system based on muscle spindle feedback. This model will form the basis for our first attempt.

Figure 3.33 diagrams the head/neck muscle system as an inverted pendulum with muscular control torques. Figure 3.34 shows Gum's model reconfigured to fit the needs of the current effort. The diagram assumes that the system is always acting to keep the head upright and that angles always remain small. Muscle dynamics and spindle feedback transfer functions were based largely on neurophysiological data, head natural frequency and damping ratio were determined empirically from a single subject, and head moment of inertia (I_h) was approximated by using a simple geometric model (see Gum, 1973). Neck joint receptors are not considered, at least initially.

Other factors probably contribute to the head/neck control system and need to be investigated further. For instance, the vestibular sensors, as well as the muscle spindles provide feedback tending to stabilize the head. There are also proprioceptive systems besides the head/neck system that are important enough to warrant study and eventual inclusion in a unified model. Proprioceptive mechanisms in the arms and legs are of particular interest for application to aircraft pilots since these limbs are used to manipulate controls (joystick, rudder pedals, etc.).

I_h is the moment of inertia of the head about the neck pivot,

B_n is the damping due to other muscles and neck tissue not involved in active motion,

K_n is the elastance due to other muscles and neck tissue not involved in active motion,

M_h is the mass of the head,

r is the distance from the pivot to the center of mass,

g is the acceleration due to gravity and

θ is the displacement angle.

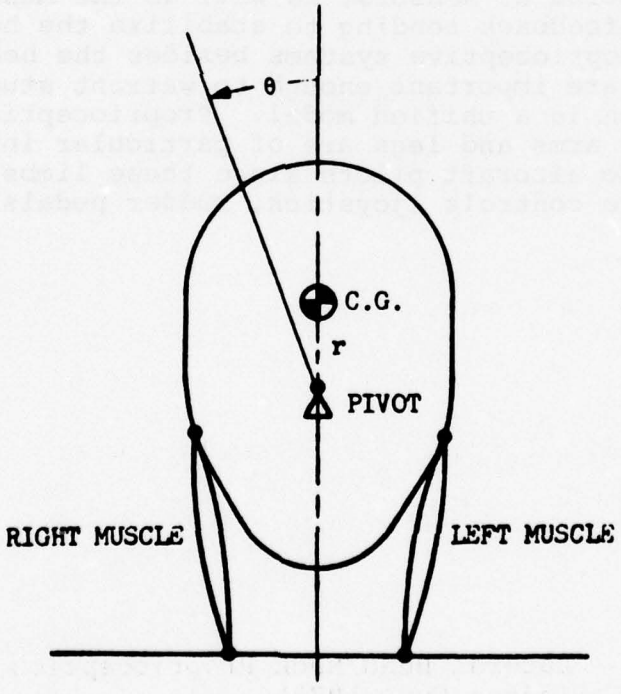

Figure 3.33 Head/Muscle System. (From Gum, 1973)

77370

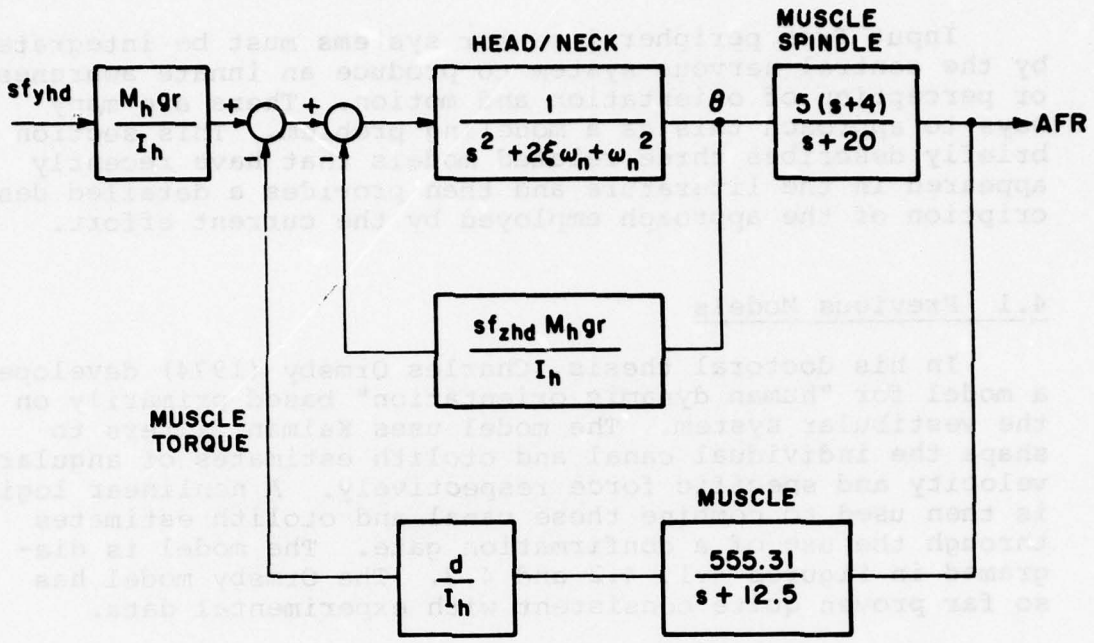

$d \equiv$ muscle lever arm = .075 m

$I_h \equiv$ head moment of inertia = .0304 kg

$M_h \equiv$ head mass = 4.6 kg

$\omega_h \equiv 7.81 \frac{rad}{sec}$

$r \equiv$ inverted pendulum length = .0498 m

$sf_{zhd} \equiv$ specific force parallel to body axis

$sf_{yhd} \equiv$ lateral specific force

Figure 3.34 Lateral Head/Neck Proprioception Model (after Gum, 1973).

4.0 UNIFIED MODEL

Input from peripheral sensor systems must be integrated by the central nervous system to produce an innate awareness or perception of orientation and motion. There are many ways to approach this as a modeling problem. This section briefly describes three related models that have recently appeared in the literature and then provides a detailed description of the approach employed by the current effort.

4.1 Previous Models

In his doctoral thesis, Charles Ormsby (1974) developed a model for "human dynamic orientation" based primarily on the vestibular system. The model uses Kalman filters to shape the individual canal and otolith estimates of angular velocity and specific force respectively. A nonlinear logic is then used to combine these canal and otolith estimates through the use of a confirmation gate. The model is diagramed in Figures 4.1, 4.2 and 4.3. The Ormsby model has so far proven quite consistent with experimental data.

Zacharias and Young (1977) have proposed a model to handle visual-vestibular interaction in the yaw rotation mode. The model is diagramed in Figure 4.4 and has shown a good fit to data obtained during a yaw motion manual control task.

Curry, Hoffman and Young (1976) have extended the pilot optimal control model of Kleinman, Baron and Levison (1970) to consider both visual and vestibular inputs to a Kalman filter/predictor. It is closely related to the present effort but with a slightly different goal and approach. The model is designed for analysis of statistical parameters of pilot performance as opposed to time domain outputs of perceptual quantities. Frequency analysis of the model shows good agreement with data gathered during a roll-controlled tracking task for all but the very low frequency range.

4.2 Approach to Present Modeling Effort

The goal of the current effort is to develop a general model able to encompass four sensor system modalities: vestibular, visual, tactile and proprioceptive. The desired output of the model is a time domain prediction of orientation and motion perception. For an initial attempt we have assumed a completely naive subject whose only task

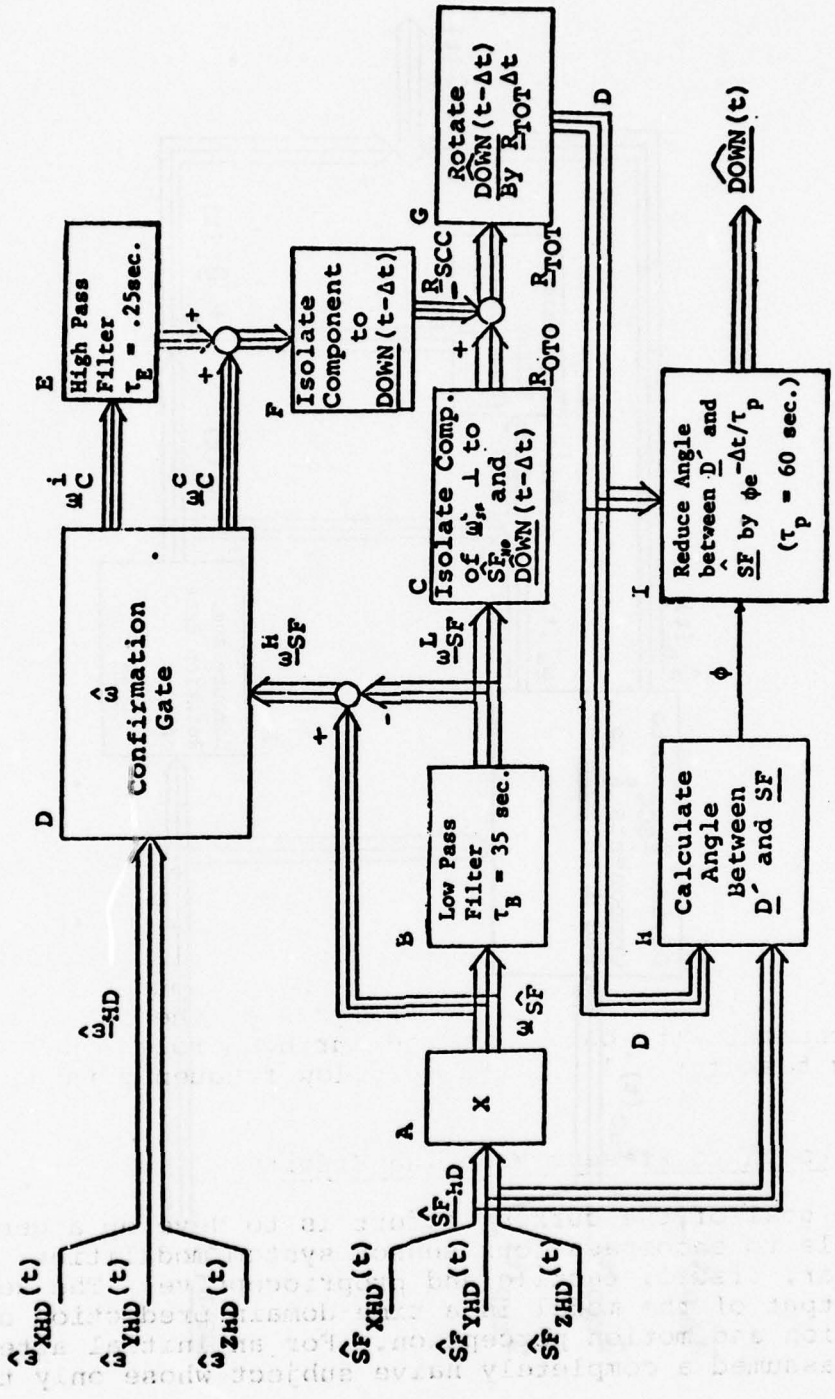

Figure 4.1 $\hat{\text{DOWN}}$ Estimator (from Ormsby, 1974).

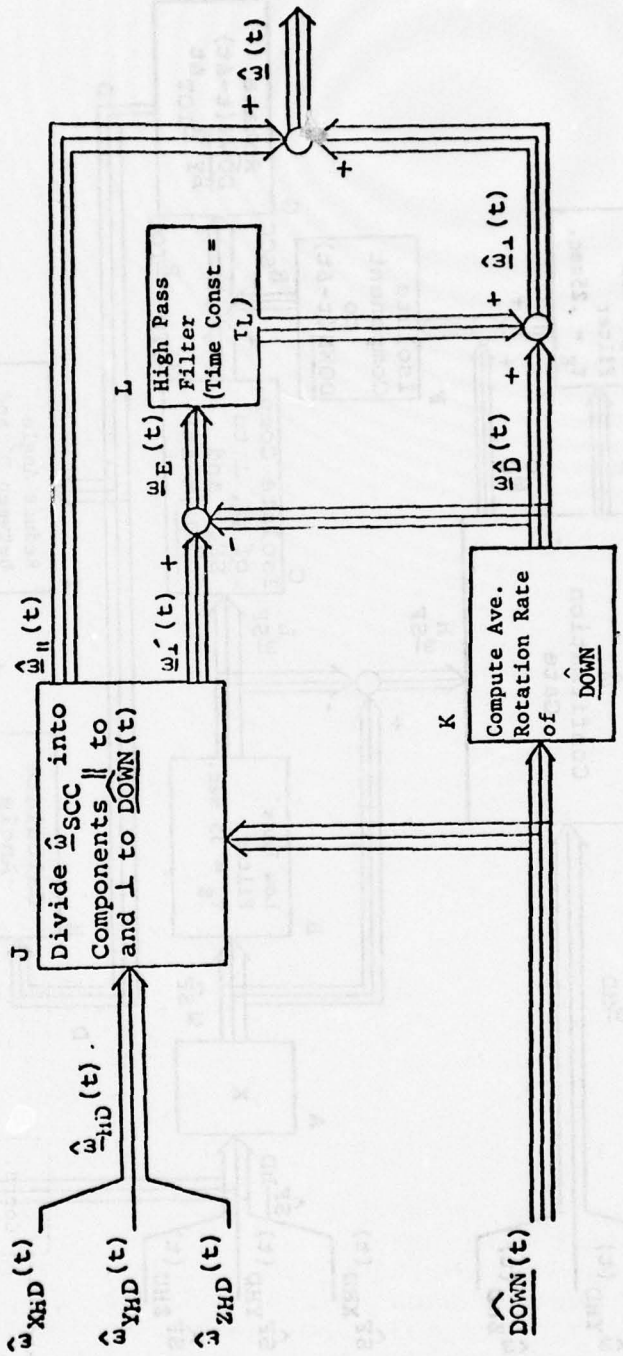

Figure 4.2 $\hat{\omega}$ Estimator (from Ormsby, 1974).

77373

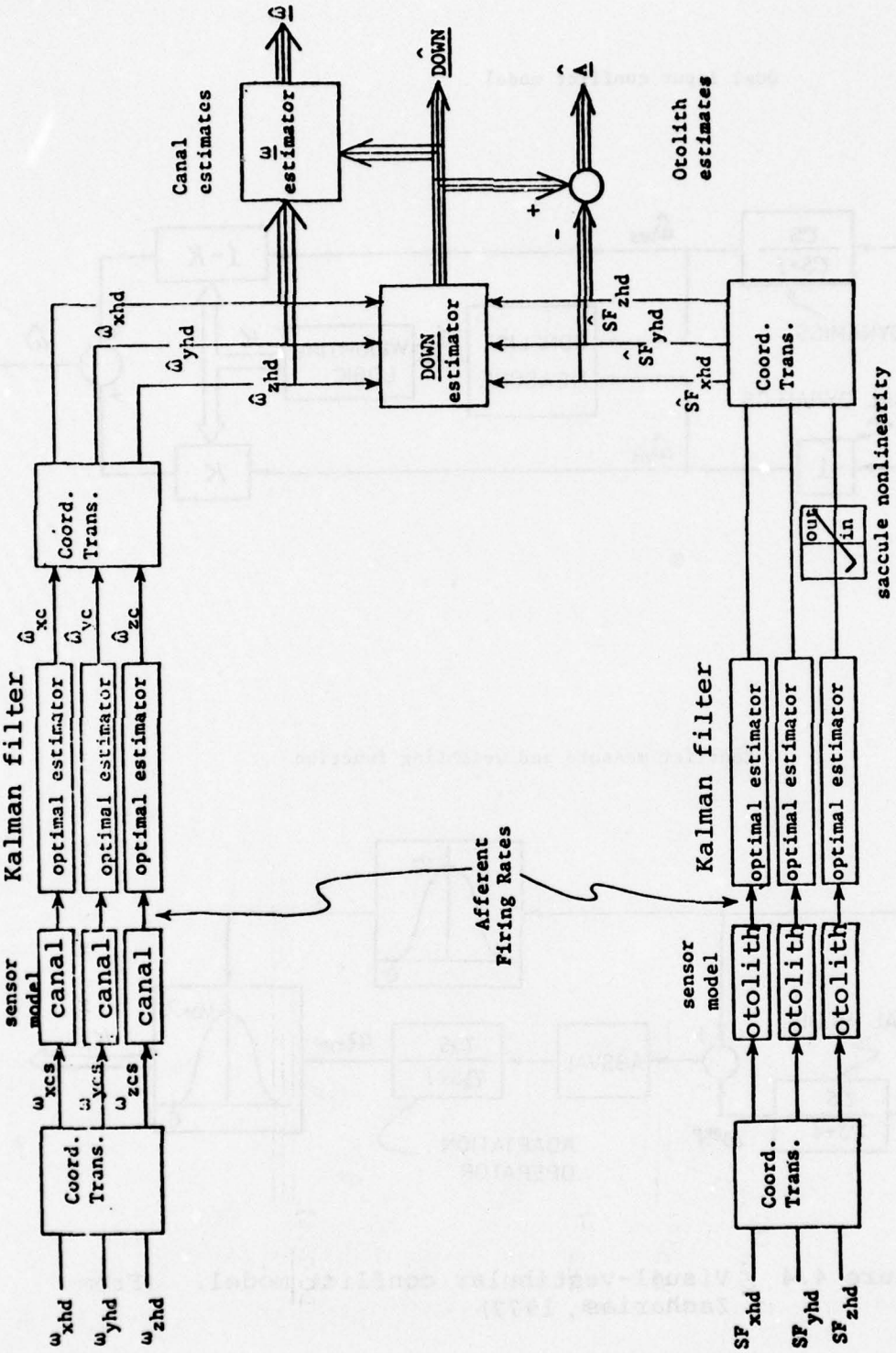

Figure 4.3 Ormsby Model.

Dual input conflict model

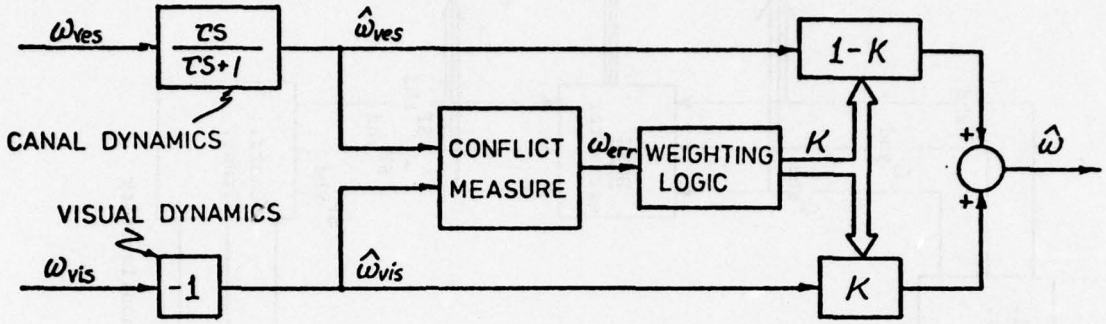

Conflict measure and weighting function

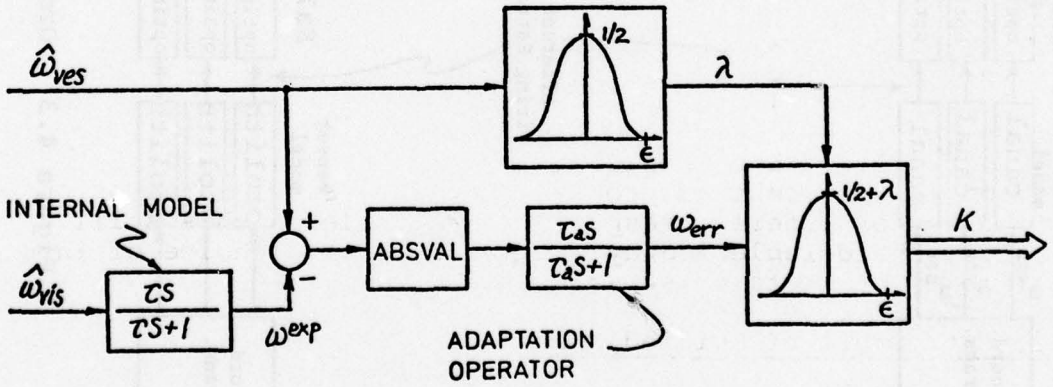

Figure 4.4 Visual-vestibular conflict model. (From Zacharias, 1977)

is to try to remain aware of his inertial state. Figure 4.5 shows a basic view of such a system. As of this writing the model has been exercised only with the vestibular sensor system components; however, work is continuing to include the other sensory modalities as well.

The sensor model blocks of Figure 4.5 are occupied by the individual sensor models described in the last section and to a large extent are physiologically based. It is not possible to decode central nervous system wiring in order to deduce a central processor algorithm; however, the problem can be approached by assuming that some sort of an optimization process is involved. If given a task similar to that of the neural central processor, the simplest technique would be to assume a linear system with white input and measurement noise, in which case the optimal estimator is the well-known Kalman filter. If, in addition, the noise processes are assumed to be stationary, the filter reduces to a steady-state Kalman or Weiner filter and has the form shown in Figure 4.6. Figure 4.7 is a generalized diagram of a Kalman filter blending model for motion and orientation perception.

There are many other possible schemes that can be used to model the central processor. A leading candidate is the cue hierarchy approach in which the central processor relies on a certain subset of available measurements depending upon specific conditions. A hybrid scheme involving both linear filter blending and cue hierarchy switching is probably closest to reality.

The Kalman filter approach is, none the less, very appealing at this stage. It has a certain conceptual simplicity since conflicting measurements are blended according to a mathematical optimization algorithm, and the filter alone may prove capable of matching available data satisfactorily. It has, therefore, been decided to pursue a Kalman filter formulation for the central processor model. Since information about sensor afferent response is incomplete, this still leaves considerable leeway, primarily in the choice of internal model parameters and structure.

4.3 Structure of Unified Model

Use of the Kalman filter blending model involves two basic operations. First, optimal parameters for the filter must be derived based on an "internal model." These parameters are then used in real-time implementation of the filter to obtain time history responses to deterministic stimuli.

77376

77302

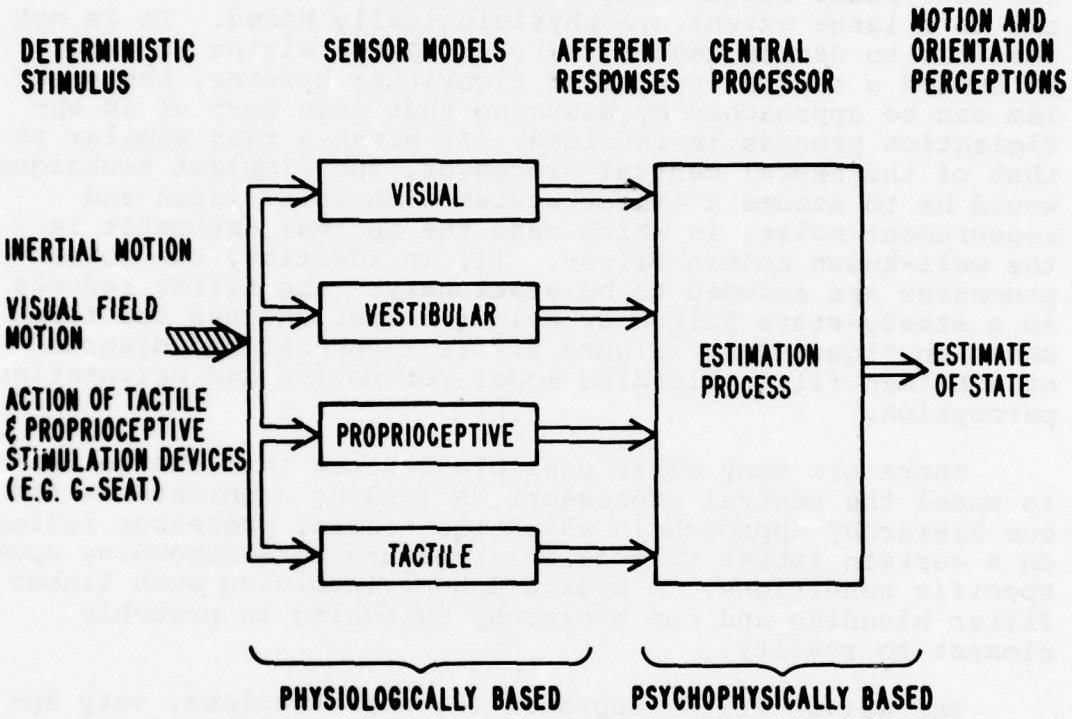

Figure 4.5 Basic structure of unified motion and orientation perception model.

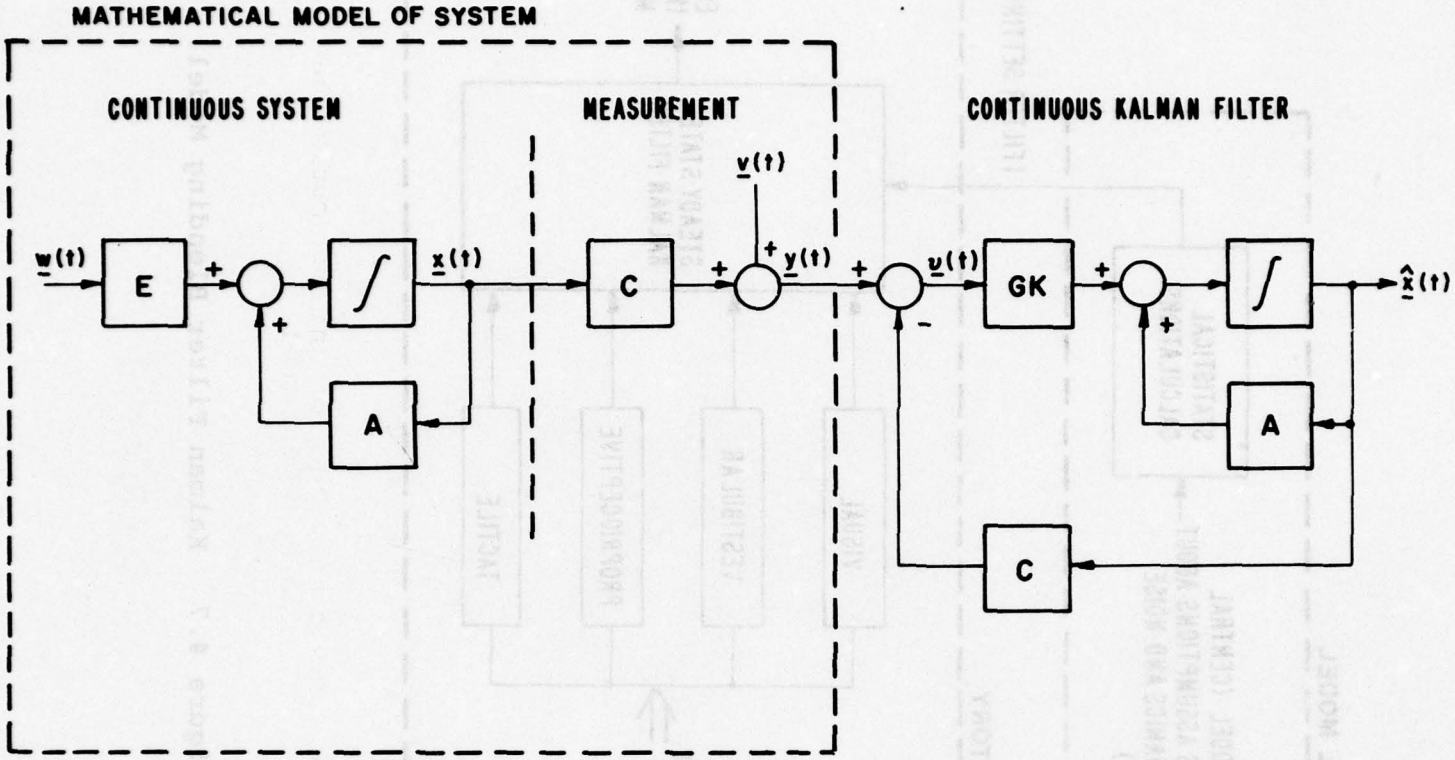

Figure 4.6 Continuous, steady state Kalman filter. (Redrawn from Gelb, 1974)

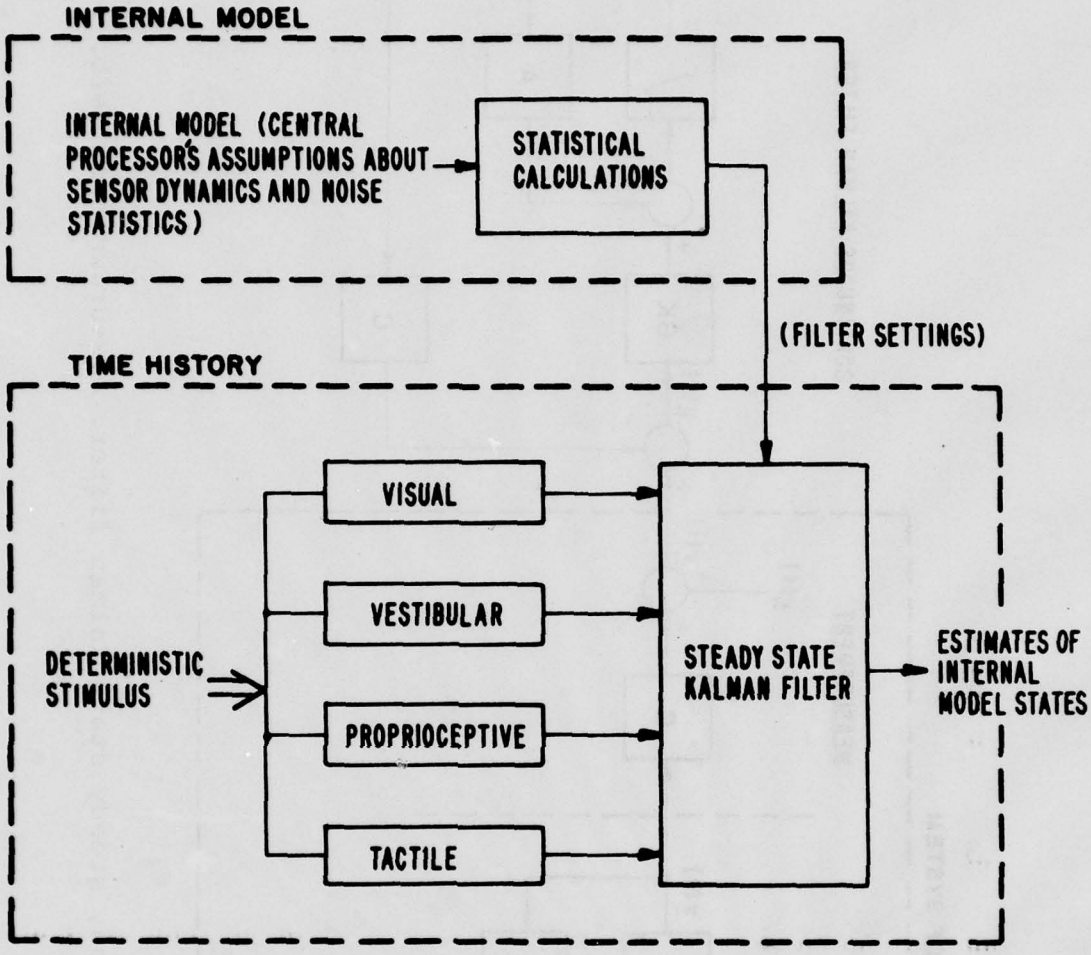

Figure 4.7 Kalman Filter Blending Model.

4.3.1 Internal Model

The internal model is the central processor's conception or view of the relation between the real world and the biological sensor systems. It is used only to derive optimal filter parameters, in our case Kalman gains, and must be linear since we are employing a linear filter. The only a priori knowledge specified by the internal model is an expected rms stimulus magnitude, an expected stimulus bandwidth, and an expected white measurement noise of known power.

Figure 4.8 shows the internal model structure used for the "vestibular system only" version of the Kalman filter blending model. The semicircular canal and otolith blocks are defined by the linear part of the sensor models derived in Section 3.2. All quantities of Figure 4.8 are defined in the head fixed coordinates system shown in Figure 4.9. The variables and parameters of Figure 4.8 are defined as follows:

$\underline{W}$	white noise process
$\underline{vel}$	velocity vector
$\underline{acc}$	acceleration vector (in gravity units)
$\underline{\gamma}$	rotation vector (integral of angular velocity) in radians
$\underline{\omega}$	angular velocity vector
$\vec{go}$	unit gravity vector when head is in upright position
$\underline{\Delta g}$	linearized difference between current unit gravity vector ($\vec{g}$) and $\vec{go}$
$\underline{sf}$	specific force (= $\underline{acc}$ - $\underline{g}$)
$\underline{v}$	measurement noise
$\underline{Y}$	neural afferent signals.

Note that the relations between $\underline{\gamma}$ and $\underline{\omega}$, and between $\underline{acc}$, $\underline{\gamma}$ and $\underline{sf}$ are accurate only for small γ and have been linearized about a 1g, head upright, condition.

77379

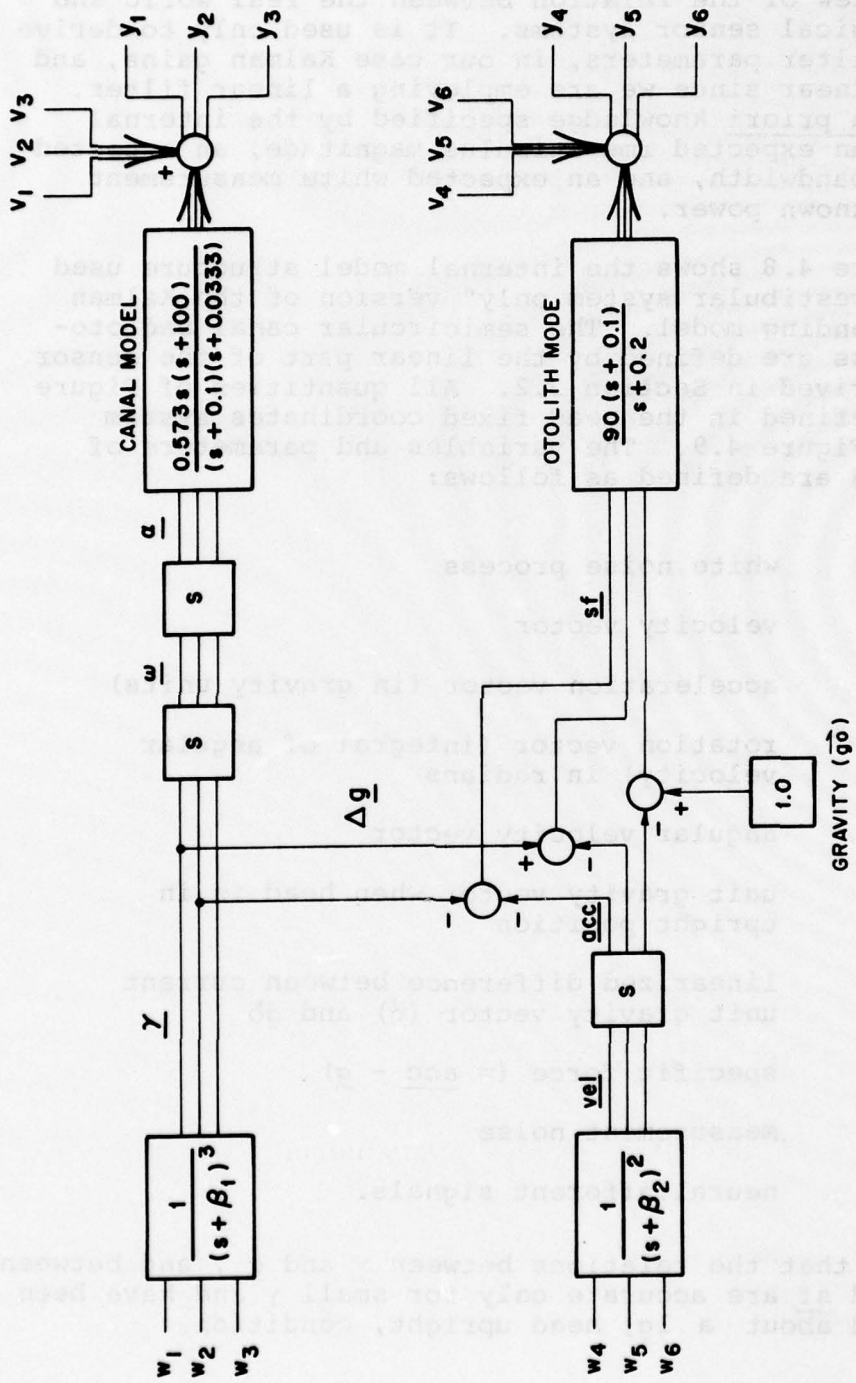

Figure 4.8 Internal Model with Vestibular System only.

77380

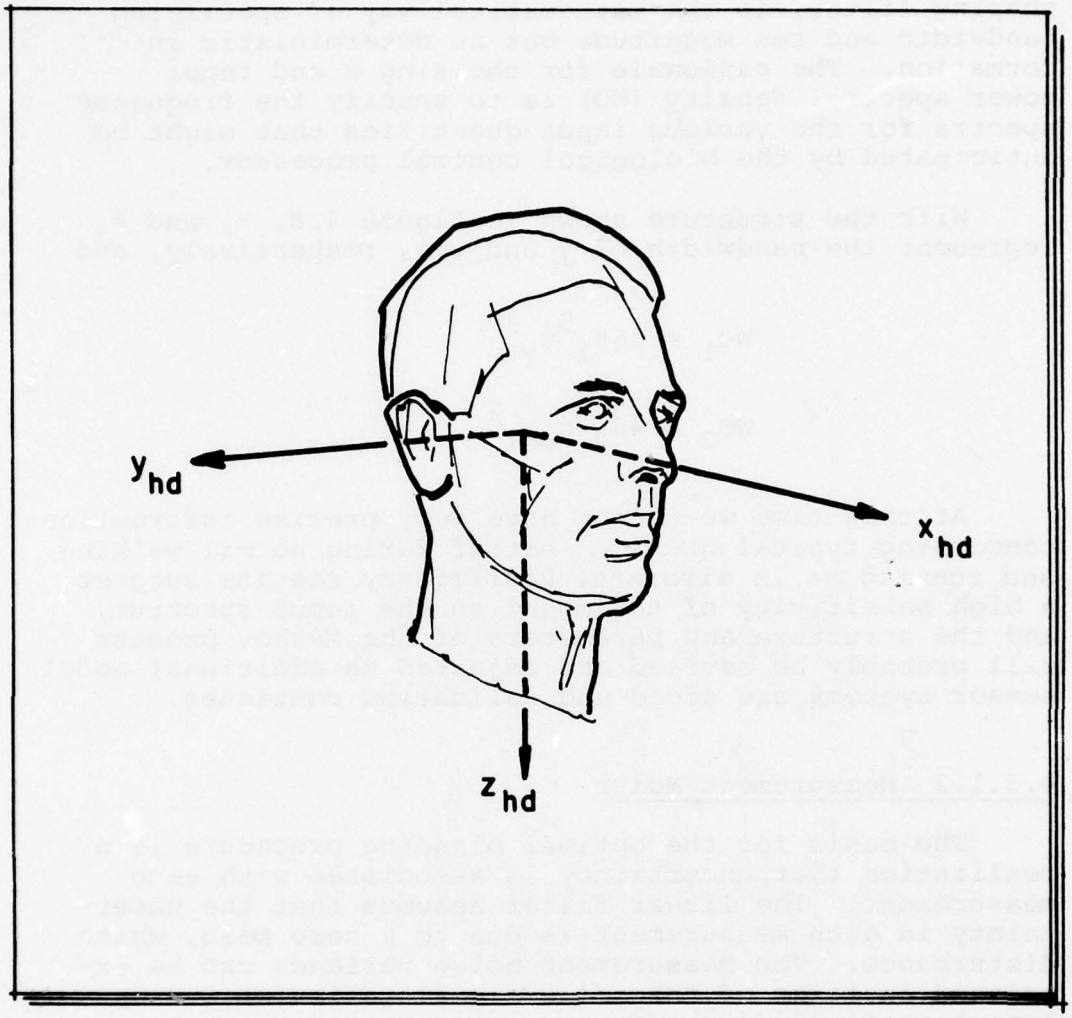

Figure 4.9 Head Coordinates.

4.3.1.1 Markov Process

The Markov process, a white noise followed by a shaping filter, is the mathematical way of specifying bandwidth and rms magnitude but no deterministic information. The rationale for choosing β and input power spectral density (WO) is to specify the frequency spectra for the various input quantities that might be anticipated by the biological central processor.

With the structure shown in Figure 4.8, β_1 and β_2 represent the bandwidth of $\dot{\gamma}$ and $\underline{vel}$, respectively, and

$$WO_1 = 16\beta_1^5\sigma_\gamma^2$$
$$WO_2 = 4\beta_2^3\sigma_{vel}^2 \qquad (4.1)$$

At this time we do not have very precise information concerning typical spectra, either during normal walking and running or in aircraft. Preliminary results suggest a high sensitivity of the model to the input spectrum, and the structure and parameters of the Markov process will probably be revised and adjusted as additional model sensor systems are added and validation continues.

4.3.1.2 Measurement Noise

The basis for the optimal blending procedure is a realization that uncertainty is associated with each measurement. The linear filter assumes that the uncertainty in each measurement is due to a zero mean, white disturbance. The measurement noise variance can be expressed in terms of the noise/signal ratio (ρ) and an output variance (σ_y^2) as

$$V_i = \rho_i\sigma_{y_i}^2 \qquad (4.2)$$

If nonlinearities are present, their effect can be included in terms of a describing function gain (see Section 4.3.1.3). If it is assumed that the central processor is dividing its attention between several tasks, attention fraction may also be included yielding

$$V_i = \frac{\rho_i \sigma_{y_i}^2}{(fa_i)(fn_i)^2} \qquad (4.3)$$

where fn is a random input describing function gain and fa is an attention fraction. This is the formulation used by Levison et. al. (1971).

Since we presently have no data that allow us to unambiguously distinguish the effects of ρ and fa, it has been decided to arbitrarily take fa as 1 for the case of a subject whose only task is to keep track of his orientation. As a starting value of ρ for the vestibular system contribution we have used .05, as computed from Shirley's data (Shirley, 1968) by Curry et. al. (1976). Preliminary results using this value appear to be reasonable (see Section 5.0). As the validation process continues, this parameter, along with input noise power and Markov process spectrum, will be adjusted to "tune" the model so that it matches known data as closely as possible. Eventually, when the "active pilot" is considered, fa will be adjusted as a function of differential pilot task loading.

4.3.1.3 Random Input Describing Function

Although the internal model must be linear for use in calculating Kalman gains, the biological central processor may have evolved to account, in its estimates, for some sensor nonlinearities. This can be handled in the model with random input describing functions (RIDFs). An RIDF consists of a linear gain (fn), chosen such that expected rms input values will result in the same rms outputs produced by the real nonlinearity.

The proper value of fn is determined by assuming that input to the nonlinearity is gaussian, and then minimizing the mean squared error of the describing function approximation. It can be shown that for a non-biased gaussian input

$$fn = \frac{1}{\sqrt{2\pi}\sigma^3} = \int_{-\infty}^{\infty} y(x) e^{(-x^2/2\ ^2)} dx \qquad (4.4)$$

where x = Gaussian input

σ = Standard deviation of input

y = Output from the nonlinearity as a function of x

For a threshold nonlinearity of the type shown in Figure 3.8 and 3.10 this reduces to

$$fn = 2\{1-PI(\frac{TH}{\sigma})\} + \frac{TH}{\sigma}\{(2)PF(\frac{TH}{\sigma})\} \qquad (4.5)$$

The functions PI and PF are plotted in Figure 4.10. For a rigorous derivation of random input describing functions see Gelb and VanderVelde (1968).

In the case of the semicircular canal model (see Section 3.2.1) σ is the standard deviation of the afferent output (calculation of covariance is described in Section 4.3.1.4). In the case of the otolith model (see Section 3.2.2) σ is the standard deviation of the state variable representing mechanical deflection of the otolith (calculation of state covariance is described in Section 4.3.1.5). The saccule nonlinearity (discussed in Section 3.2.2) is not represented by a describing function. The reason is that the nonlinearity was designed to produce the Aubert, Müller and elevator illusion affects--presuming the system does not try to correct for the nonlinearity when making estimates. The filter is, therefore, not "told" about the saccule nonlinearity.

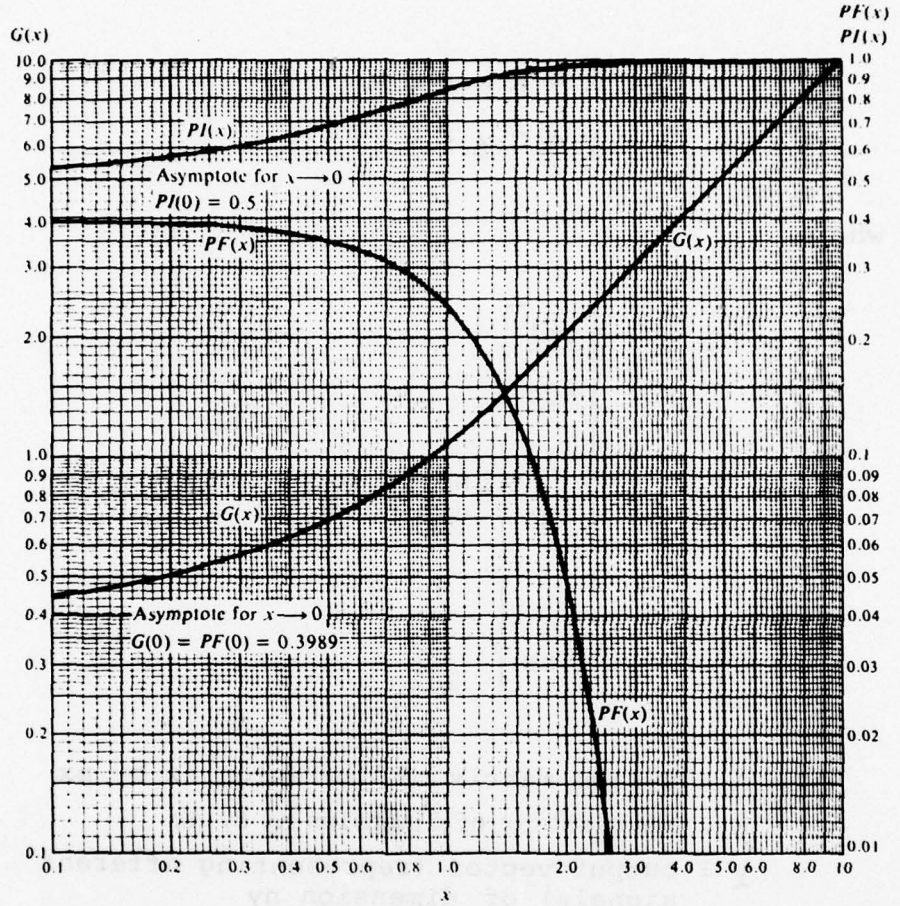

Figure 4.10 Graph of PF(x), PI(x), and G(x). (From Gelb & VanderVelde, 1968) (Copyright [1968] by McGraw Hill Book Co., used with permission of McGraw Hill Book Co.)

4.3.1.4 Steady State Kalman Filter Gain Calculation

The entire internal model of Figure 4.8 can be expressed in state vector form as

$$\dot{\underline{x}} = A\,\underline{x} + E\,\underline{w}$$
$$\underline{y} = C\,\underline{x} + \underline{v} \qquad (4.6)$$

where

$$\underline{x} = \begin{bmatrix} \underline{vel} \\ \underline{acc} \\ \underline{\gamma} \\ \underline{\omega} \\ \vdots \\ x_{nx} \end{bmatrix} \equiv \text{State vector of dimension nx}$$

A ≡ system matrix of dimension nx by nx

E ≡ input matrix of dimension nx by nw

$\underline{y}$ ≡ output vector (representing afferent signals) of dimension ny

C ≡ output observation matrix of dimension ny by nx

$\underline{v}$ ≡ measurement noise vector of dimension ny

nx ≡ number of state variables

nw ≡ number of white noise inputs

ny ≡ number of output observations

Appendix B contains the A, E, and C matrices used to obtain the results shown in Section 5.0. Note that $\underline{\gamma}$, $\underline{\omega}$, $\underline{vel}$, and $\underline{acc}$ (see Figure 4.9) must appear as state variables since the estimates of these states will represent the perceptual quantities desired. The remaining state variables need not have any physical significance.

Optimal steady-state Kalman filter gains are determined from the model of Equation 4.6 by solving the following well-known matrix equations.

1. Covariance of state (X).

   X is the solution of the linear matrix equation.

$$\dot{X} = 0 = AX + XA' + E\ WO\ E' \tag{4.7}$$

2. Covariance of observation (Y).

$$Y = C\ X\ C' \tag{4.8}$$

3. Error Covariance of the Kalman filter (S).

   S is the solution of the Matrix Riccati equation.

$$\dot{S} = 0 = A\ S + S\ A' + E\ WO\ E' - S\ C'\ V^{-1}\ C\ S \tag{4.9}$$

4. Covariance of the Kalman filter estimate (XH).

$$XH = X - S \tag{4.10}$$

5. Steady state Kalman filter gain matrix (GK)

$$GK = S\ C'\ V^{-1} \tag{4.11}$$

6. Filter system matrix (F)

$$F = (A - GK\ C) \tag{4.12}$$

4.3.2 Time History Response to Deterministic Stimuli

Once optimal Kalman gains have been calculated the filter can be implemented by satisfying

$$\dot{\hat{\underline{x}}} = F\,\hat{\underline{x}} + Gk\,\underline{y} \tag{4.13}$$

y_i are afferent signals received by the filter and x_i are the filter's estimates of internal model states. Figure 4.11 diagrams the time history calculation for the "vestibular system only" model.

The linear portion of each sensor model can be represented in state variable form as

$$\begin{aligned} \dot{\underline{x}} &= A\,\underline{x} + B\,\underline{u} \\ \underline{y} &= C\,\underline{x} \end{aligned} \tag{4.14}$$

where $\underline{x} \equiv$ sensor state vector
$B \equiv$ sensor input matrix
$\underline{u} \equiv$ deterministic stimulus
$\underline{y} \equiv$ afferent response
$C \equiv$ sensor output matrix

Equation 4.14 can be implemented on a computer by the discrete formulation

$$\underline{x}(t) = \Phi(\Delta t)\,\underline{x}(t-\Delta t) + DM(\Delta t)\,\underline{u}(t) \tag{4.15}$$

$$\Phi(\Delta t) = e^{A\,\Delta t} \tag{4.16}*$$

$$DM = \left[\int_0^{\Delta t} \Phi(v)\,dv\right]B \tag{4.17}$$

This formulation assumes that u(t) is approximated by a series of Δt duration steps.

---

* For a square matrix A, the matrix exponential is defined as:

$$e^A = I + A + \frac{A^2}{2!} + \frac{A^3}{3!} + \cdots\cdots$$

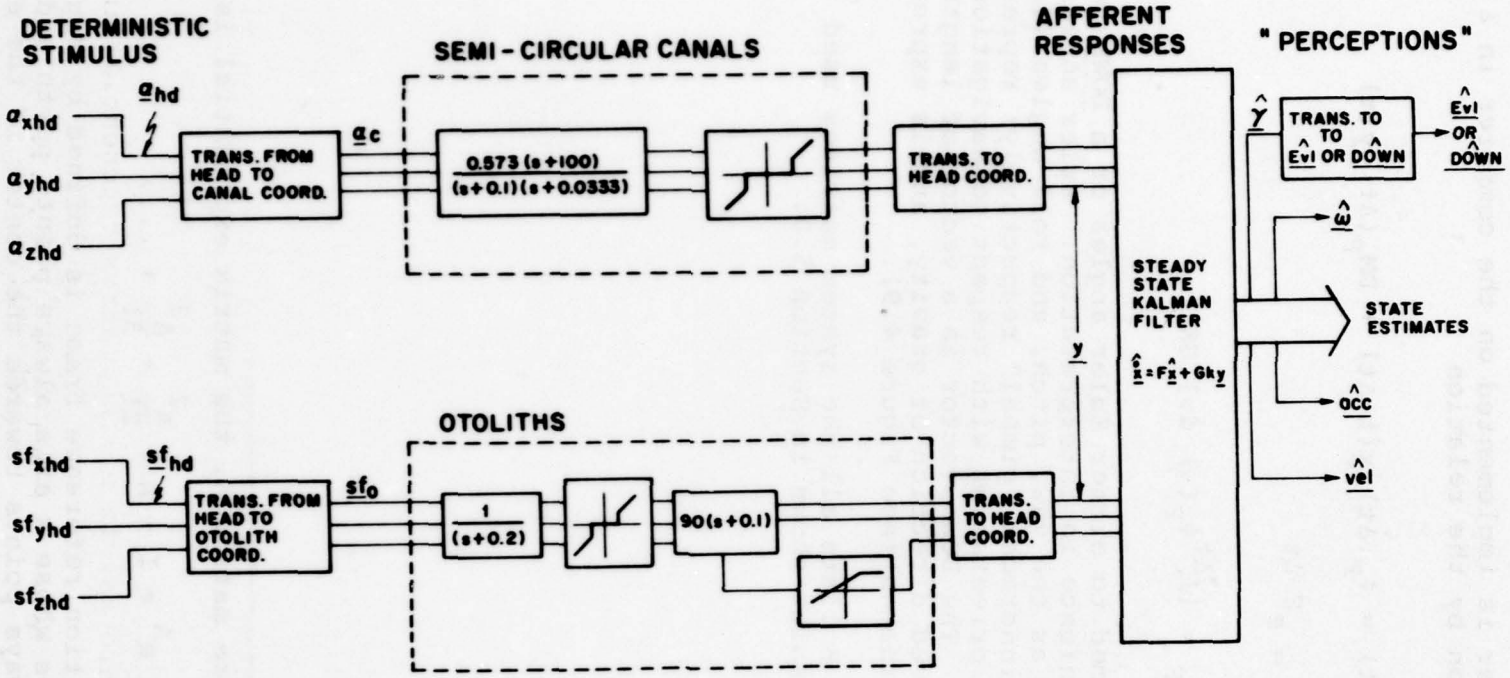

Figure 4.11 Time History Model with Vestibular System only.

The filter is implemented on the computer in a similar fashion by the relation

$$\underline{x}(t) = \Phi_F(\Delta t)\ \underline{x}(t-\Delta t) + DM_F(\Delta t)\ \underline{y}(t) \qquad (4.18)$$

$$\Phi_F = e^{F\ \Delta t} \qquad (4.19)^*$$

$$DM_F = [\int_o^{\Delta t} \Phi_F(\nu)\ d\nu]\ GK \qquad (4.20)$$

$\hat{\underline{y}}$ is transformed to either Euler angles or a DOWN vector for convenience in interpretation. Euler angles are expressed as the yaw, pitch, and roll angles (from outermost to innermost "gimbal" respectively) representing perceived orientation with respect to navigation coordinates.† The DOWN vector is a vector of length 1g in the perceived direction of gravity, and is expressed in head coordinates (see Figure 4.9).

Appendix B lists all the system matrices used to obtain the results shown in Section 5.0.

---

* For a square matrix A, the matrix exponential is defined as:

$$e^A = I + A + \frac{A^2}{2!} + \frac{A^3}{3!} + \ldots.$$

† The navigation reference frame is defined by right-handed coordinates whose x axis always points north and whose z axis always points towards the center of the earth.

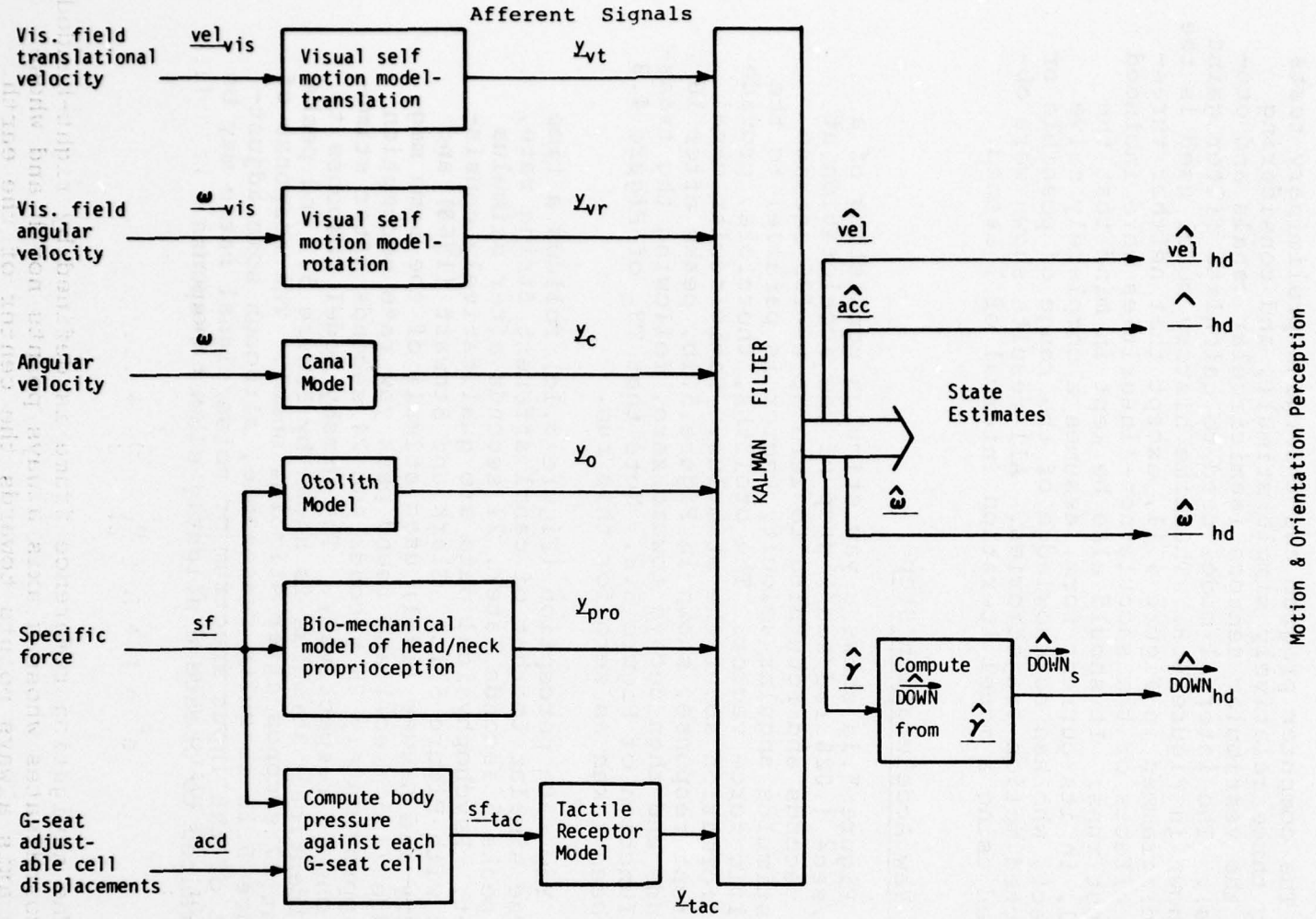

Figure 4.12 General Time History Model. (Has not been tested with visual, tactile and proprioceptive components.)

5.0 PRELIMINARY RESULTS

The computer program has undergone preliminary tests using three relatively simple stimuli, and considering only the vestibular sensors (semicircular canals and otoliths). The internal model used to calculate filter gains is shown in Figure 4.8. The time history model used is the one diagrammed in Figure 4.11, except that neither threshold effects or the saccule non-linearities were included in test runs. It should also be kept in mind that the model, in its current form, assumes a completely naive subject, who has no knowledge of the range of possible or expected motion trajectories. All results shown were obtained using a model iteration interval of 1 second.

5.1 Yaw Acceleration Step

Figure 5.1a shows a yaw stimulus consisting of a $1.5°/sec^2$ ($.026$ rad/sec^2) step of yaw acceleration at $t = 5$ seconds and returning to zero at $t = 125$ seconds. The stimulus angular velocity vector is parallel to the specific force vector. The otoliths, therefore, provide no information about the stimulus. Semicircular canal afferent response, shown in Figure 5.1b, peaks after 16 seconds and then decays toward zero, following the transfer function of Figure 3.8. Note that TH_c of Figure 4.8 has been taken as zero for this run.

Yaw rate perception (Figure 5.1c) follows a time course similar to that of canal afferent firing rate, but peaks 5 seconds later, 21 seconds after stimulus onset. Psychophysical data are qualitatively consistent with Figure 5.1c. Clark and Stewart (1968) and Guedry and Lauver (1961) used stimuli of the same magnitude ($1.5°/sec^2$) and found peak yaw rate perception at approximately 35 seconds and 24 seconds after stimulus onset, respectively. The Ormsby model response to an identical stimulus is shown by Figure 5.2 and peaks about 27 seconds after stimulus onset. The response of Figure 5.1c is quite reasonable, although some adjustment of the input spectrum or noise/signal ratio may be warranted to create a slightly slower response.

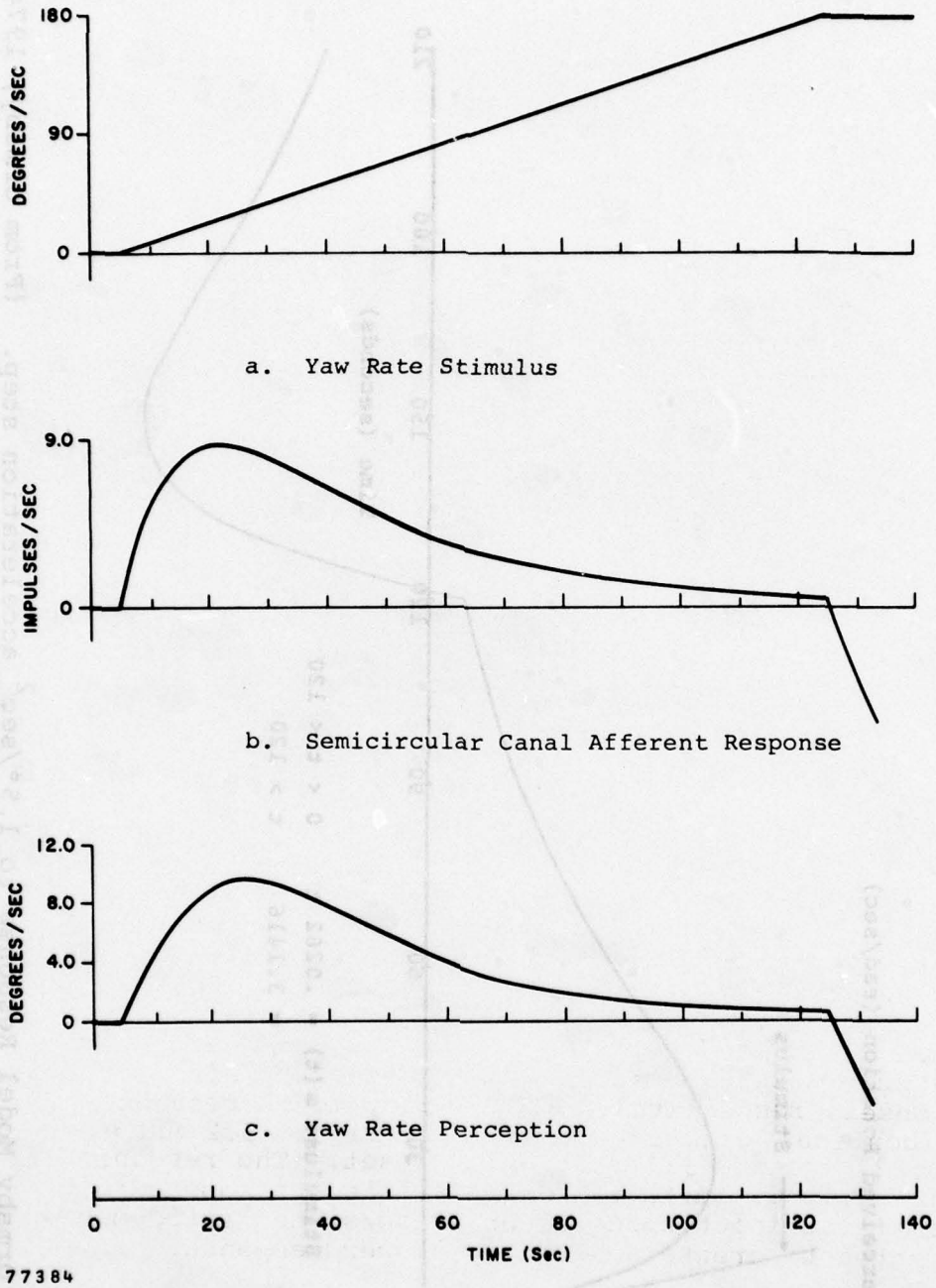

Figure 5.1 Model Response to 1.5°/sec^2 Yaw Acceleration Step.

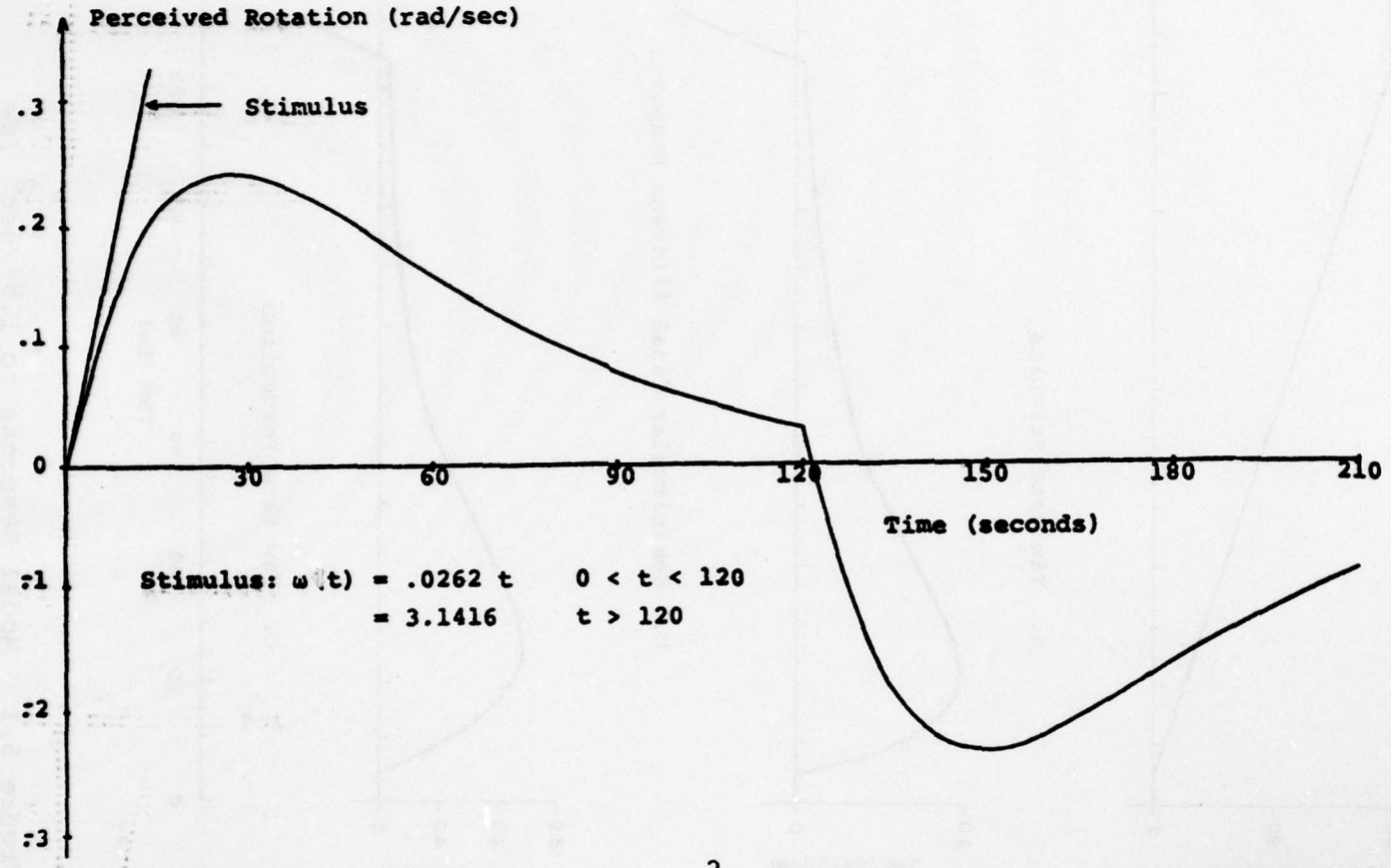

Figur 5.2 Ormsby Model Response to 1.5°/sec^2 acceleration step. (From Ormsby, 1974)

AD-A049 278 GULF AND WESTERN APPLIED SCIENCE LABS WALTHAM MA F/G 6/16
SENSORY MECHANISM MODELING.(U)
OCT 77 J BORAH, L R YOUNG, R E CURRY F33615-76-C-0039
UNCLASSIFIED AFHRL-TR-77-70 NL

2 OF 2
AD
A049278

END
DATE
FILMED
3-78
DDC

5.2 Forward Acceleration Step

Figure 5.3 shows the model response to a .2g step in forward acceleration. The stimulus causes the specific force vector to elongate and to rotate approximately .2 radians with respect to head fixed coordinates. This rotation is signaled by the otoliths (see Figure 5.3c). The head, however, has not rotated with respect to inertial space and the semicircular canals maintain a zero signal.

The model initially "trusts" the canals and attributes the specific force change to acceleration (see acceleration perception curve in Figure 5.3a). The initial acceleration perception then decays, and is replaced by a pitched-back sensation (see Figure 5.3a). In the steady state, the specific force direction is attributed primarily to pitch orientation, or stated another way, specific force direction is perceived to be the direction of gravity.

This type of response has long been observed by pilots during aircraft catapult launchings. Cohen et. al. (1973), using centrifuge simulations of the catapult launch, have obtained psychophysical data documenting a pitch-back sensation during forward acceleration.

Figure 5.3b indicates that there is never a very significant feeling of pitch velocity, (the semicircular canals continue to signal zero velocity) and pitch rate is not consistent with pitch attitude perception. We presently know of no data against which to check Figure 5.3b (angular velocity perception). The magnitudes shown in the figure are actually below the resolution of most psychophysical data. There are, however, well-documented situations which produce discrepancies between perceived orientation and perceived angular rate. A most dramatic instance occurs during visual circularvection about a horizontal axis. This stimulus causes the subject to feel a constant tilt angle with respect to gravity, and the contradictory sensation of constant horizontal angular velocity.

As in the case of the yaw stimulus, the responses of Figure 5.3a appear qualitatively correct, but validity of the time constants and magnitudes cannot be determined quantitatively from Figure 5.3. A more quantitative

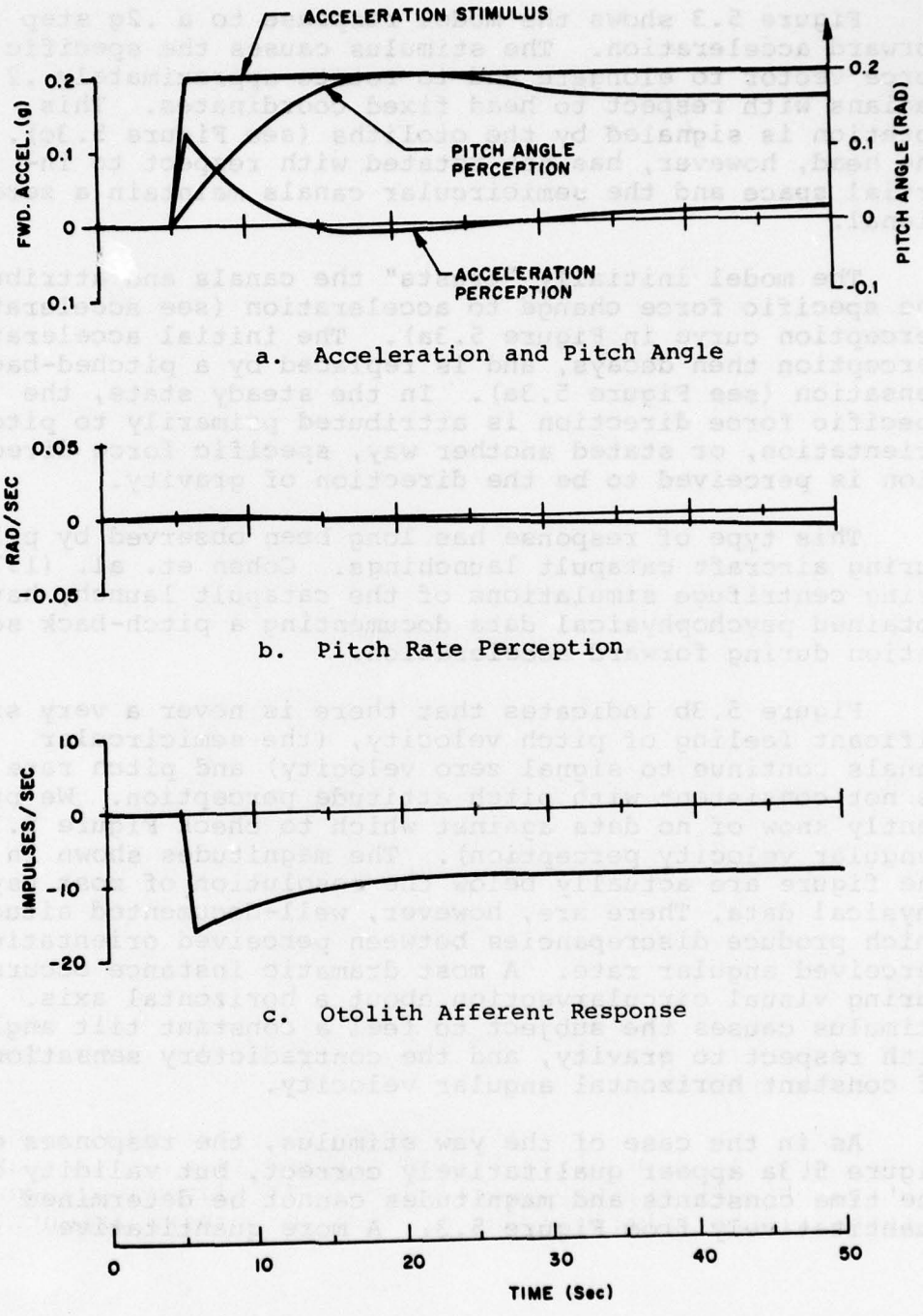

Figure 5.3 Model Response to .2g Forward Acceleration Step.

analysis can be performed by precisely inputting the Cohen et. al. (1973) catapult launch simulation profile, and comparing model output with those results. In addition, the frequency response of the model output can be determined and compared with Young and Meiry's (1968) velocity perception, frequency response data.

5.3 Pitch-Up to Constant Angle

A trapezoidal pitch rate stimulus was used to bring pitch angle to .2 rad over a 3-second period (see Figure 5.4a). Responses are evoked from both the semicircular canals and the otoliths during this stimulus (Figures 5.4c and 5.4d), with the semicircular canals responding to pitch specific force direction. Note that at a pitch of .2 rad (11.5°) the specific force vector has the same orientation with respect to head coordinates as during the .2g acceleration step.

Steady-state perception of pitch, pitch rate and forward acceleration (Figures 5.4a and 5.4b) are the same as the steady-state response to the .2g acceleration step (Figures 5.3a and 5.3b). The initial response, however, is quite different. Pitch perception (Figure 5.4a) now closely follows the time course of the pitch stimulus, pitch rate perception (Figure 5.4b) is consistent with attitude perception, and there is no longer a large initial perception of acceleration (Figure 5.4a). The semicircular canals have effectively "told" the system that the initial change in specific force direction is due to a change in pitch attitude, rather than forward acceleration, and the stimulus is correctly interpretted as such from its onset.

Experimental evidence does indicate that people are able to track both angular velocity and changes in their orientation with a fair degree of accuracy. Figures 5.5 and 5.6 are examples of subjective orientation angle and angular velocity tracking results.

The steady-state pitch perception in Figure 5.4a is smaller than true pitch but is within the standard deviation of most psychophysical data. The literature contains a substantial amount of data concerning orientation

77387

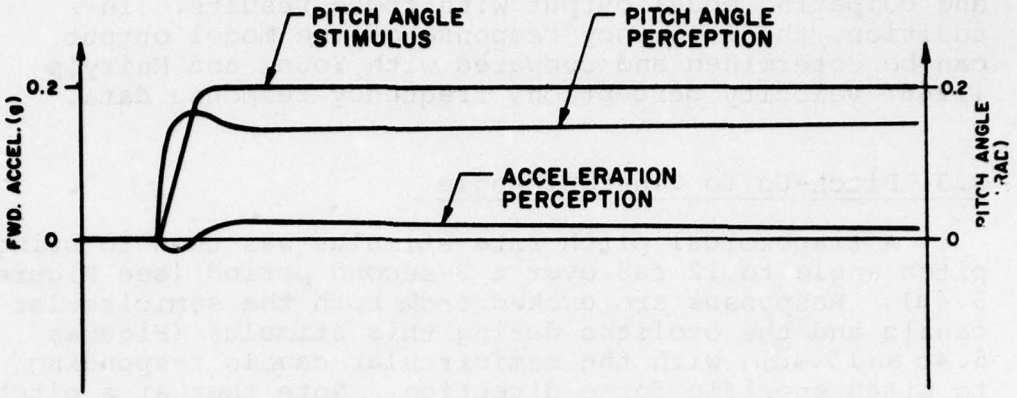

a. Acceleration and Pitch Angle

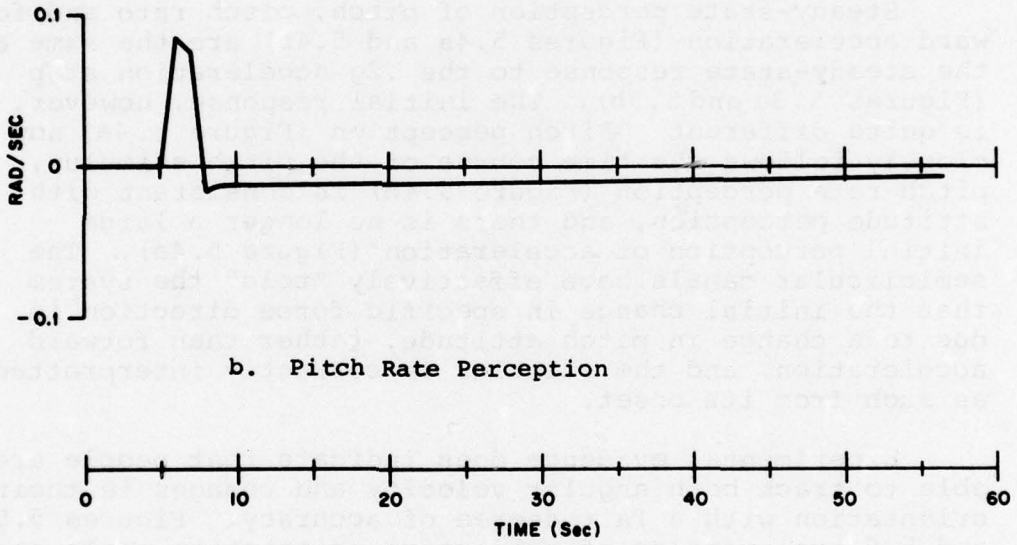

b. Pitch Rate Perception

Figure 5.4 Model Response to .2rad Pitch Up Stimulus.

77388

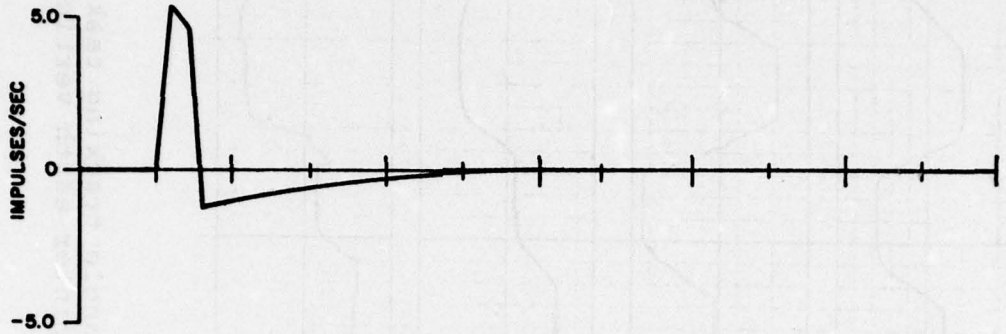

c. Canal Afferent Response

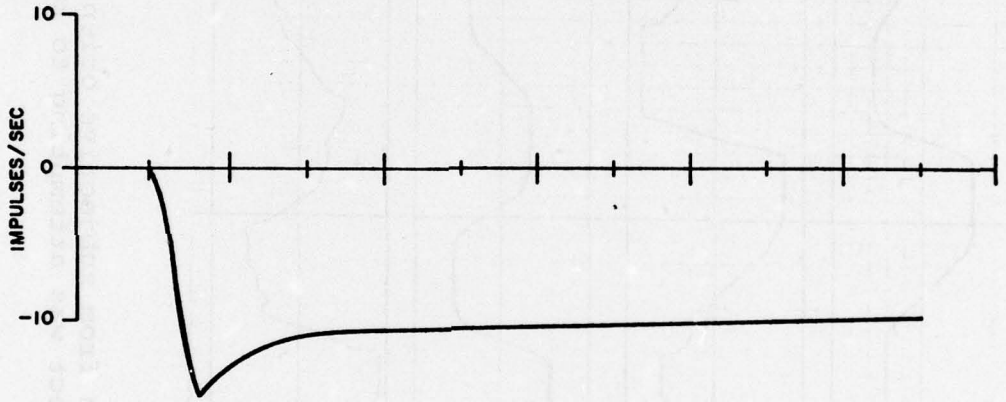

d. Otolith Afferent Response

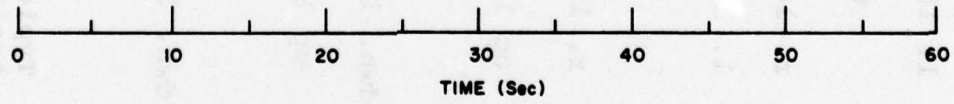

Figure 5.4 (Cont'd.) Model Response to .2rad Pitch Up Stimulus.

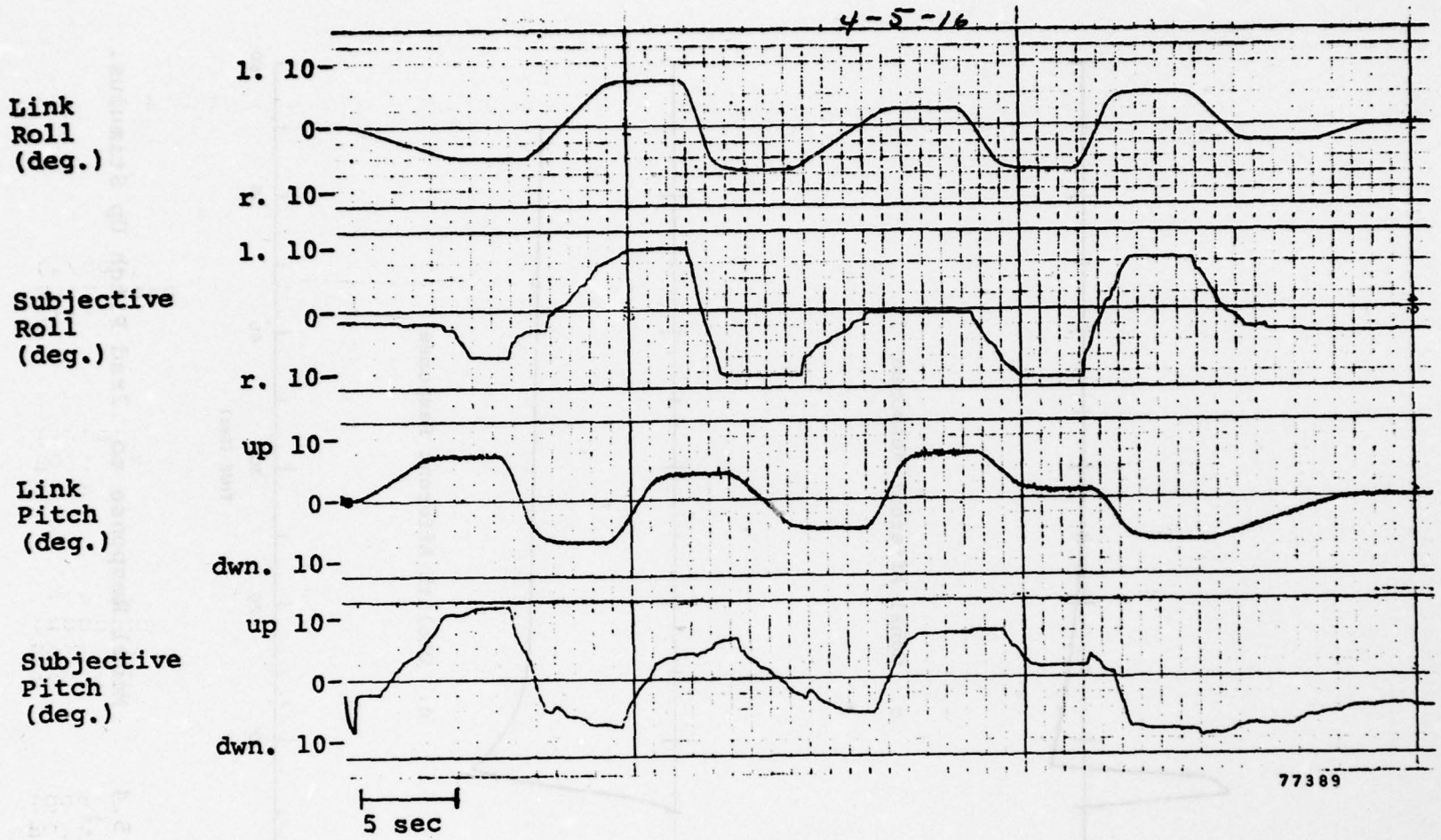

Figure 5.5 Typical results from subjective orientation angle tracking task in a Link trainer. Subject was attempting to keep a pointer earth vertical. (From Borah, 1976)

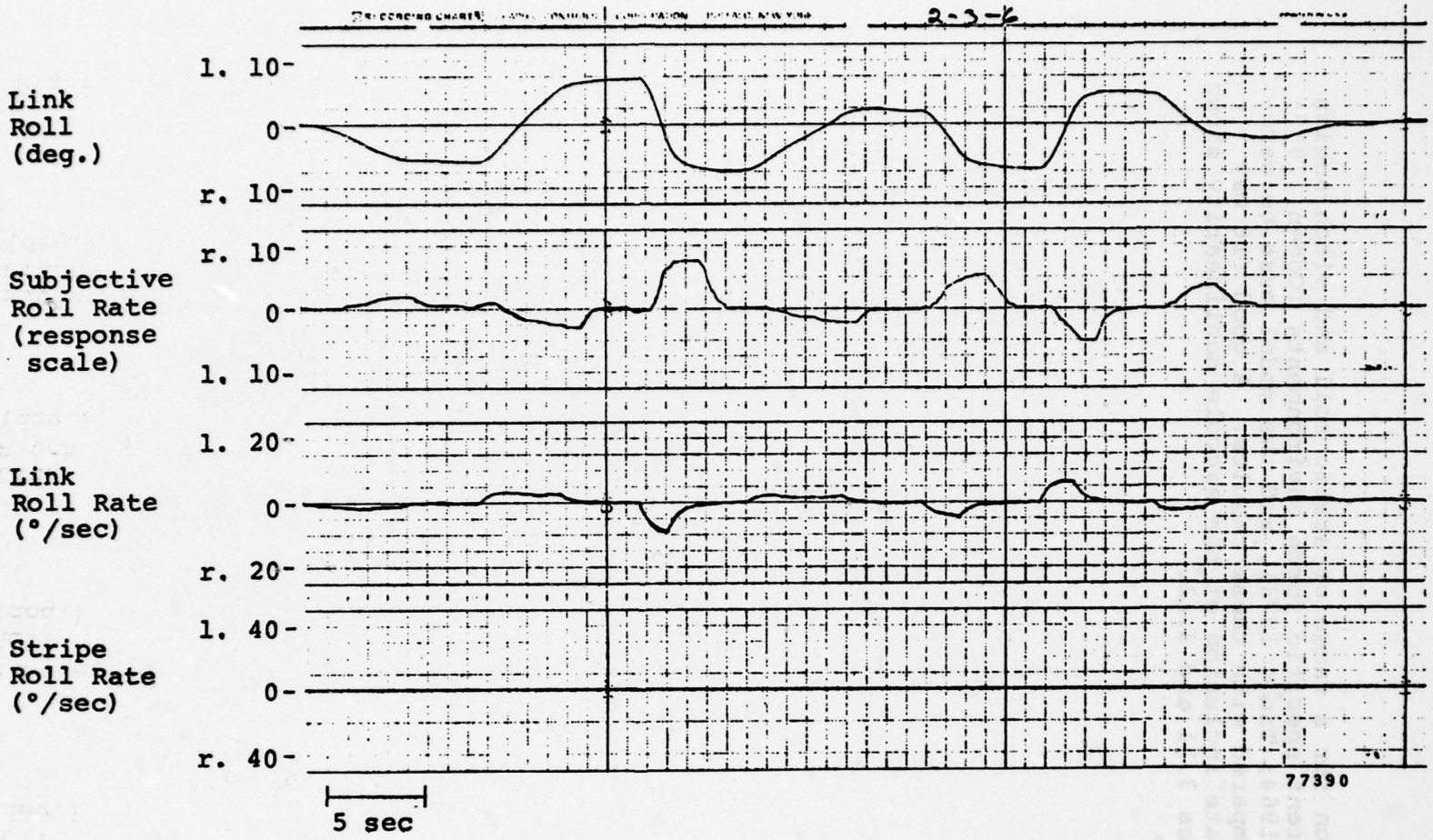

Figure 5.6 Subjective roll velocity magnitude estimation in a Link trainer. (From Borah, 1976).

perception for a range of static roll and pitch angles in different specific force environments (Cohen, 1973; Schöne, 1964; Tang, 1974), and the model must be carefully compared with these results. A good fit may necessitate inclusion of the saccule nonlinearity shown in Figures 3.11 and 3.12.

6.0 CONCLUSION AND RECOMMENDATIONS

6.1 Conslusion

Our goal has been to lay the groundwork for a unified motion and orientation perception model based upon integration of several different sensory modalities. The literature has been surveyed for available material concerning vestibular, visual, tactile, and proprioceptive systems as they relate to perception of motion and orientation. Although there are certainly gaps in our knowledge, a great deal is already known about how the visual and vestibular systems act individually and how they interact to influence subjective orientation and motion. This material has been reviewed, and is presented along with the individual vision and vestibular system models considered to be best suited to the problem at hand.

The tactile and proprioceptive modalities are less well-defined in terms of their relation to motion and orientation perception. A computer literature search was conducted in order to help identify available mechanoreceptor data. A tactile model has been proposed based on the observed dynamics of three distinct peripheral receptors, two of which are found near the skin surface and a third in subcutaneous tissue. The proposed model is aimed at analyzing the effect of seat pressure acting against various body surfaces. More data is needed, however, pertaining to wide area stimulation of skin surfaces and subjective interpretation of such stimuli.

The proprioceptive system is perhaps the least well-defined of the four modalities. It presents an especially difficult modeling problem because it is present at many locations over the body and involves different mechanical structures at each. As an initial attempt to include proprioception in a unified model, an adaptation of Gum's (1973) head/neck system model is proposed.

A detailed structure for a unified model has been outlined, using a Kalman filter blending approach to integration of different sensory modalities. The model structure has been translated into a flexible FORTRAN IV computer program, designed to output time history predictions of perceptual quantities given a time doman stimulus profile.

Preliminary trials of the program are quite promising but have so far included only the vestibular sensors (semicircular canals and otoliths) and have not yet considered threshold phenomena. Ongoing work is directed at further exercise and validation of the vestibular portion of the model, as well as implementation of the additional modalities. Modifications are expected as this work is pursued.

6.2 Recommendations for Additional Study

The required data concerning receptor physiology and the results of sensory interaction is by no means complete. Additional data in the following areas would be extremely helpful to modeling efforts:

1. Conflicting Otolith and Semicircular Canal Cues. There are several basic motion cue situations that commonly occur in aircraft, but are never experienced during normal walking and running. It would be useful to have more complete psychophysical data concerning acceleration, orientation, and angular velocity perception during sustained acceleration. Such data would be especially useful during "coordinated" maneuvers.

2. Visual-Vestibular Interaction During Rotation About a Horizontal Axis. There is significant work in the literature describing horizontal circularvection combined with various static orientation angles. The dynamic interaction between horizontal, inertial and visual field rotations needs further study.

3. Broad Surface Area Tactile Stimulation. The tactile cue processing model currently employed is based primarily on data generated from neural recordings or vibrotactile threshold measures in which small area stimuli were applied to the forearm or hand. The tactile cues of importance in motion simulation, however, include broad area, low frequency contact forces between the seat and the pilot's legs, buttocks and back. The use of a "g-seat" permits one to vary the surface distribution if not the total magnitude of supporting force. Study is required of the relationships among pressure threshold, surface area and psychophysical frequency response to tactile stimuli applied to these load bearing areas. Such experiments require the use of a controlled displacement, variable frequency vibrator, capable of applying and recording various pre-load forces, and equipped with contact heads of various sizes. Finally, definitive studies are required to generate the data base for g-seat generated sensations of tilt or linear acceleration, in the presence or absence of associated platform motion.

4. Typical Angular and Translational Velocity and Acceleration Spectra. Since the Kalman filter estimator is very sensitive to assumed input spectra, it would be particularly useful to have more complete information

about such spectra during aircraft flight (perhaps broken down by type of aircraft and/or type of mission), and during normal walking and running motions.

5. Effects of Pilot Workload and Level of Training on Threshold of Motion Detection. Thresholds for human detection of angular and translational accelerations play an important role in simulator motion drive design, and their accurate representation will also significantly enhance the utility of sensory system models. Most threshold figures currently available represent optimal detection conditions and may be unrealistic for application to a busy pilot performing demanding tasks. Experiments are needed to clarify the effect of workload and pilot skill, so that thresholds can be properly incorporated in perception models and applied to simulation problems. For example, pilots with different experience levels may be asked to signal their first feeling of angular motion while continuously performing a visual tracking task of varying difficulty. At each level of pilot skill and side task difficulty, threshold can be determined according to a standard double staircase technique for approaching the minimum detectable level from above and below.

References

1. Allum, J.H.J., Graf, W., Dichgans, J., Schmidt, C.L., "Visual-Vestibular Interactions in the Vestibular Nuclei of the Gold fish," Exp. Brain Res., 25:463-485, (1976).

2. Berthoz, A., Pavard, B., Young, L.R., "Perception of Linear Horizontal Self-Motion Induced by Peripheral Vision (Linearvection): Basic Characteristics and Visual-Vestibular Interactions," Exp. Brain Res., 23:471-489, (1975).

3. Borah, J., "Human Dynamic Orientation Model Applied to Motion Simulation," S.M. Thesis, Department of Aeronautics and Astronautics, MIT, (1976).

4. Burgess, P.R., "Cutaneous Mechanoreceptors," Handbook of Perception, Carterette and Friedman (Eds.), Academic Press, New York, (1973).

5. Chambers, M.R., Andres, K.H., Duering, M., Iggo, A., "The Structure & Function of the Slowly Adapting Type II Mechanoreceptor in Hairy Skin," Quart. J. Exp. Physiol., 57:417-455, (1972).

6. Chu, W., "Dynamic Response of Human Linearvection," S.M. Thesis, Department of Aeronautics and Astronautics, MIT, (1976).

7. Clark, B, Stewart, J.D., "Magnitude Estimates of Rotational Velocity During and Following Prolonged Increasing, Constant, and Zero Acceleration," J. Exp. Psychol., 78:329-339, (1968).

8. Cohen, M.M., "Elevator Illusion: Influence of Otolith Organ Activity and Neck Proprioception," Perception & Psychophysics, 14(3):401-406, (1973).

9. Cohen, M.M., Crosbie, R.J., Blackburn, L.H., "Disorienting Effects of Aircraft Catapult Launchings," Aerospace Med., 44(1):37-39, (1973).

10. Curry, R.E., Hoffman, W.C., Young, L.R., "Pilot Modeling for Manned Simulation," AFFDL-TR-76-124, (1976).

11. Daunton, N.G., Thomsen, D.D., "Otolith-Visual Interactions in Single Units of Cat Vestibular Nuclei," Neuroscience Abstracts, 2:1057, (1976).

12. Dichgans, J., Schmidt, C.L., Graf, W., "Visual Input Improves the Speedometer Function of the Vestibular Nuclei in the Goldfish," Exp. Brain Res., 18:319-322, (1973).

13. Fernandez, C., Goldberg, J.M., "Physiology of Peripheral Neurons Innervating Otolith Organs of the Squirrel Monkey, I, II, and III," J. Neurophysiol., 39:970-1008, (1976).

14. Gelb, A., (ed.), Applied Optimal Estimation, Cambridge, MIT Press, 1974.

15. Gelb, A., VanderVelde, W.E., Multiple Input Describing Functions and Nonlinear System Design, New York, McGraw-Hill, (1968).

16. Goldberg, J.M., Fernandez, C., "Physiology of Peripheral Neurons Innervating Semicircular Canals of the Squirrel Monkey, I, II, and III," J. Neurophysiol., 34:661-675, (1971).

17. Guedry, F.E., Lauver, L.S., "Vestibular Reactions During Prolonged Constant Angular Acceleration," J. Appl. Physiol., Vol. 16, (1961).

18. Gum, D.R., "Modeling of the Human Force and Motion-Sensing Mechanisms," AFHRL-TR-72-54, (1973).

19. Henn, V., Young, L.R., Finley, C., "Vestibular Nucleus Units in Alert Monkeys are also Influenced by Moving Visual Field," Brain Res., 71:144-149, (1974).

20. Houk, J., Henneman, E., "Responses of Golgi Tendon Organs to Active Contractions of the Soleus Muscle of the Cat," J. Neurophysiol., 30:466-481, (1967).

21. Howard, I.P., Templeton, W.B., Human Spatial Orientation, John Wiley & Sons, New York, (1966).

22. Iggo, A., Muir, A.R., "The Structure and Functions of a Slowly Adapting Touch Corpuscle in Hairy Skin," J. Physiol., 300:762-69, (1969).

23. Kenton, B., Kruger, L., Woo, M., "Two Classes of Slowly Adapting Mechanoreceptive Fibers in Reptile Cutaneous Nerve, J. Physiol., 212:21-44, (1971).

24. Kleinman, D.L. Baron, S. Levison, W.H., "An Optimal Control Model of Human Response, Part 1: Theory & Validation," Automatica, Vol. 6, 357-369, (1970).

25. Knibestol, M., Vallbo, A.B., "Single Unit Analysis of Mechamoreceptor Activity from the Human Glabrous Skin," Acta Physiol. Scand., 80:178-195, (1970).

26. Kruger, L., Kenton, B., "Quantitative Neural and Psychophysical Data for Cutaneous Mechanorecpetor Function," Brain Res., 49:1-24, (1973).

27. Levison, W.H., Elkind, J.I., Ward, J.L., "Studies of Multivariable Manual Control Systems: A Model for Task Interference," NASA CR-1746, (1971).

28. Lowenstein, W.R., "Mechano-electric Transduction in the Pacinian Corpuscle, Initiation of Sensory Impulses in Mechanoreceptors," Handbook of Sensory Physiology, Vol. I, W.R. Lowenstein (ed.), Springer-Verlag, Berlin, (1971).

29. Makarov, P.O., Matoyan, D.S., "Topaxia: The Significance of the Spatial Factor in the Excitability of the Cutaneous Sensory System in Man," Biofizika, 13(4):662-669, (1968).

30. Meiry, J.L., "The Vestibular System and Human Dynamic Space Orientation," Sc.D. Thesis, Department of Aeronautics and Astronautics, MIT, (1965).

31. Mountcastle, V.B., "Sensory Receptors and Neural Encoding: Introduction to Sensory Processes," Medical Physiology, 13th Edition, V.B. Mountcastle (ed.), C.V. Mosby Company, St. Louis, (1974).

32. Mountcastle, V.B., "The Problem of Sensing and the Neural Coding of Sensory Events," The Neurosciences, Rockefeller Univ. Press., New York, (1967).

33. Nashner, L.M., "Sensor Feedback in Human Posture Control," Sc.D. Thesis, Department of Aeronautics & Astronautics, MIT, (1970).

34. Ormsby, C., "Model of Human Dynamic Orientation," Ph.D. Thesis, Department of Aeronautics and Astronautics, MIT, (1974).

35. Ormsby, C., Young, L.R., "Perception of Static Orientation in a Constant Gravitoinertial Environment," Aviation Space and Environ. Med., 47:159-164, (1976).

36. Shirley, R.S., "Motion Cues in Man-Vehicle Control," ScD. Thesis, MIT, Man-Vehicle Lab, Report MVT-68-1, (1968).

37. Shöne, H., "On the Role of Gravity in Human Spatial Orientation," Aerospace Med., 35, 1964.

38. Talbot, S.A., Gessner, V., Systems Physiology, New York, Wiley, 1973.

39. Tang, J., "Interaction Between Visually Induced and Real Lateral Tilts," S.M. Thesis, Department of Aeronautics and Astronautics, MIT, (1974).

40. Verrillo, R.T., "Vibrotactile Thresholds for Hairy Skin," J. Exp. Psychol., 73:47-50, (1966).

41. Waespe, W., Henn, V., "Neuronal Activity in the Vestibular Nuclei of the Alert Monkey During Vestibular and Optikenetic Stimulation," Exp. Brain Res., (In Press), (1977).

42. Werner, G., Mountcastle, V.B., "Neural Activity in Mechano-Receptive Cutaneous Afferents: Stimulus-Response Relations, Weber Functions, and Information Transmission," J. Neurophysiol., 28:359-397, (1965).

43. Young, L.R., Dichgans, J., Murphy, R., Brandt, T., "Interaction of Optokinetic and Vestibular Stimuli in Motion Perception," Acta Otolaryng, 76:24-31, (1973).

44. Young, L.R., Meiry, J.C., "A Revised Dynamic Otolith Model," Aerospace Med., 39(6):606-608, (1968).

45. Young, L.R., Oman, C.M., "Model for Vestibular Adaptation to Horizontal Rotation," Aerospace Med., 40:1076-1080, (1969).

46. Zacharias, G.L., Young, L.R., "Manual Control of Yaw Motion with Combined Visual and Vestibular Cues," Annual Conference of Manual Control, MIT, (1977).

47. Zacharias, "Motion Sensation Dependence on Visual and Vestibular Cues," Ph.D. Thesis, Department of Aeronautics and Astronautics, MIT, 1977.

APPENDIX A

MECHANORECEPTOR LITERATURE SEARCH RESULTS

TACTILE SENSOR SYSTEMS

Neurophysiology

1. Burgess, P.R., "Cutaneous Mechanoreceptors," Handbook of Perception, Vol. III, Carterette and Friedman, (eds.), Academic Press, New York, (1973).

2. Byrne, Castellucci, and Kandel, "Receptive Fields and Response Properties of Mechanoreceptor Neurons Innervating Siphon Skin and Mantle Shelf in Aplysia," J. Neurophysiol., 37(5):1041-64, (1974).

3. Chambers, M.R., Andres, K.H., Duering, M., and Iggo, A., "The Structure & Function of the Slowly Adapting Type II Mechanoreceptor in Hairy Skin," Quart. J. Exp. Physiol., 57:417-445, (1972).

4. Darian-Smith, I., Rowe, M.J., Sessle, B.J., "Tactile Stimulus Intensity: Information Transmission by Relay Neurons in Different Trigeminal Nuclei," Science, 160: 781-94, (1968).

5. Harrington, T., Merzenich, M.M., "Neural Coding in the Sense of Touch," Exp. Brain Res., 10:251-264, (1970).

6. Iggo, A., Muir, A.R., "The Structure and Function of a Slowly Adapting Touch Corpuscle in Hairy Skin," J. Physiol., 200:762-69, (1969)

7. Janig, W., Schmidt, R.F., and Zimmermann, M., "Single Unit Responses and the Total Afferent Outlaw from the Cat's Foot Pad Upon Mechanical Stimulation," Exp. Brain Res., (1968).

8. Janig, W., Schmidt, R.F., and Zimmermann, R., "Two Specific Feedback Pathways to the Central Afferent Terminals of Phase and Tonic Mechanoreceptors," Exp. Brain Res., (1968).

9. Janig, W., "Morphology of Rapidly and Slowly Adapting Mechanoreceptors in the Hairless Skin of the Cats Hind Foot," Brain Res., 28:217-231, (1971).

10. Kenton, B., Kruger, L., and Woo, M., "Two Classes of Slowly Adapting Mechanoreceptor Fibers in Reptile Cutaneous Nerve," J. of Physiol., 212:21-44, (1971).

Neurophysiology (Cont'd.)

11. Knibestol, M., "Stimulus-Response Functions of Rapidly Adapting Mechanoreceptors in the Human Glabrous Skin Area," J. Physiol., 232:427-52, (1973).

12. Knibestol, M., and Vallbo, A.B., "Single Unit Analysis of Mechanoreceptor Activity from the Human Glabrous Skin," Acta Physiol. Scand., 80:178-95, (1970).

13. Loewenstein, W.R. (ed.) "Mechano-electric Transduction in the Pacinian Corpuscle, Initiation of Sensory Impulses in Mechanoreceptors," Handbook of Sensory Physiology, Vol. I, W. R. Loewenstein (ed.), Springer-Verlag, Berlin, (1971).

14. Mountcastle, V.B., "The Problem of Sensing and the Neural Coding of Sensory Events," The Neurosciences, Vol. I, (1971).

15. Mountcastle, V.B., Talbot, William, H., Kornhuber, H.H., "The Neural Transformation of Mechanical Stimuli Delivered to the Monkey's Hand," Ciba Foundation Symposium; Touch Heat and Pain, London, 325-351, (1966).

16. Paul, R.L., Merzenich, M., Goodman, H., "Representation of Slowly and Rapidly Adapting Cutaneous Mechanoreceptors of the Hand in Brodmann's Areas 3 and 2 of Macaca Mulatta," Brain Res., 35(2):229-249, (1972).

17. Pasechnik, V.I., "Possible Mechanism of the Work of an Elementary Mechanosensitive Centre," Biofizika, No. 6, 1020-1024, (1974).

18. Pasechnik, V.I., "Fluctuations in the Receptor Potential of the Pacini Corpuscle," Biofizika, No. 1, 82-87, (1975).

19. Pyatigorskii, B. Ya., "Spontaneous Activity of Primary Central Neurons of the Ascending Pathways for Cutaneous Sensitivity," Biofizika,. 516-523, (1967).

20. Werner, G., Mountcastle, "Quantitative Relations Between Mechanical Stimuli to the Skin and Neural Responses Evoked by Them," Skin Senses, 112-137, (1968).

21. Werner, G., Mountcastle, V.B., "Neural Activity in Mechano-Receptive Cutaneous Afferents: Stimulus-Response Relations Weber Functions, and Information Transmission," J. Neurophysiol., 28:359-397, (1965).

Psychophysics

1. Bliss, J.C., Crane, H.D., "Experiments in Tactual Perception," NASA-CR-322, (1965).

2. Bliss, J.C., Brody, W.R., Crane, H.D., Lane, B., Link, S.W., "Tactual Perception--Experiments and Models," NASA-CR-623, (1967).

3. Bliss, J.C., "Tactual Perception--Experiments and Models Final Report," NASA-CR-73135, (1967).

4. Bliss, J.C., Hill, J.W., Wilber, B.M., "Characteristics of Tactile Information Channel," NASA-CR-1389, (1969).

5. Craig, J.C., "Vibrotactile Difference Thresholds for Intensity and the Effect of a Masking Stimulus," Perception & Psychophysics, Vol. 15(1), 1974.

6. Gardner, E.P., Spencer, W.A., "Sensory Funnelling: I. Psychophysical Observations of Human Subjects and Responses of Cutaneous Mechanoreceptive Afferents in the Cat to Patterned Skin Stimuli," J. Neurophysiol., Vol. 35(6), (1972).

7. Makarov, P.O., Matoyan, D.S., "Topaxia: The Significance of the Spatial Factor in the Excitability of the Cutaneous Sensory System in Man," Biofizika, 13(4): 662-669, (1968).

8. Moore, T.J., Mundie, J.R., "Measurement of Specific Mechanical Impedance of the Skin: Effects of Static Force, Site of Stimulation, Area of Probe, and Presence of a Surround," J. Acoust. Soc. Am., Vol. 52, (1972).

9. Talbor, W.H., Darian-Smith, I., Kornhuber, H.H., Mountcastle, V.B., "The Sense of Flutter-Vibration: Comparison of the Human Capacity with Response Patterns Mechanoreceptive Afferents from the Monkey Hand," J. Neurophysiol., Vol. 31, (1968).

10. Verrillo, R.T., "Temporal Summation of Vibratactile Sensitivity," J. Acoust. Soc. Am., Vol. 37, (1965).

11. Verrillo, R.T., "Effect of Spatial Parameters on the Vibrotactile Threshold," J. Exp. Psychol., Vol. 71, (1966).

12. Verrillo, R.T., "Vibrotactile Thresholds for Hairy Skin," J. Exp. Psychol., Vol. 72, (1966).

Neurophysiology & Psychophysics

1. Kruger, L., Kenton, B., "Quantitative Neural and Psychophysical Data for Cutaneous Mechanoreceptor Function," Brain Res., Vol. 49:1-24, (1973).

PROPRIOCEPTIVE SENSOR SYSTEMS

Neurophysiology

1. Anderson, J.H., "Dynamic Characteristics of Golgi Tendon Organs," Brain Res., Vol. 67, (1974).

2. Chaplain, R.A., "Small-Signal Analysis of the Encoder Mechanism in the Lobster Receptor and the Frog and Cat Muscle Spindle," Biol. Cybernetics, 19(2):95-104, (1975).

3. Clark, F.J., Burgess, P.R., "Slowly Adapting Receptors in Cat Knee Joint: Can they signal joint angle?" J. Neurophysiol., Vol. 38(6):1448-1463, (1975).

4. Coenen, R., Chaplain, R.A., "Systems Analysis of Biological Receptors," Kybernetik, 13(4):183-93, (1973).

5. Hasan, Z., Houk, J.C., "Transition in Sensitivity of Spindle Receptors that Occurs when Muscle is Stretched More than a Fraction of a Millimeter," J. Neurophysiol., 38(3):673-89, (1975).

6. Hasan, Z , Houk, J.C., "Analysis of Response Properties of Deefferented Mammalian Spindle Receptors Based on Frequency Response," J. Neurophysiol., 38(3):663-72, (1975).

7. McCall, W.D., Jr., Farias, M.C., Williams, W.J., BeMent, S.L., "Static and Dynamic Responses of Slowly Adapting Joint Receptors," Brain Res., 70:221-243, (1974).

8. Milgram, P., Gideon, F.I., "Distortion Suppression in Neuromuscular Information Transmission Due to Interchannel Dispersion in Muscle Spindle Firing Thresholds," IEEE Transactions on Biomedical Engineering, Vol. BME-23, No. 1, (1976).

9. Murphy, J.T., Wong, Y.C., Kwan, H.C., "Afferent-Efferent Linkages in Motor Cortex for Single Forelimb Muscles," J. Neurophysiol., 38(4):990-1014, (1975).

10. Naeige, M., Crowe, A., deKlerk, H., "Model of the Firing Frequency of the Chelonian Muscle Spindle," Biol. Cybernetics, 21(1):53-60, (1976).

11. Taylor, A., "G. Progress with Modelling Neuromuscular Control Systems," Nature, 250(463):265-6, (1974).

Psychophysics

1. Horch, K.W., Clark, F.J., Burgess, P.R., "Awareness of Knee Joint Angle Under Static Conditions," J. Neurophysiol., Vol. 38(6):1436-1447, (1975).

GENERAL MECHANORECEPTOR MODELS AND PHYSIOLOGY

1. Goldman, D.E., "The Transducer Action of Mechanoreceptor Membranes," Cold Spring Harbar Symposia on Quantitative Biology, Vol. 30:59-68, (1965).

2. Teorell, T., "A Biophysical Analysis of Mechano-Electrical Transduction," Handbook of Sensory Physiology, Vol. I, Principles of Receptor Physiology, W.R. Loewenstein (ed.), Springer-Verlag, Berlin, (1971).

APPENDIX B

PARAMETERS AND MATRICES USED FOR MODEL RESULTS PRESENTED IN SECTION 5.0

INTERNAL MODEL: $\dot{\underline{x}} = A\,\underline{x} + E\,\underline{w}$

$\underline{y} = C\,\underline{x} + \underline{v}$

A

1	-0.	-0.	-0.	1.000	-0.
	-0.	-0.	-0.	-0.	-0.
	-0.	-0.	-0.	-0.	-0.
	-0.	-0.	-0.	-0.	-0.
	-0.	-0.	-0.	-0.	-0.
2	-0.	-0.	-0.	-0.	1.000
	-0.	-0.	-0.	-0.	-0.
	-0.	-0.	-0.	-0.	-0.
	-0.	-0.	-0.	-0.	-0.
	-0.	-0.	-0.	-0.	-0.
3	-0.	-0.	-0.	-0.	-0.
	1.000	-0.	-0.	-0.	-0.
	-0.	-0.	-0.	-0.	-0.
	-0.	-0.	-0.	-0.	-0.
	-0.	-0.	-0.	-0.	-0.
4	-0.	-0.	-0.	-0.	-0.
	-0.	1.000	-0.	-0.	-0.
	-0.	-0.	-0.	-0.	-0.
	-0.	-0.	-0.	-0.	-0.
	-0.	-0.	-0.	-0.	-0.
5	-0.	-0.	-0.	-0.	-0.
	-0.	-0.	1.000	-0.	-0.
	-0.	-0.	-0.	-0.	-0.
	-0.	-0.	-0.	-0.	-0.
	-0.	-0.	-0.	-0.	-0.
6	-0.	-0.	-0.	-0.	-0.
	-0.	-0.	-0.	1.000	-0.
	-0.	-0.	-0.	-0.	-0.
	-0.	-0.	-0.	-0.	-0.
	-0.	-0.	-0.	-0.	-0.
7	-1.000	-0.	-0.	-3.000	-0.
	-0.	-3.000	-0.	-0.	-0.
	-0.	-0.	-0.	-0.	-0.
	-0.	-0.	-0.	-0.	-0.
	-0.	-0.	-0.	-0.	-0.

8	-0.	-1.000	-0.	-0.	-3.000
	-0.	-0.	-3.000	-0.	-0.
	-0.	-0.	-0.	-0.	-0.
	-0.	-0.	-0.	-0.	-0.
	-0.	-0.	-0.	-0.	-0.
9	-0.	-0.	-1.000	-0.	-0.
	-3.000	-0.	-0.	-3.000	-0.
	-0.	-0.	-0.	-0.	-0.
	-0.	-0.	-0.	-0.	-0.
	-0.	-0.	-0.	-0.	-0.
10	-0.	-0.	-0.	-0.	-0.
	-0.	-0.	-0.	-0.	-0.
	-0.	-0.	1.000	-0.	-0.
	-0.	-0.	-0.	-0.	-0.
	-0.	-0.	-0.	-0.	-0.
11	-0.	-0.	-0.	-0.	-0.
	-0.	-0.	-0.	-0.	-0.
	-0.	-0.	-0.	1.000	-0.
	-0.	-0.	-0.	-0.	-0.
	-0.	-0.	-0.	-0.	-0.
12	-0.	-0.	-0.	-0.	-0.
	-0.	-0.	-0.	-0.	-0.
	-0.	-0.	-0.	-0.	1.000
	-0.	-0.	-0.	-0.	-0.
	-0.	-0.	-0.	-0.	-0.
13	-0.	-0.	-0.	-0.	-0.
	-0.	-0.	-0.	-0.	-1.000
	-0.	-0.	-2.000	-0.	-0.
	-0.	-0.	-0.	-0.	-0.
	-0.	-0.	-0.	-0.	-0.
14	-0.	-0.	-0.	-0.	-0.
	-0.	-0.	-0.	-0.	-0.
	-1.000	-0.	-0.	-2.000	-0.
	-0.	-0.	-0.	-0.	-0.
	-0.	-0.	-0.	-0.	-0.
15	-0.	-0.	-0.	-0.	-0.
	-0.	-0.	-0.	-0.	-0.
	-0.	-1.000	-0.	-0.	-2.000
	-0.	-0.	-0.	-0.	-0.
	-0.	-0.	-0.	-0.	-0.
16	-0.	-0.	-0.	-0.	-0.
	-0.	-0.	-0.	-0.	-0.
	-0.	-0.	-0.	-0.	-0.
	-0.	-0.	-0.	-0.	-0.
	-0.	-0.	-0.	-0.	-0.
17	-0.	-0.	-0.	-0.	-0.
	-0.	-0.	-0.	-0.	-0.
	-0.	-0.	-0.	-0.	-0.
	-0.	-0.	1.000	-0.	-0.
	-0.	-0.	-0.	-0.	-0.

18	-0.	-0.	-0.	-0.	-0.
	-0.	1.000	-0.	-0.	-0.
	-0.	-0.	-0.	-0.	-0.
	-0.	-.3333E-02	-.1333	-0.	-0.
	-0.	-0.	-0.	-0.	-0.
19	-0.	-0.	-0.	-0.	-0.
	-0.	-0.	-0.	-0.	-0.
	-0.	-0.	-0.	-0.	-0.
	-0.	-0.	-0.	-0.	1.000
	-0.	-0.	-0.	-0.	-0.
20	-0.	-0.	-0.	-0.	-0.
	-0.	-0.	1.000	-0.	-0.
	-0.	-0.	-0.	-0.	-0.
	-0.	-0.	-0.	-.3333E-02	-.1333
	-0.	-0.	-0.	-0.	-0.
21	-0.	-0.	-0.	-0.	-0.
	-0.	-0.	-0.	-0.	-0.
	-0.	-0.	-0.	-0.	-0.
	-0.	-0.	-0.	-0.	-0.
	-0.	1.000	-0.	-0.	-0.
22	-0.	-0.	-0.	-0.	-0.
	-0.	-0.	-0.	1.000	-0.
	-0.	-0.	-0.	-0.	-0.
	-0.	-0.	-0.	-0.	-0.
	-.3333E-02	-.1333	-0.	-0.	-0.
23	-0.	-1.000	-0.	-0.	-0.
	-0.	-0.	-0.	-0.	-0.
	-0.	-0.	-1.000	-0.	-0.
	-0.	-0.	-0.	-0.	-0.
	-0.	-0.	-.2000	-0.	-0.
24	1.000	-0.	-0.	-0.	-0.
	-0.	-0.	-0.	-0.	-0.
	-0.	-0.	-0.	-1.000	-0.
	-0.	-0.	-0.	-0.	-0.
	-0.	-0.	-0.	-.2000	-0.
25	-0.	-0.	-0.	-0.	-0.
	-0.	-0.	-0.	-0.	-0.
	-0.	-0.	-0.	-0.	-1.000
	1.000	-0.	-0.	-0.	-0.
	-0.	-0.	-0.	-0.	-.2000

E

1	-0.	-0.	-0.	-0.	-0.
	-0.				
2	-0.	-0.	-0.	-0.	-0.
	-0.				
3	-0.	-0.	-0.	-0.	-0.
	-0.				
4	-0.	-0.	-0.	-0.	-0.
	-0.				
5	-0.	-0.	-0.	-0.	-0.
	-0.				
6	-0.	-0.	-0.	-0.	-0.
	-0.				
7	1.000	-0.	-0.	-0.	-0.
	-0.				
8	-0.	1.000	-0.	-0.	-0.
	-0.				
9	-0.	-0.	1.000	-0.	-0.
	-0.				
10	-0.	-0.	-0.	-0.	-0.
	-0.				
11	-0.	-0.	-0.	-0.	-0.
	-0.				
12	-0.	-0.	-0.	-0.	-0.
	-0.				
13	-0.	-0.	-0.	1.000	-0.
	-0.				
14	-0.	-0.	-0.	-0.	1.000
	-0.				
15	-0.	-0.	-0.	-0.	-0.
	1.000				
16	-0.	-0.	-0.	-0.	-0.
	-0.				
17	-0.	-0.	-0.	-0.	-0.
	-0.				
18	-0.	-0.	-0.	-0.	-0.
	-0.				
19	-0.	-0.	-0.	-0.	-0.
	-0.				
20	-0.	-0.	-0.	-0.	-0.
	-0.				
21	-0.	-0.	-0.	-0.	-0.
	-0.				
22	-0.	-0.	-0.	-0.	-0.
	-0.				
23	-0.	-0.	-0.	-0.	-0.
	-0.				
24	-0.	-0.	-0.	-0.	-0.
	-0.				
25	-0.	-0.	-0.	-0.	-0.
	-0.				

WC

	.5000	.5000	.5000	1.000	1.000
	1.000				

C

1	-0.	-0.	-0.	-0.	-0.
	-0.	.5724	-0.	-0.	-0.
	-0.	-0.	-0.	-0.	-0.
	-0.	-.1908E-02	57.17	-0.	-0.
	-0.	-0.	-0.	-0.	-0.
2	-0.	-0.	-0.	-0.	-0.
	-0.	-0.	.5724	-0.	-0.
	-0.	-0.	-0.	-0.	-0.
	-0.	-0.	-0.	-.1908E-02	57.17
	-0.	-0.	-0.	-0.	-0.
3	-0.	-0.	-0.	-0.	-0.
	-0.	-0.	-0.	.5724	-0.
	-0.	-0.	-0.	-0.	-0.
	-0.	-0.	-0.	-0.	-0.
	-.1908E-02	57.17	-0.	-0.	-0.
4	-0.	-90.00	-0.	-0.	-0.
	-0.	-0.	-0.	-0.	-0.
	-0.	-0.	-90.00	-0.	-0.
	-0.	-0.	-0.	-0.	-0.
	-0.	-0.	-9.000	-0.	-0.
5	90.00	-0.	-0.	-0.	-0.
	-0.	-0.	-0.	-0.	-0.
	-0.	-0.	-0.	-90.00	-0.
	-0.	-0.	-0.	-0.	-0.
	-0.	-0.	-0.	-9.000	-0.
6	-0.	-0.	-0.	-0.	-0.
	-0.	-0.	-0.	-0.	-0.
	-0.	-0.	-0.	-0.	-90.00
	90.00	-0.	-0.	-0.	-0.
	-0.	-0.	-0.	-0.	-9.000

TH (threshold)

0.	-0.	-0.	-0.	-0.	-0.
-0.					

VA (additive noise)

0.	-0.	-0.	-0.	-0.	-0.
-0.					

VM (noise/signal ratio)

.5000E-01	.5000E-01	.5000E-01	.5000E-01	.5000E-01	.5000E-01
.5000E-01					

FA (attention fraction)

1.000	1.000	1.000	1.000	1.000	1.000
1.000					

KALMAN FILTER: $\hat{\underline{x}} = F\,\hat{\underline{x}} + GK\,\underline{y}$

$\hat{\underline{x}}(t) = \Phi_F(\Delta t)\,\hat{\underline{x}}(t-\Delta t) + DM_F(\Delta t)\,\underline{y}(t)$

F

1	-.4495	0.	0.	1.000	0.
	0.	-.5389E-03	0.	0.	0.
	0.	0.	0.	.4496	0.
	0.	.2129E-05	-.6380E-01	0.	0.
	0.	0.	0.	.4496E-01	0.
2	0.	-.4495	0.	0.	1.000
	0.	0.	-.5389E-03	0.	0.
	0.	0.	-.4496	0.	0.
	0.	0.	0.	.2129E-05	-.6380E-01
	0.	0.	-.4496E-01	0.	0.
3	0.	0.	0.	0.	0.
	1.000	0.	0.	.1287E-01	0.
	0.	0.	0.	0.	0.
	0.	0.	0.	0.	0.
	-.4290E-04	1.285	0.	0.	0.
4	-.4817E-01	0.	0.	0.	0.
	0.	.9680	0.	0.	0.
	0.	0.	0.	.4817E-01	0.
	0.	.1065E-03	-3.191	0.	0.
	0.	0.	0.	.4817E-02	0.
5	0.	-.4817E-01	0.	0.	0.
	0.	0.	.9680	0.	0.
	0.	0.	-.4817E-01	0.	0.
	0.	0.	0.	.1065E-03	-3.191
	0.	0.	-.4817E-02	0.	0.
6	0.	0.	0.	0.	0.
	0.	0.	0.	.9679	0.
	0.	0.	0.	0.	0.
	0.	0.	0.	0.	0.
	.1069E-03	-3.202	0.	0.	0.
7	-.9078	0.	0.	-3.000	0.
	0.	-3.058	0.	0.	0.
	0.	0.	0.	-.9217E-01	0.
	0.	.1946E-03	-5.832	0.	0.
	0.	0.	0.	-.9217E-02	0.
8	0.	-.9078	0.	0.	-3.000
	0.	0.	-3.058	0.	0.
	0.	0.	.9217E-01	0.	0.
	0.	0.	0.	.1946E-03	.832
	0.	0.	.9217E-02	0.	0.

9	0.	0.	-1.000	0.	0.
	-3.000	0.	0.	-3.061	0.
	0.	0.	0.	0.	0.
	0.	0.	0.	0.	0.
	.2040E-03	-6.112	0.	0.	0.
10	0.	1.133	0.	0.	0.
	0.	0.	-.1238E-01	0.	0.
	0.	0.	2.138	0.	0.
	0.	0.	0.	.4126E-04	-1.236
	0.	0.	.1138	0.	0.
11	-1.138	0.	0.	0.	0.
	0.	.1238E-01	0.	0.	0.
	0.	0.	0.	2.138	0.
	0.	-.4126E-04	1.236	0.	0.
	0.	0.	0.	.1138	0.
12	0.	0.	0.	0.	0.
	0.	0.	0.	0.	0.
	0.	0.	0.	0.	1.319
	-.3189	0.	0.	0.	0.
	0.	0.	0.	0.	.3189E-01
13	0.	-6.040	0.	0.	0.
	0.	0.	.1978E-03	0.	-1.000
	0.	0.	-8.040	0.	0.
	0.	0.	0.	-.6593E-06	.1975E-01
	0.	0.	-.6040	0.	0.
14	6.040	0.	0.	0.	0.
	0.	-.1978E-03	0.	0.	0.
	-1.000	0.	0.	-8.040	0.
	0.	.6593E-06	-.1975E-01	0.	0.
	0.	0.	0.	-.6040	0.
15	0.	0.	0.	0.	0.
	0.	0.	0.	0.	0.
	0.	-1.000	0.	0.	-9.239
	7.239	0.	0.	0.	0.
	0.	0.	0.	0.	-.7239
16	0.	0.	0.	0.	0.
	0.	0.	0.	0.	0.
	0.	0.	0.	0.	.4243E-14
	-.4243E-14	0.	0.	0.	0.
	0.	0.	0.	0.	.4243E-15
17	-.2432	0.	0.	0.	0.
	0.	-.3408E-02	0.	0.	0.
	0.	0.	0.	.2432	0.
	0.	.1136E-04	.6597	0.	0.
	0.	0.	0.	.2432E-01	0.
18	-.1093E-01	0.	0.	0.	0.
	0.	.9684	0.	0.	0.
	0.	0.	0.	.1093E-01	0.
	0.	-.3228E-02	-3.286	0.	0.
	0.	0.	0.	.1093E-02	0.

19	0.	-.2432	0.	0.	0.
	0.	0.	-.3408E-02	0.	0.
	0.	0.	-.2432	0.	0.
	0.	0.	0.	.1136E-04	.6597
	0.	0.	-.2432E-01	0.	0.
20	0.	-.1093E-01	0.	0.	0.
	0.	0.	.9684	0.	0.
	0.	0.	-.1093E-01	0.	0.
	0.	0.	0.	-.3228E-02	-3.236
	0.	0.	-.1093E-02	0.	0.
21	0.	0.	0.	0.	0.
	0.	0.	0.	.3239E-03	0.
	0.	0.	0.	0.	0.
	0.	0.	0.	0.	0.
	-.1079E-05	1.032	0.	0.	0.
22	0.	0.	0.	0.	0.
	0.	0.	0.	.9676	0.
	0.	0.	0.	0.	0.
	0.	0.	0.	0.	0.
	-.3225E-02	-3.368	0.	0.	0.
23	0.	-.2317	0.	0.	0.
	0.	0.	-.5809E-02	0.	0.
	0.	0.	-.2317	0.	0.
	0.	0.	0.	.1936E-04	-.5802
	0.	0.	-.1232	0.	0.
24	.2317	0.	0.	0.	0.
	0.	.5809E-02	0.	0.	0.
	0.	0.	0.	-.2317	0.
	0.	-.1936E-04	.5802	0.	0.
	0.	0.	0.	-.1232	0.
25	0.	0.	0.	0.	0.
	0.	0.	0.	0.	0.
	0.	0.	0.	0.	-.6311
	.6311	0.	0.	0.	0.
	0.	0.	0.	0.	-.1581

GK

1	.1116E-02	0.	0.	0.	.4936E-02
	0.				
2	0.	.1115E-02	0.	-.4996E-02	0.
	0.				
3	0.	0.	-.2249E-01	0.	0.
	0.				
4	.5582E-01	0.	0.	0.	.5352E-03
	0.				
5	0.	.5582E-01	0.	-.5352E-03	0.
	0.				
6	0.	0.	.5600E-01	0.	0.
	0.				
7	.1020	0.	0.	0.	-.1024E-02
	0.				
8	0.	.1020	0.	.1024E-02	0.
	0.				
9	0.	0.	.1069	0.	0.
	0.				
10	0.	.2162E-01	0.	.1264E-01	0.
	0.				
11	-.2162E-01	0.	0.	0.	.1254E-01
	0.				
12	0.	0.	0.	0.	0.
	.3544E-02				
13	0.	-.3455E-03	0.	-.6711E-01	0.
	0.				
14	.3455E-03	0.	0.	0.	-.6711E-01
	0.				
15	0.	0.	0.	0.	0.
	-.3044E-31				
16	0.	0.	0.	0.	0.
	.4714E-16				
17	.5953E-02	0.	0.	0.	.2703E-02
	0.				
18	.5514E-01	0.	0.	0.	.1215E-03
	0.				
19	0.	.5953E-02	0.	-.2703E-02	0.
	0.				
20	0.	.5514E-01	0.	-.1215E-03	0.
	0.				
21	0.	0.	-.5658E-03	0.	0.
	0.				
22	0.	0.	.5658E-01	0.	0.
	0.				
23	0.	.1015E-01	0.	.8537E-02	0.
	0.				
24	-.1015E-01	0.	0.	0.	.8537E-02
	0.				
25	0.	0.	0.	0.	0.
	.3544E-02				

FILTER INITIAL STATE

0.	-0.	-0.	-0.	-0.	
-0.	-0.	0.	-0.	-0.	
-0.	-0.	-0.	-0.	-0.	
1.000	-0.	-0.	-0.	-0.	
-0.	-0.	-0.	-0.	5.000	

Φ_F(1 sec)

1	.8269	0.	0.	.8137	0.
	0.	.4544E-01	0.	0.	0.
	-.4184E-01	0.	0.	.4025E-01	0.
	0.	.3962E-03	-.6725	0.	0.
	0.	0.	0.	.1352E-01	0.
2	0.	.8269	0.	0.	.8137
	0.	0.	.4544E-01	0.	-.4184E-01
	0.	0.	-.4025E-01	0.	0.
	0.	0.	0.	.9952E-03	-.6725
	0.	0.	-.1352E-01	0.	0.
3	0.	0.	.9220	0.	0.
	.7387	0.	0.	.1216	0.
	0.	0.	0.	0.	0.
	0.	0.	0.	0.	0.
	.1846E-03	-.3683	0.	0.	0.
4	-.5926E-01	0.	0.	.7952	0.
	0.	.4884E-02	0.	0.	0.
	-.1345E-02	0.	0.	.3684E-05	0.
	0.	.2371E-02	-.8333	0.	0.
	0.	0.	0.	.3296E-03	0.
5	0.	-.5925E-01	0.	0.	.7952
	0.	0.	.4884E-02	0.	-.1345E-02
	0.	0.	-.3684E-05	0.	0.
	0.	0.	0.	.2371E-02	-.8333
	0.	0.	-.3296E-03	0.	0.
6	0.	0.	-.5532E-01	0.	0.
	.7998	0.	0.	.4397E-02	0.
	0.	0.	0.	0.	0.
	0.	0.	0.	0.	0.
	.2383E-02	-.3394	0.	0.	0.
7	-.1433	0.	0.	-.6833	0.
	0.	-.5156E-01	0.	0.	0.
	.1093E-01	0.	0.	-.8659E-02	0.
	0.	-.1841E-03	.6199	0.	0.
	0.	0.	0.	-.3357E-02	0.
8	0.	-.1433	0.	0.	-.5833
	0.	0.	-.5156E-01	0.	-.1093E-01
	0.	0.	.8659E-02	0.	0.
	0.	0.	0.	-.1841E-03	.6199
	0.	0.	.3357E-02	0.	0.

9	0.	0.	-.1695	0.	0.
	-.5726	0.	0.	-.6743E-01	0.
	0.	0.	0.	0.	0.
	0.	0.	0.	0.	0.
	-.2193E-04	.5614	0.	0.	0.
10	0.	-.2077	0.	0.	.7617E-01
	0.	0.	-.6292E-01	0.	.7860
	0.	0.	.2256	0.	0.
	0.	0.	0.	.7652E-03	-.2673
	0.	0.	-.2422E-01	0.	0.
11	.2077	0.	0.	-.7617E-01	0.
	0.	.6292E-01	0.	0.	0.
	.7860	0.	0.	.2256	0.
	0.	-.7652E-03	.2673	0.	0.
	0.	0.	0.	-.2422E-01	0.
12	0.	0.	0.	0.	0.
	0.	0.	0.	0.	0.
	0.	.8776	0.	0.	.1309
	.5683	0.	0.	0.	0.
	0.	0.	0.	0.	-.5442E-01
13	0.	-.6108	0.	0.	-.5561
	0.	0.	-.2348E-01	0.	-.1301
	0.	0.	.4936E-02	0.	0.
	0.	0.	0.	-.6715E-03	.4764
	0.	0.	-.5562E-01	0.	0.
14	.6108	0.	0.	.5561	0.
	0.	.2348E-01	0.	0.	0.
	-.1301	0.	0.	.4936E-02	0.
	0.	.6715E-03	-.4764	0.	0.
	0.	0.	0.	-.5662E-01	0.
15	0.	0.	0.	0.	0.
	0.	0.	0.	0.	0.
	0.	-.1006	0.	0.	-.9494E-02
	.7148	0.	0.	0.	0.
	0.	0.	0.	0.	-.6508E-01
16	0.	0.	0.	0.	0.
	0.	0.	0.	0.	0.
	0.	-.3347E-15	0.	0.	.4020E-15
	1.000	0.	0.	0.	0.
	0.	0.	0.	0.	.1273E-15
17	-.9343E-01	0.	0.	-.1127	0.
	0.	.3054E-01	0.	0.	0.
	-.2168E-01	0.	0.	.1968E-01	0.
	0.	.9996	.2086	0.	0.
	0.	0.	0.	.6902E-02	0.
18	-.4494E-01	0.	0.	-.1880	0.
	0.	.4364E-03	0.	0.	0.
	.2013E-02	0.	0.	-.3093E-02	0.
	0.	-.3977E-03	.1359	0.	0.
	0.	0.	0.	-.7436E-03	0.

19	0.	-.9343E-01	0.	0.	-.1127
	0.	0.	.3054E-01	0.	.2168E-01
	0.	0.	-.1968E-01	0.	0.
	0.	0.	0.	.9996	.2086
	0.	0.	-.5902E-02	0.	0.
20	0.	-.4494E-01	0.	0.	-.1890
	0.	0.	.4364E-03	0.	-.2113E-02
	0.	0.	.3093E-02	0.	0.
	0.	0.	0.	-.8977E-03	.1359
	0.	0.	.7436E-03	0.	0.
21	0.	0.	-.3344E-01	0.	0.
	-.1121	0.	0.	.5151E-01	0.
	0.	0.	0.	0.	0.
	0.	0.	0.	0.	0.
	.9994	.2709	0.	0.	0.
22	0.	0.	-.4955E-01	0.	0.
	-.1819	0.	0.	-.4042E-02	0.
	0.	0.	0.	0.	0.
	0.	0.	0.	0.	0.
	-.9465E-03	.1163	0.	0.	0.
23	0.	-.4894E-01	0.	0.	.2717E-01
	0.	0.	-.3299E-01	0.	.2048E-01
	0.	0.	-.1916E-01	0.	0.
	0.	0.	0.	.3440E-03	-.1257
	0.	0.	.8982	0.	0.
24	.4994E-01	0.	0.	-.2717E-01	0.
	0.	.3299E-01	0.	0.	0.
	.2048E-01	0.	0.	-.1916E-01	0.
	0.	-.3440E-03	.1267	0.	0.
	0.	0.	0.	.8982	0.
25	0.	0.	0.	0.	0.
	0.	0.	0.	0.	0.
	0.	.5398E-01	0.	0.	-.5363E-01
	.2043	0.	0.	0.	0.
	0.	0.	0.	0.	.8356

DM_p (1 sec)

1	.1245E-01	0.	0.	0.	.1690E-02
2	0.	.1245E-01	0.	-.1690E-02	0.
3	0.	0.	.6545E-02	0.	0.
4	.1624E-01	0.	0.	0.	.4417E-04
5	0.	.1624E-01	0.	-.4417E-04	0.
6	0.	0.	.1634E-01	0.	0.
7	-.1095E-01	0.	0.	0.	-.4226E-03
8	0.	-.1095E-01	0.	.4226E-03	0.
9	0.	0.	-.9810E-02	0.	0.
10	0.	.5212E-02	0.	-.2827E-02	0.
11	-.5212E-02	0.	0.	0.	-.2827E-02
12	0.	0.	0.	0.	0.
13	0.	-.8795E-02	0.	-.7553E-02	0.
14	.8795E-02	0.	0.	0.	-.7553E-02
15	0.	0.	0.	0.	0.
16	0.	0.	0.	0.	0.
17	.1352E-01	0.	0.	0.	.8653E-03
18	.1445E-01	0.	0.	0.	-.9010E-04
19	0.	.1352E-01	0.	-.8653E-03	0.
20	0.	.1445E-01	0.	.9010E-04	0.
21	0.	0.	.1228E-01	0.	0.
22	0.	0.	.1484E-01	0.	0.
23	0.	.2459E-02	0.	.9751E-02	0.
24	-.2459E-02	0.	0.	0.	.9751E-02
25	0.	0.	0.	0.	0.

.1584E-16

.8173E-02

INDIVIDUAL SENSOR SYSTEMS: iteration interval = 1 sec

SENSOR SYSTEM LINEAR DYNAMICS
- INIT. STATES (X)
- SYST. MTX (A)
- INPUT MTX (B)
- OUTPUT MTX (C)
- TRANSITION MTX (TM)
- DRIVING MTX (DM)

SEMICIRCULAR CANALS

XS

1	0.	-0.	-0.
2	0.	-0.	-0.

AS

1	0.	1.000
2	-.3333E-02	-.1333

BS

0.	1.000

CC

1	-.1909E-02	57.17	.5724

TMC

1	.9984	.9357
2	-.3119E-02	.8737

DMC

.4784	.9357

OTOLITHS

XO

1	-2.113	0.	4.532

AO

-.2000

BO

1.000

CO

1	-9.000	90.00

TMO

.8187

DMO

.9063

SENSOR SYSTEM THRESHOLDS (TH)

THC =-0.

THO =-0.

☆ U.S. GOVERNMENT PRINTING OFFICE: 1977—771-122/62